

**TIME-SERIES ANALYSIS OF PRESSURE
FLUCTUATION IN GAS-SOLID FLUIDIZED BEDS**

by

ROWEN GYAN

Submitted in fulfilment of the academic requirements of

Master of Science

in Engineering

School of Chemical Engineering

College of Agriculture, Engineering and Science

University of KwaZulu-Natal

Durban

South Africa

2015

LIBRARY COPY

ABSTRACT

Fluidized beds have been used extensively in chemical process industries for several years. The success of fluidized operations is largely dependent on a well-defined and stable contact regime. Hence, the ability to understand the flow regime behaviour plays a vital role in the design and operation of fluidized bed units in order to achieve a particular stable fluid dynamic state. Fluidization regime is dependent on factors such as particle properties (size, density and geometry), column properties (size and geometry) as well as the fluidizing medium properties (density, viscosity and velocity) (Fan, et al., 1981).

In order to expand the understanding of the hydrodynamics of a fluidized bed system, a substantial amount of research has been committed to the measurement and analysis of pressure fluctuations in a fluidized bed. This is due to the strong relationship between pressure fluctuation and the hydrodynamic factors which include bubble size, bubble rising velocity and the motion of the bed surface with time (Hartman, et al., 2009). Identification of each regime could be accomplished through the time-series analysis of the pressure fluctuation in the time domain, frequency domain and state space domain (van Ommen, et al., 2011).

The main focus of this dissertation was to apply time-series analysis in the frequency domain, for the characterisation of the different fluidization regimes (particulate, bubbling, slugging and turbulent) in a gas-solid fluidized bed. This was achieved through the use of spectral analysis and the mathematical tool known as the Fast Fourier Transform (FFT) was used to analyse and interpret the pressure fluctuation in the fluidized bed. Analysis was also performed in the time domain by analysing the time-pressure behaviour as well as the change in the standard deviation of pressure fluctuations. Experimental measurements were conducted in three different columns with varying column height and diameter. Three different solid particles were used namely, sand particles (Geldart Group B), plastic beads (Geldart Group D) and spent Fluid Cracking Catalyst (Geldart Group A). The sampling frequency used for pressure measurements in this work was fixed at 500 Hz with a sampling time of 30 minutes.

Results indicated that the pressure fluctuation signal is useful in providing information about fluidized bed behaviour. Analysis in the time domain revealed that this technique could be used primarily to identify whether fluidization has occurred or not. Analysis in the frequency domain indicated a better representation of the fluidization behaviour and the different regimes could

clearly be identified and distinguished based on a dominant frequency. In the 5 cm diameter column, the Geldart Group B particles displayed a distinct dominant frequency for the bubbling regime while a dominant frequency could not be obtained for the Group A and D particles respectively. In the 11 cm diameter column, the Geldart Group B materials were observed to fluidize very easily, with three dominant frequencies corresponding to the bubble, slugging and turbulent regimes, being identified. The Geldart Group D particles were found to fluidize at high velocities in the 11 cm diameter column with the bubbling and slugging regimes being identified. Geldart Group A particles were found to behave very differently from the other two materials. A noticeable bed expansion was seen before fluidization actually occurred. The only regime achieved with the Group A particles was the bubbling regime. Results for the 29 cm diameter column indicated a dominant frequency for the bubbling regime for the Group B particles while measurements could not be performed using other materials due to limitations on the pressure transmitter. It was further observed that the dominant frequencies were much more pronounced at higher bed heights. In addition, a change in the aspect ratio (bed height: column diameter) had a significant influence on the dominant frequency as a visible shift was apparent. An increase in the aspect ratio indicated a noticeable decrease in the dominant frequency component. This was valid for all fluidization regimes investigated.

ACKNOWLEDGMENTS

I would like to extend my deepest gratitude to the following people/organizations for their contributions in this work:

- Firstly, my supervisors, Professor M. Carsky and Mr M.G. Ntunka for their invaluable support, guidance, wisdom and enthusiastic encouragement throughout this work. Working with them has been a privilege and a great learning experience.
- The School of Chemical Engineering technical staff, in particular, Danny Singh, Sanjay Naidoo, Thobikile Mafekeng and Xoli Hadebe for their ever-willing assistance and contributions to this project.
- To my mother, Aishnee, my brother, Kyle, my grandparents, late grandmother, aunts, uncles and cousins for their unconditional love, selfless sacrifices and words of encouragement throughout every facet in my life. They have made me realise that anything is possible in life, as long as you have the desire and determination to achieve your goals.
- Lastly, to Suvigya, for her love, support, strength and inspiration throughout this research. Your tolerance and ever-willingness to assist has been greatly appreciated.

The financial assistance of the National Research Foundation (NRF) towards this research is hereby acknowledged. Opinions expressed and conclusions arrived at, are those of the author and are not necessarily to be attributed to the NRF.

TABLE OF CONTENTS

	<u>Page</u>
PREFACE.....	ii
DECLARATION 1: PLAGIARISM.....	iii
DECLARATION 2: PUBLICATIONS	iv
ABSTRACT.....	v
ACKNOWLEDGMENTS	vii
TABLE OF CONTENTS.....	viii
LIST OF TABLES.....	xi
LIST OF FIGURES	xii
NOMENCLATURE.....	xvi
CHAPTER 1: INTRODUCTION	1
1.1 Fluidization and Applications.....	1
1.2 Motivation and Research Aims	3
1.3 Research Contributions.....	3
1.4 Contribution to Literature.....	4
1.5 Outline of Dissertation Structure.....	4
CHAPTER 2: LITERATURE REVIEW	5
2.1 Phenomena of Fluidization.....	5
2.1.1 Fluidized Beds.....	6
2.1.2 Fluidization Regimes	8
2.1.3 Minimum Fluidization Velocity.....	10
2.1.4 Minimum Bubbling Velocity	13
2.1.5 Maximum Bubble Size.....	13
2.1.6 Minimum Slugging Velocity.....	14
2.1.7 Transition Velocity from Bubbling to Turbulent Regime.....	15
2.1.8 Gas Hold-up	17
2.1.9 Geldart Powder Classification.....	17
2.2 Time-series Analysis Techniques using in-bed Pressure Measurements	20
2.2.1 Time Domain Analysis	21
2.2.1.1 Standard Deviation or Variance.....	21
2.2.1.2 Additional Time Domain Methods.....	21
2.2.2 Frequency Domain Analysis	22

2.2.3	State Space Domain	25
CHAPTER 3:	EQUIPMENT DESCRIPTION	27
3.1	The Gas-Solid Fluidized Bed Apparatus	27
3.1.1	Fluidized Bed Column	29
3.1.2	The Bed Region.....	30
3.1.3	The Distributor Plate	30
3.1.4	The Plenum Chamber.....	30
3.1.5	Flow measurement and Control	31
3.1.6	Pressure measurement and Control	31
CHAPTER 4:	EXPERIMENTAL PROCEDURE	33
4.1	Particle Selection and Characterization	33
4.1.1	Particle Selection.....	33
4.1.2	Particle Characterization	34
4.1.2.1	Particle density	34
4.1.2.2	Particle size.....	35
4.2	Preparation of the Experimental Equipment.....	36
4.2.1	Cleaning of the Gas-Solid Fluidized Bed Apparatus	36
4.2.2	Detection of penetration of solid particles through distributor plate.....	36
4.3	Operation of the Experimental Equipment	37
4.4	Processing of Pressure Fluctuation Signals	38
CHAPTER 5:	RESULTS AND DISCUSSION	39
5.1	Comparison to Literature Data	40
5.2	Analysis in the time domain	42
5.2.1	Time-pressure behaviour.....	42
5.2.2	Standard Deviation or Variance	47
5.2.2.1	Experimental regime transition velocity.....	47
5.2.2.2	Prediction of the regime transition velocity.....	48
5.3	Analysis in the frequency domain	49
5.3.1	Fluidized bed 1 (Internal diameter of 5 cm and height of 200 cm).....	50
5.3.1.1	Sand Particles	50
5.3.1.2	Other Materials.....	54
5.3.2	Fluidized bed 2 (Internal diameter of 11 cm and height of 153 cm).....	54
5.3.2.1	Sand Particles	54
5.3.2.2	Plastic Beads.....	60
5.3.2.3	Spent FCC	63

5.3.3	Fluidized bed 3 (Internal diameter of 29 cm and height of 507.5 cm)	65
5.3.3.1	Sand Particles	65
5.3.3.2	Other Materials	67
5.3.4	Summary of frequency domain analysis	67
CHAPTER 6: CONCLUSION		73
CHAPTER 7: RECOMMENDATIONS		76
REFERENCES		77
APPENDIX A: ADDITIONAL FREQUENCY DOMAIN RESULTS		83
APPENDIX B: MATLAB CODE FOR IMPLEMENTATION OF THE FFT		89
APPENDIX C: DATA CAPTURE AND DESCRIPTION OF SOFTWARE INTERFACE		93

LIST OF TABLES

<u>Table</u>	<u>Page</u>
Table 2.1 Correlations for predicting the minimum fluidization velocity	13
Table 2.2 Correlations for predicting the minimum slugging velocity	14
Table 2.3 Correlations for predicting the transition velocity from the bubbling to turbulent regime	16
Table 4.1 Physical characteristics of solid particles.....	36
Table 4.2 Operational Conditions of Gas-Solid Fluidized System	38
Table 5.1 Correlations and predictions for <i>u_c</i> using sand in the 11 cm I.D column and a bed height of 11 cm	49

LIST OF FIGURES

<u>Figure</u>	<u>Page</u>
Figure 2.1 Schematic of a Fluidized Bed	6
Figure 2.2 Schematic representation of the different fluidization regimes that occur with increasing superficial gas velocity in fluidized beds (Kunii & Levenspiel, 1991)	10
Figure 2.3 Amplitude of pressure fluctuation across the fluidized bed with increasing superficial gas velocity (Basu, 2006).....	15
Figure 2.4 Geldart's Classification of Powders (Geldart, 1973).....	18
Figure 3.1 Experimental Setup of the Fluidized Bed System	28
Figure 3.2 Schematic representation of the experimental gas-solid fluidized bed apparatus	29
Figure 5.1 Power spectrum of the bubbling regime for FCC with 80 μm , bed height 21 cm and column I.D 11 cm; Experimental	41
Figure 5.2 Power spectrum of the bubbling regime for FCC with 92 μm , bed height 20.5 cm and column I.D 11.15 cm; Alberto et al. (2004).....	41
Figure 5.3 Time sequences of the pressure fluctuation signals measured in the bubbling regime using spent FCC in the 11 cm I.D column at the indicated bed heights	43
Figure 5.4 Time sequences of the pressure fluctuation signals measured in various regimes using sand in the 11 cm I.D column at a bed height of 11 cm	44
Figure 5.5 Time sequences of the pressure fluctuation signals measured in various regimes using sand in the 11 cm I.D column at a bed height of 21 cm	45
Figure 5.6 Time sequences of the pressure fluctuation signals measured in the indicated regimes using plastic beads in the 11 cm I.D column at a bed height of 11 cm.....	46
Figure 5.7 Time sequences of the pressure fluctuation signals measured in the indicated regimes using plastic beads in the 11 cm I.D column at a bed height of 28 cm	46
Figure 5.8 Standard deviation of pressure fluctuation as a function of superficial gas velocity for sand particles at a bed height of 11 cm	48

Figure 5.9 Power spectrum of the slugging regime of sand particles in the 5 cm I.D column with a bed height of 8 cm.....	51
Figure 5.10 Power spectrum of the turbulent regime of sand particles in the 5 cm I.D column with a bed height of 8 cm.....	51
Figure 5.11 Power spectrum of the slugging regime of sand particles in the 5 cm I.D column with a bed height of 30 cm.....	53
Figure 5.12 Power spectrum of the turbulent regime of sand particles in the 5 cm I.D column with a bed height of 30 cm.....	53
Figure 5.13 Power spectrum of the bubbling regime of sand particles in the 11 cm I.D column with a bed height of 11 cm.....	56
Figure 5.14 Power spectrum of the slugging regime of sand particles in the 11 cm I.D column with a bed height of 11 cm.....	56
Figure 5.15 Power spectrum of the turbulent regime of sand particles in the 11 cm I.D column with a bed height of 11 cm.....	57
Figure 5.16 Power spectrum of the bubbling regime of sand particles in the 11 cm I.D column with a bed height of 21 cm.....	58
Figure 5.17 Power spectrum of the slugging regime of sand particles in the 11 cm I.D column with a bed height of 21 cm.....	59
Figure 5.18 Power spectrum of the turbulent regime of sand particles in the 11 cm I.D column with a bed height of 21 cm.....	59
Figure 5.19 Power spectrum of the bubbling regime of plastic beads in the 11 cm I.D column with a bed height of 11 cm.....	61
Figure 5.20 Power spectrum of the slugging regime of plastic beads in the 11 cm I.D column with a bed height of 11 cm.....	61
Figure 5.21 Power spectrum of the bubbling regime of plastic beads in the 11 cm I.D column with a bed height of 21 cm.....	62
Figure 5.22 Power spectrum of the slugging regime of plastic beads in the 11 cm I.D column with a bed height of 21 cm.....	63

Figure 5.23 Power spectrum of the bubbling regime of spent FCC in the 11 cm I.D column with a bed height of 11 cm.....	64
Figure 5.24 Power spectrum of the bubbling regime of spent FCC in the 11 cm I.D column with a bed height of 16 cm.....	65
Figure 5.25 Power spectrum of the bubbling regime of sand particles in the 29 cm I.D column with a bed height of 32 cm.....	66
Figure 5.26 Power spectrum of the bubbling regime of sand particles in the 29 cm I.D column with a bed height of 80 cm.....	67
Figure 5.27 Summary of the relationship between dominant frequency and L/D ratio for the indicated regimes using sand in the 5 cm I.D column	68
Figure 5.28 Summary of the relationship between dominant frequency and L/D ratio for the indicated regimes using sand in the 11 cm I.D column	69
Figure 5.29 Summary of the relationship between dominant frequency and L/D ratio for the indicated regimes using plastic beads in the 11 cm I.D column	70
Figure 5.30 Summary of the relationship between dominant frequency and L/D ratio for the bubbling regime using spent FCC in the 11 cm I.D column.....	71
Figure 5.31 Summary of the relationship between dominant frequency and L/D ratio for the bubbling regime using sand particles in the 29 cm I.D column.....	72
Figure A.1 Power spectra of the bubbling regime of sand particles in the 11 cm I.D column with a bed height of 16 cm.....	84
Figure A.2 Power spectra of the slugging regime of sand particles in the 11 cm I.D column with a bed height of 16 cm.....	84
Figure A.3 Power spectra of the turbulent regime of sand particles in the 11 cm I.D column with a bed height of 16 cm.....	85
Figure A.4 Power spectra of the bubbling regime of plastic beads in the 11 cm I.D column with a bed height of 16 cm.....	86
Figure A.5 Power spectra of the slugging regime of plastic beads in the 11 cm I.D column with a bed height of 16 cm.....	86

Figure A.6 Power spectra of the bubbling regime of plastic beads in the 11 cm I.D column with a bed height of 28 cm.....	87
Figure A.7 Power spectra of the slugging regime of plastic beads in the 11 cm I.D column with a bed height of 28 cm.....	88
Figure C.1 Main window configuration.....	94
Figure C.2 Instrument menu displayed in working pane once the instrument has been connected.....	95
Figure C.3 Data logger menu displayed in working pane once the instrument had been connected	96

NOMENCLATURE

English Letters

A	Cross-sectional area [m^2]
Ar	Archimedes Number
AR	Autoregressive
C_1	Constant in modified Ergun Equation, Equation 2-7
C_2	Constant in modified Ergun Equation, Equation 2-7
CFB	Circulating Fluidized Bed
D_b	Bubble diameter [m]
D_c	Column diameter [m]
d_p	Particle diameter [m]
F	Mass fraction of solids with diameter less than $45 \mu m$
f	Frequency [Hz]
FCC	Fluid Catalytic Cracking
g	Acceleration due to gravity [m/s^2]
H, L	Bed height [m]
$I.D$	Inner column diameter [m]
m	Mass [kg]
N	Number of data points
P	Pressure [Pa]
Re	Reynolds Number
SFB	Stationary Fluidized Bed
t	Time [s]
t_n	Total sampling time [s]
U	Superficial gas velocity [m/s]
u_c	Onset of turbulent regime velocity [m/s]
u_k	End of turbulent regime velocity [m/s]
u_{mb}	Minimum bubbling velocity [m/s]
u_{mf}	Minimum fluidization velocity [m/s]
u_{ms}	Minimum slugging velocity [m/s]
u_t	Terminal velocity [m/s]

u_t^*	Terminal velocity of solid particles with diameter 2.7 times that of the average particle diameter [m/s]
V	Volume [m^3]
X	Amplitude of sinusoidal $x(t)$
$x(t)$	Time-dependent variable

Greek Letters

Δ	Denotes a change in a property
ε	Bed voidage
\emptyset	Sphericity of solid particles
ρ	Density [kg/m^3]
σ	Standard deviation of pressure [Pa]
μ	Fluid viscosity [$Pa \cdot s$]

Subscript/Superscript

f	Denotes fluid
g	Denotes gas phase
l	Denotes liquid
max	maximum
mb	Minimum bubbling
mf	Minimum fluidization
ms	Minimum slugging

1

CHAPTER 1

INTRODUCTION

1.1 Fluidization and Applications

Fluidization phenomenon refers to a unit operation which involves the direct contact between a bed of solid particles and an upward flow of fluid. The solid particles are fluidized alike to the state of the liquid with the fluidizing medium being either a gas or liquid (Kunii & Levenspiel, 1991). Gas-solid fluidized beds have gained increased popularity due to the numerous advantages such as: enhanced heat and mass transfer, excellent particle mixing, relatively low pressure drop together with a large effective surface contact (Johnsson, et al., 2000). The application of fluidized beds can be seen in a wide range of industries including the petroleum, chemical, metallurgical, pharmaceutical as well as food industries.

Processes which implement fluidized bed technology include coal combustion and gasification, synthetic fuel catalytic cracking, drying and coating of solids as well as gas adsorption. The application of fluidized beds in these industries has been used for many years with significant progress being made in the design and development of these units (Hartman, et al., 2009). In addition, the success of a fluidized bed largely depends on a well-defined and stable fluidization regime. As a result, the ability to understand the flow regime behaviour plays a vital function in

the design and operation of fluidized bed units in order to achieve a particular stable fluid dynamic state.

There are six main fluidization regimes that exist in gas-solid fluidization. These can be described as: fixed bed, minimum fluidization, bubbling fluidization, slugging (typical for narrow vessels), turbulent fluidization, and pneumatic conveying (Kunii & Levenspiel, 1991). Each regime is strongly related to the hydrodynamic factors of the fluidized bed. The hydrodynamic factors include bubble size, bubble rising velocity as well as the motion of the bed surface with time. These factors are very complex and are difficult to measure as the behaviour in the fluidized bed is unsteady, opaque and non-uniform (Croxford & Gilbertson, 2011). In addition, it is known that the fluidization regimes described above have a strong influence on the pressure fluctuation (Fan, et al., 1981). The approximate relationship between pressure fluctuation and the state of fluidization provides vital information about the process taking place in a fluidized bed vessel. As a result, pressure fluctuation is widely used by researchers in order to understand the hydrodynamic behaviour of a fluidized bed system.

The measurement of the pressure fluctuation signal is simple to make even under severe, industrial conditions. Measurements are performed using a pressure transducer that is connected with a thin tube to a measurement point in the fluidized bed. This is typically a hole positioned in the wall of the vessel (Sasic, et al., 2007). In addition, the use of pressure fluctuation to monitor the fluid flow behaviour represents a simple, robust and non-intrusive method. However, the downfall of using pressure fluctuation signals is that the interpretation is not straightforward. The pressure fluctuation signals are complex and unsteady in nature and this makes techniques for the characterization of these signals essential.

Characterization of the time-series data of the pressure fluctuation signals in fluidized beds can be performed using several available methods. These methods can be classified into three predominant categories: time domain methods, frequency domain methods and state space methods (van Ommen, et al., 2011). Analysis in the time domain represents the simplest approach which relies on studying the amplitude of the pressure signals. This is commonly expressed as standard deviation or variance. Analysis in the time domain is used predominantly for the identification of the different fluidization regimes. However, the downfall with analysis in the time domain is that this technique represents an indirect measure of the dynamics of the bed and it is often unreliable. Analysis in the frequency domain is the commonly adopted technique. This is achieved by using the pressure fluctuation signals in conjunction with the Fast

Fourier Transform (FFT) to construct a power spectrum. The different fluidization regimes are thereafter identified by analysing the power spectra for a dominant frequency component. Analysis in the state space domain is still a relatively new development which requires a more complex calculation procedure. This method is convenient for non-linear analysis and can serve as a useful basis for future analysis.

1.2 Motivation and Research Aims

Literature presents several studies in which the pressure fluctuation signal is used to understand the dynamic behaviour of a fluidized bed. However, this phenomenon is not yet fully understood (Johnsson, et al., 2000; van Ommen, et al., 2011). As a result, the purpose of this research is to improve the understanding of the pressure fluctuations in gas-solid fluidized beds. The primary focus will be to indicate the dependence of the fluidizing behaviour on the various process variables i.e. bed characteristics and fluidizing medium characteristics through the application of the FFT and analysis in the frequency domain. The secondary aim will be to assess the use of the pressure fluctuation signal as a diagnostic tool to monitor fluidized bed hydrodynamics through identification of the various fluidization regimes. This will be achieved by measuring the pressure fluctuation in the fluidized bed with a pressure transmitter connected to a data acquisition system. The pressure signals would thereafter be used to generate a power spectrum. The dominant frequency from the power spectrum may then be used to identify the fluidization regime in which the bed is operating.

1.3 Research Contributions

Currently, the majority of literature focuses on observing the dominant frequency for a single fluidized bed vessel using different materials at various bed heights. Limited research has been conducted with different fluidized bed columns and the effect of the column diameter on the dominant frequency has not been addressed (Guevara, 2010). This research will address the applicability of the use of pressure fluctuations for identification of the different fluidization states as well as the influence of the material, column diameter and bed height on the dominant frequency as observed from the power spectra. Understanding the influence of each characteristic on the dynamics of a fluidized bed would play a vital role in improving the efficiency of a fluidized bed.

1.4 Contribution to Literature

Gyan, R., Ntunka, M. G., & Carsky, M. (2014). Time-series analysis of pressure fluctuations in gas-solid fluidized beds. *The South African Journal of Chemical Engineers*, 9-21.

1.5 Outline of Dissertation Structure

This dissertation is organised in seven chapters. Chapter 1 introduces the concepts of fluidization, its applications, fluidization regimes and the techniques available to distinguish between regimes. It outlines the motivation and objective of the research and includes the scope. In chapter 2, a review of the relevant principles and characteristics of fluidization is presented in the Literature Review. This includes fundamental fluidization phenomena concepts as well as a review of the methods for time-series analysis for gas-solid fluidized beds.

Chapter 3 presents a detailed description of the experimental set-up and measurement techniques employed in this work. A description of the data capture process and software interface is also included.

In Chapter 4, a description of the experimental procedures is presented. This consists of the selection and characterization of particles, the methods for the preparation and operation of the apparatus described in Chapter 3 as well as the techniques used to process the pressure fluctuation signals.

Chapter 5 consists of the results and discussion which includes a comprehensive description of the findings from this research. Comparison to literature data, analysis in the time domain as well as results for the analysis in the frequency domain is presented.

Chapter 6 is the overall conclusion of this dissertation, where the main findings are summarized. Potential improvements and further work is included in the Recommendations in Chapter 7.

2

CHAPTER 2

LITERATURE REVIEW

This chapter provides a review of the important principles and characteristics of fluidization that are necessary to understand the concepts used in this research project. An overview of concepts such as fluidized beds, fluidization regimes, minimum fluidization velocity, minimum bubbling velocity, minimum slugging velocity, transition velocity from the bubbling to turbulent regime, gas hold-up as well as the Geldart classification can be seen under Phenomena of Fluidization in Section 2.1. Section 2.2 reviews the methods for time-series analysis in order to understand the hydrodynamics of gas-solid fluidized beds from in-bed pressure measurements for the various fluidization regimes.

2.1 Phenomena of Fluidization

Fluidization represents a well-established fluid contacting operation. It is a process in which a bed of solid particles are transformed from the static solid-like state to a dynamic fluid-like state by contact with a fluidizing medium. The process occurs when the fluidizing medium, a stream of either a gas or liquid, is allowed to pass through vertically upward through the bed of solid particles (Kunii & Levenspiel, 1991).

2.1.1 Fluidized Beds

Fluidized Beds are vessels that contain solid particles through which a fluid, either a gas or liquid, flows. In addition, there exists a number of different types and geometries of fluidized beds. However, most of these vessels have the same key components which include: a plenum chamber, a distributor, a bed region as well as a freeboard region. The plenum chamber is the location where the fluidizing medium enters the bed. The fluid then passes through a distributor plate which ensures uniform distribution of the fluid at the base of the bed. Distributor types include: porous plates, straight-hole distributors, pipe grid distributor plates as well as bubble cap or nozzles distributors (Basu, 2006). The solid granular particles are positioned above the distributor plate in the bed region. The riser or freeboard region occurs above the bed chamber and this region comprises of solid particles that have been ejected from the fluidized bed. A schematic of a typical fluidized bed can be observed in Figure 2.1.

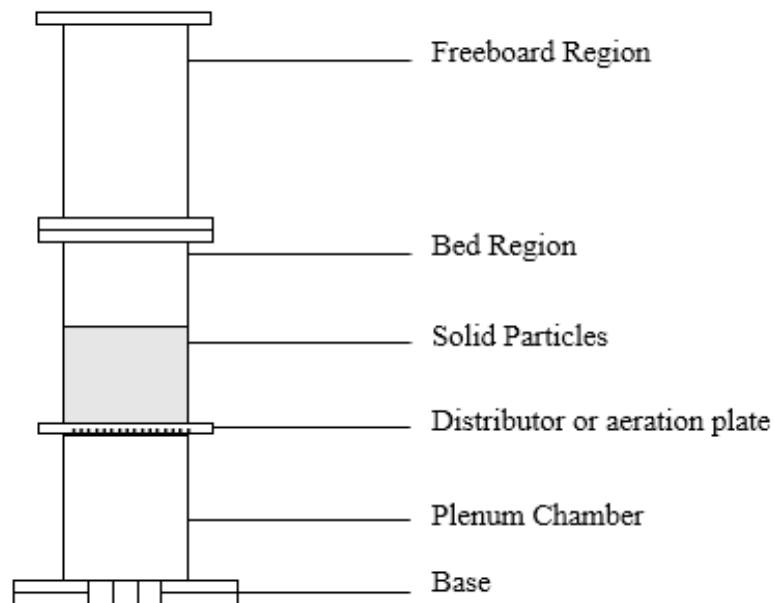


Figure 2.1 Schematic of a Fluidized Bed

The emergence of gas-solid fluidized beds as chemical reactors can largely be attributed to the numerous advantages which include: excellent heat and mass transfer due to intense particle mixing, relatively low pressure drop, uniform temperature distribution as well as a large effective surface contact as a result of the small particle size. In addition, gas-solid fluidized

beds are further applicable for both small as well as large scale operations and they allow continuous processing (Kunii & Levenspiel, 1991).

As mentioned before, there exists a number of different types and geometries of fluidized beds. The possible geometries include cylindrical, square or rectangular in cross-section while the most common types include the Stationary Fluidized Beds (SFB) and Circulating Fluidized Beds (CFB) (Crowe, 2006). SFB involves fluidized beds in which the solid particles tend to remain within the fluidized bed. On the other hand, CFB refers to fluidized beds in which the fluidizing medium is at a high velocity which is enough to suspend the solid particles such that most of the particles are transported with the fluid out of the bed. The entrained particles are generally re-circulated back into the fluidized bed via an external loop which is achieved by the use of a cyclone.

Currently, fluidization technologies can be seen in a broad range of commercial applications which can be divided into two predominant categories (Kumar, et al., 2014):

- Chemical operations which involve reactions of gases on solid catalysts as well as reactions of solids with gases.
- Physical operations which include processes such as absorption, heating, drying, mixing of fine powders as well as transportation.

Reactions of gases on solid catalyst particles represent a well-established chemical operation and a typical example of this type of reaction is Fluid Catalytic Cracking (FCC). In this gas catalytic reaction, the reaction occurs on the surface of the solid catalyst with the reactants and products typically existing in the same phase. FCC converts the low value heavy hydrocarbon components of crude oil into lighter and more valuable products which include gasoline and other olefinic gases (Sadeghbeigi, 2000). The reaction of solids with gases is typically seen in the processes of combustion and gasification.

In these processes, the reactants are either gases or a combination of both, gas and solid particles. Combustion is commonly employed in the process of power generation and this is achieved through the use of CFB's. In the combustion process, coal or biomass undergoes a series of chemical reactions, in an oxygen rich environment, in order to produce energy in the form of heat. Water and carbon dioxide are produced as by-products. Combustion in fluidized

beds can lead to an improvement in the overall combustion efficiency by approximately 96-98 % as well as a significant improvement in the rate of heat transfer by 60-80 times than that of conventional combustors (Abdullah, et al., 2003).

Gasification represents a process that is commonly achieved at high temperatures (700 - 900 °C) by contacting biomass with air, oxygen or steam in order to produce a gaseous fuel. The process consists of four steps: heating and drying, pyrolysis, gas-solid reactions and gas-phase reactions. Gasification in fluidized beds result in an efficiency of 70-90% and this is often used due to the fuel flexibility as well as ease of scale-up (Basu, 2006).

Physical operations typically involve processes in which no chemical reactions take place. These processes are employed due to the fluidized bed exhibiting a rapid drying rate, a high thermal efficiency as well as lower operating costs. Physical operations are often used in the chemical, food, ceramic as well as the pharmaceutical industries (Basu, 2006).

2.1.2 Fluidization Regimes

During the process of fluidization, when a fluid comes into contact with a bed of solid particles, the fluidized bed tends to behave differently. As the operating conditions such as the velocity as well as the gas and solid properties are varied, different contact regimes can be produced in the fluidized bed vessel. These regimes are established based on the superficial gas velocity and this can be seen in Figure 2.2.

For very low flow rates, the gas merely flows through the void spaces in the solid particles without disturbing the bed. The solid particles tend to vibrate in fixed positions with no visible change in the bed height. In addition, the particles are in direct contact with each other and are able to support each other's weight. The bed displays behavior similar to a porous medium and this regime is classified as the fixed bed regime (Figure 2.2 A).

With an increase in superficial gas velocity, the bed expands slightly with particles being suspended such that the drag force imparted by the upward moving fluid equals the weight of the solid particles. This represents the onset of fluidization and is referred to as the minimum fluidization regime (Figure 2.2 B). The system is now considered to be a fluidized bed as fluid-like properties are apparent. The velocity of the superficial gas is referred to as the minimum fluidization velocity, u_{mf} .

Depending on whether the fluidizing medium is a gas or liquid, the behavior of the fluidized bed tends to differ with increasing gas velocity following the minimum fluidization state. In the case of the fluid being a liquid, a smooth progressive bed expansion can be seen with an absence of large scale instabilities and heterogeneities such as the formation of bubbles. This is typical for systems where the liquid and solids have similar density properties. However, in gas-solid systems, the formation of bubbles tends to impose a great deal of instability in the system after the minimum fluidization regime. This regime is classified as the bubbling regime (Figure 2.2 C). The velocity of the superficial gas is now referred to as the minimum bubbling velocity, u_{mb} .

With a further increase in superficial gas velocity, the bubbles in the bubbling fluidized bed tend to coalesce and grow as they rise up the column. If the bed is sufficiently deep and the ratio of the height to the diameter of bed (aspect ratio) is high enough, the bubbles are able to coalesce and grow such that the bubble size is approximately 66 % of the column diameter (Yang, 2003). This is now known as the slugging regime (Figure 2.2 D).

If the particles are fluidized at a high enough gas flow rate such that the velocity exceeds the terminal or critical velocity, u_c of the particles, the upper bed surface tends to disappear. In addition, instead of bubbles being visible, a turbulent motion of solid particle clusters with voids of gas of different shapes and sizes can be seen. This regime is called the turbulent regime (Figure 2.2 E).

With a further increase in superficial gas velocity, the rate of particle entrainment with the gas increases and conditions of extreme turbulence can be observed. This eventually leads to the bed forming an entrained bed in which disperse, dilute or lean fluidized bed exists which effectively leads to a pneumatic transport of solids (Figure 2.2 F).

Depending on the application, most conventional fluidized bed systems function in the bubbling and/or turbulent fluidization regimes. However, operation in the pneumatic transport regime has expanded in recent years largely due to new developments in CFB reactors. The turbulent and pneumatic transport regimes are achieved at high gas velocities and operation in these regimes offer several advantages which include: more uniform solids distribution due to less gas bypass, improved gas-solids contact efficiency as well as a higher gas throughput (Crowe, 2006).

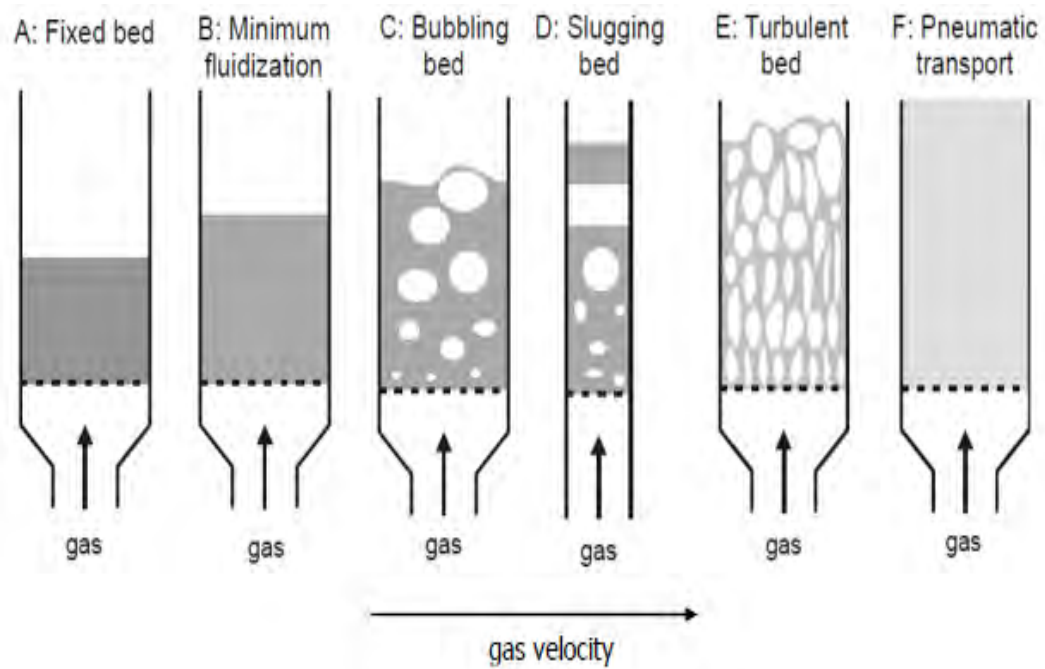


Figure 2.2 Schematic representation of the different fluidization regimes that occur with increasing superficial gas velocity in fluidized beds (Kunii & Levenspiel, 1991)

2.1.3 Minimum Fluidization Velocity

As mentioned before, the minimum fluidization velocity (u_{mf}) refers to the superficial fluid velocity at which the drag force exerted by the upward flowing fluid is equal to the apparent weight of the solid particles (Pell, 1990). The minimum fluidization velocity is a parameter that represents the point of incipient fluidization and this variable plays a critical role in the characterization of the hydrodynamics of a fluidized bed (Ramos, et al., 2002). The minimum fluidization velocity is dependent on several factors which include: particle properties (density, size and shape) as well as fluidizing medium properties (density and viscosity) (Liao, 2013). The minimum fluidization velocity can be obtained either experimentally or predicted through several correlations reported in literature.

The Ergun equation represents the first attempt at expressing the minimum fluidization velocity in a packed bed based on the pressure drop. Due to the condition of the pressure drop at the point of onset of fluidization being equal for a packed bed and a fluidized bed, the Ergun equation may be used to predict the minimum fluidization velocity at this point. The derivation for the minimum fluidization velocity from the Ergun equation is as follows:

$$\frac{(-\Delta P)}{H} = 150 \frac{\mu U (1 - \varepsilon)^2}{g \phi^2 d_p^2 \varepsilon^3} + 1.75 \frac{\rho_f U^2 (1 - \varepsilon)}{g \phi d_p \varepsilon^3} \quad (2-1)$$

where $-\Delta P$ is the frictional pressure drop across the bed, H refers to the bed height, μ denotes the fluid viscosity, ρ_f is the density of the fluid, ϕ and d_p refer to the sphericity and equivalent diameter of solid particles, U denotes the superficial gas velocity, ε is the voidage of the fixed bed and g is the gravitational acceleration constant.

During the process of fluidization, the pressure drop remains constant and does not depend on the superficial gas velocity. This can be described by Equation (2-2).

$$-\Delta P = g(1 - \varepsilon_{mf})(\rho_p - \rho_f)H \quad (2-2)$$

where ε_{mf} represents the voidage at minimum fluidization and ρ_p is the density of the solid particles.

Substitution of Equation (2-2) into the Ergun equation leads to a quadratic equation for the minimum fluidization velocity:

$$g(\rho_p - \rho_f) = 150 \frac{\mu U_{mf} (1 - \varepsilon_{mf})}{\phi^2 d_p^2 \varepsilon_{mf}^3} + 1.75 \frac{\rho_f U_{mf}^2}{\phi d_p \varepsilon_{mf}^3} \frac{1}{\varepsilon_{mf}^3} \quad (2-3)$$

In order to simplify Equation (2-3), two dimensionless numbers, the Archimedes Number (Ar) and Reynolds Number (Re), have been introduced. The Archimedes Number (Ar) is defined as the ratio of the gravitational forces to the viscous forces:

$$Ar = \frac{d_p^3 \rho_f (\rho_p - \rho_f) g}{\mu^2} \quad (2-4)$$

The Reynolds Number (Re) is defined as the ratio of inertial forces to viscous forces at the onset of fluidization:

$$Re_{mf} = \frac{d_p U_{mf} \rho_f}{\mu} \quad (2-5)$$

By substituting Equations (2-4) and (2-5) into the Ergun equation at incipient fluidization, Equation (2-3), the following equation is obtained:

$$Ar = 150 \frac{(1 - \varepsilon_{mf})}{\varphi^2 \varepsilon_{mf}^3} Re_{mf} + 1.75 \frac{1}{\varphi \varepsilon_{mf}^3} Re_{mf}^2 \quad (2-6)$$

However, Equation (2-6) requires values for sphericity, φ and voidage, ε_{mf} at minimum fluidization. Several researchers including Wen and Yu (1966), Kunii and Levenspiel (1991) and Benyahia and O'Neill (2005) have focussed on the relationship between voidage and sphericity. It was found that an increase in sphericity results in a decrease in the voidage. However, the problem arises as the relationship between the two parameters could not be distinctly identified with a single function as each value of sphericity corresponds to a number of values for voidage. This effectively led to a modification of the Ergun equation with the objective of replacing the coefficients $\frac{(1-\varepsilon_{mf})}{\varphi^2 \varepsilon_{mf}^3}$ and $\frac{1}{\varphi \varepsilon_{mf}^3}$ from Equation (2-6) with two constants, C_1 and C_2 . The modified Ergun equation then simplifies to:

$$Ar = C_1 \cdot Re_{mf} + C_2 \cdot Re_{mf}^2 \quad (2-7)$$

The minimum fluidization velocity can then be determined by re-arranging and solving the quadratic equation, Equation (2-7). Several researchers have developed values for the constants, C_1 and C_2 and this then allowed for the prediction of the minimum fluidization velocity. The most common correlation for solving for the minimum fluidization velocity is by the equation proposed by Wen and Yu (1966) which can be seen by Equation (2-8) below.

$$Re_{mf} = [(33.7)^2 + 0.0408Ar]^{0.5} - 33.7 \quad (2-8)$$

However, the predictive model is only applicable for limited conditions and involves a significant error of approximately 30 to 40 % (Liao, 2013). Furthermore, the relationships of $C_1 = \frac{(1-\varepsilon_{mf})}{\varphi^2 \varepsilon_{mf}^3}$ and $C_2 = \frac{1}{\varphi \varepsilon_{mf}^3}$ are only applicable for certain values of φ and ε_{mf} . Predictions for the minimum fluidization velocity from other researchers, based on the same method and different values for the constants, is indicated in Table 2.1.

Table 2.1 Correlations for predicting the minimum fluidization velocity

Author	Correlation
(Bourgeois & Grenier, 1968)	$Re_{mf} = [(25.46)^2 + 0.0382Ar]^{0.5} - 25.46$
(Hilal, et al., 2001)	$Re_{mf} = [(13.07)^2 + 0.0263Ar]^{0.5} - 13.07$
(Reina, et al., 2000)	$Re_{mf} = [(48)^2 + 0.045Ar]^{0.5} - 48$
(Chitester, et al., 1984)	$Re_{mf} = [(28.7)^2 + 0.0494Ar]^{0.5} - 28.7$

2.1.4 Minimum Bubbling Velocity

An increase in the superficial gas velocity above a value defined as the minimum bubbling velocity, u_{mb} leads to the appearance of bubbles in the fluidized bed. For Group B and D particles, bubbles appear in the bed as soon as the minimum fluidization velocity is passed. However, for Group A particles, the bed does not bubble immediately after exceeding the minimum fluidization velocity. Instead, a noticeable bed expansion is observed (Basu, 2006). For Group A particles, the minimum bubbling velocity can be determined by Equation (2-9).

$$u_{mb} = 2.07 \exp(0.716F)d_p \left[\frac{\rho_f^{0.06}}{\mu^{0.347}} \right] \quad (2-9)$$

where F is the mass fraction of solid particles less than 45 μm and d_p is the mean surface-volume diameter of solid particles.

2.1.5 Maximum Bubble Size

Bubbles represent gas voids that comprise of very little or no solid particles. As a result of the buoyancy force, the bubbles tend to rise through the emulsion phase and in the process, by-pass the solid particles. The bubbles are capable of growing to a maximum size after which they collapse. The bubble size is influenced by three factors: the particle size, excess gas velocity and the height above the distributor. According to (Grace, 1982), the maximum stable bubble size is obtained by Equation (2-10).

$$D_{bmax} = \frac{2(u_t^*)^2}{g} \quad (2-10)$$

where u_t^* represents the terminal velocity of solid particles having a diameter 2.7 times that of the average size of solid particles from the bed.

2.1.6 Minimum Slugging Velocity

As described before, the phenomenon of slugging occurs when the size of the bubbles approximate to 66 % of the diameter of the bed (Yang, 2003). The formation of slugs is typical for fluidized beds that are characterized as narrow and deep (high aspect ratio). According to (Yang, 1976), the criteria for slug formation in a fluidized bed is given by:

$$\frac{u_t^2}{gD_c} \geq 0.123 \quad (2-11)$$

where u_t is the terminal velocity of the average sized solid particle and D_c represents the column diameter.

A well-known correlation used to determine the minimum slugging velocity, u_{ms} can be observed below (Stewart & Davidson, 1967):

$$u_{ms} = u_{mf} + 0.07(gD_c)^{0.5} \quad (2-12)$$

Predicting the minimum slugging velocity has been studied by several other researchers including Singh & Roy (2008) and Baeyens & Geldart (1974). These results can be seen in Table 2.2.

Table 2.2 Correlations for predicting the minimum slugging velocity

Author	Correlation
(Baeyens & Geldart, 1974)	$u_{ms} = u_{mf} + 0.07(gD_c)^{0.5} + 0.16(1.3D_c^{0.175} - H)^2$
(Singh & Roy, 2008)	$u_{ms} = 0.136 \left(\frac{d_p}{D_c}\right)^{0.6324} \left(\frac{D_c}{H}\right)^{0.044} \left(\frac{\rho_p}{\rho_f}\right)^{0.6559}$

2.1.7 Transition Velocity from Bubbling to Turbulent Regime

An increase in the superficial gas velocity above the minimum bubbling velocity results in a noticeable bed expansion being observed. A further increase in the gas velocity may eventually indicate a change in the appearance of the bed expansion which would represent a transition into the turbulent regime. According to Nakajima et al. (1991), the transition from the bubbling to the turbulent regime may be due to an increase in the bubble fraction, an expansion of the emulsion phase and/or thinning of the emulsion walls splitting the bubbles in the bed. Rapid coalescence and breakup of the bubbles in the turbulent regime effectively leads to rapid fluctuations in the pressure drop across the fluidized bed (Basu, 2006). The transition velocity from the bubbling to the turbulent regime can be determined either experimentally or theoretically through correlations.

The experimental technique involves graphically depicting the relationship between the standard deviation of pressure fluctuations and the superficial gas velocity. This can be seen in Figure 2.3 below.

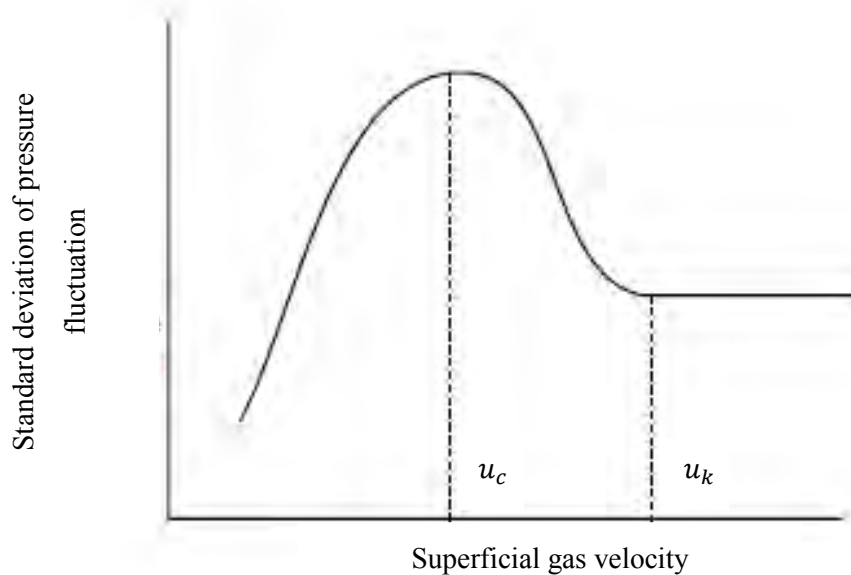


Figure 2.3 Amplitude of pressure fluctuation across the fluidized bed with increasing superficial gas velocity (Basu, 2006)

The trend that is observed is that an increase in superficial gas velocity leads to an increase in the standard deviation of pressure fluctuation, until a peak velocity, u_c is obtained. A further increase in gas velocity then results in a decrease in the standard deviation of pressure fluctuation until a steady value, u_k is achieved. The transition from the bubbling to the turbulent regime initiates at the critical velocity, u_c and is completed at the terminal velocity, u_k .

Basu (2006) found that there are several existing correlations available for predicting the transition from the bubbling to the turbulent regime. However, the problem arises as literature lacks a well-established correlation that is capable of predicting the transition with reasonable accuracy. In addition, most correlations predict the transition independent to the height of the fluidized bed and the diameter of the column. This could have a significant impact as the fluidizing behaviour is strongly influenced by these two factors. The lack of available data for large diameter fluidized bed vessels is a further barrier which prevents defining the actual extent of the effect of the column diameter on the fluidization regime.

For small diameter fluidized bed vessels with the contribution of $\rho_p d_p$ occurring in the range of 0.05 to 0.07 kg/m^2 , the onset and termination velocities for the transition can be predicted by Equations (2-13) and (2-14).

$$u_c = 3.0 \sqrt{\rho_p d_p} - 0.17 \quad (2-13)$$

$$u_k = 7.0 \sqrt{\rho_p d_p} - 0.77 \quad (2-14)$$

Several other correlations are available to predict the transition from the bubbling to the turbulent regime and this can be observed in Table 2.3.

Table 2.3 Correlations for predicting the transition velocity from the bubbling to turbulent regime

Author	Equation
(Bi, et al., 1995)	$Re_c = 0.565 Ar^{0.461}$
(Cai, et al., 1989)	$u_c = (gd_p)^{0.5} \left[\frac{0.211}{D_c^{0.27}} + \frac{2.42 \times 10^{-3}}{D_c^{1.27}} \right] \left[\frac{D_c(\rho_p - \rho_g)}{d_p \rho_g} \right]^{0.27}$

$$u_c = (gd_p)^{0.5} \left[\frac{(KD_f)(\rho_p - \rho_g)}{d_p \rho_g} \right]^{0.27}$$

(Jin, et al., 1986)

$$KD_f = 0.00367 \text{ (for free bed)}$$

$$Re_c = 0.7 Ar^{0.485}$$

(Lee & Kim, 1990)

$$Re_c = 0.633 Ar^{0.467}$$

(Nakajima, et al., 1991)

2.1.8 Gas Hold-up

In order to understand the behaviour inside a fluidized bed, it is essential to be able to measure and interpret the hydrodynamic factors of the bed. Gas hold-up represents a dimensionless parameter and is a critical variable for the characterization of fluidization quality, homogeneous mixing and process efficiency in a fluidized bed system (Guevara, 2010). Gas hold-up is defined as the volume fraction of the gas phase (occupied by gas bubbles) that exists within the bed material.

2.1.9 Geldart Powder Classification

The transition between the fluidization regimes, and at times their existence is strongly influenced by the properties of the solids in the bed (Wiens, 2010). These properties include the particle density and diameter and this dictates the fluidization behaviour. Particles having a low density and small diameter are more easily fluidized than bigger and heavier particles, as the gravity acting on the latter is much larger. In addition, the inter-particle forces on the smaller particles are much more important than the same forces on the bigger particles. This causes the smaller particles to display a certain velocity range of homogenous expansion. A cohesive bed is seen when the particles are fine or sticky. In this instance, the bed will tend to produce channels through which the aeration gas will escape rather than being dispersed through the spaces supporting the solid particles. In the other extreme, if the particles have a high density and large diameter the bed will not fluidize well either. Instead, the bed would tend to exhibit turbulent conditions and would form a spout.

Under conditions using air as the fluidizing medium at atmospheric pressure, the fluidization behaviour of solid particles can be grouped into four categories. This is referred to as the Geldart Classification and is dependent on the particle diameter and bed density (Geldart, 1986). The fluidization behaviour for these four particle groups is represented in Figure 2.4.

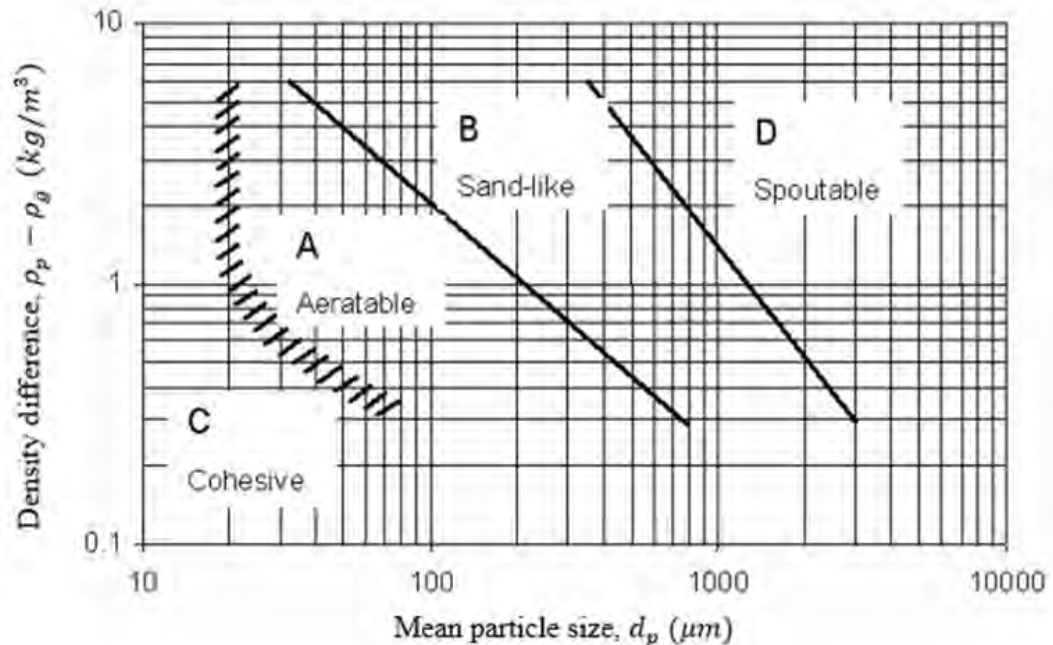


Figure 2.4 Geldart's Classification of Powders (Geldart, 1973)

Group A: Particles are referred to as 'aeratable'. Most particles from this group exist as powders which have a small mean particle size ($30 \mu\text{m} < d_p < 100 \mu\text{m}$) and/or low particle density ($< \sim 1400 \text{ kg/m}^3$). A typical example of a particle classified from this group is fluid cracking catalysts. These powders tend to fluidize easily, with uniform fluidization taking place at low superficial gas velocities without the formation of bubbles. With an increase in superficial gas velocity above the minimum fluidization velocity (U_{mf}), Group A powders tend to display a considerable bed expansion. This occurs until the minimum bubbling velocity (U_{mb}) is reached at which bubbles start to form in the bed. This behaviour is as a result of the cohesiveness of the powders. The bubbles formed in these beds tend to split and re-coalesce frequently which results in a restricted bubble size.

- Group B: Material of this group is commonly called ‘sand-like’ particles. The particles typically have a mean size of 100 to 1000 μm with a density in the range of 1000 to 4000 kg/m^3 . Group B particles possess negligible inter-particle forces and once the superficial gas velocity exceeds the minimum fluidization velocity, bubbles are observed in the bed. Coalescence represents the main bubble-bubble interaction and the bubbles can grow to a large size with no known maximum bubble size. Group B particles tend to fluidize well with a relatively small expansion in bed height. Typical examples of particles classified from this group include glass beads (ballotini) and sand particles.
- Group C: Particles of this group are characterised as fine, cohesive powders that are extremely difficult to fluidize under normal operating conditions. Material classified as Group C typically has a particle diameter of less than 30 μm . The particles tend to lift the bed as a plug or often form channels that extend from the distributor to the bed surface. This is due to the inter-particle forces being stronger than the forces that are exerted on the particles by the fluidizing gas. Fluidization using material classified as Group C can generally be made possible or even improved by making use of mechanical stirrers or vibrators that effectively break up the stable channels in the bed. Particles classified as Group C typically include flour, fly ash and cement.
- Group D: Particles are commonly referred to as ‘spoutable’. The particles generally have a large mean particle size ($d_p > 1000 \mu\text{m}$) and/or are very dense. This results in Group D particles exhibiting very poor bed mixing properties. Bubbling generally does not commence until approximately 5 cm above the distributor where the bubbles then tend to coalesce rapidly and flow to a large size thereafter. The bubbles rise more slowly than the fluidizing gas which percolates through the particles in the bed. This leads to the fluidizing gas flowing to the base of the bubble and out of the top which creates a situation of gas exchange and bypassing which is very different from that detected with Group A and B particles. Unlike the particles classified as Group B, with increasing superficial gas velocity, a jet can be created in the bed and the particles can then be carried out with the jet in a spouting motion. Materials classified as Group D include coffee beans, wheat, lead shot as well as some roasting metal ores.

2.2 Time-series Analysis Techniques using in-bed Pressure Measurements

Pressure is often the variable used to understand the hydrodynamic behaviour of gas-solid fluidized beds. The use of pressure signals possesses several advantages: it can be readily measured even under extreme industrial conditions; it is robust, cost effective and non-intrusive which effectively avoids disturbance of the flow around the measurement point (van Ommen, et al., 2011). However, the problem with pressure measurement arises in the interpretation of the pressure fluctuation signals. The analysis of the pressure signals is not straight forward and as a result, there has been a steady increase in studying and understanding the pressure fluctuations in gas-solid fluidized beds.

Van Ommen et al. (2011) did a follow-up and update on the research performed by Johnsson et al. (2000). In the work of van Ommen et al. (2011), a review of the methods for time-series analysis for the characterization of the hydrodynamics of gas-solid fluidized beds, using in-bed pressure measurements, was performed. In addition, van Ommen et al. (2011) used the same pressure time-series as Johnsson et al. (2000) and proposed additional methods for time-series analysis.

In the work of Sasic et al. (2007), a review of the techniques for understanding the hydrodynamic behaviour of gas-solid fluidized beds through the use of pressure fluctuation signals, was conducted. Sasic et al. (2007) further investigated the use of various models and their applicability in understanding the fluidization behaviour. The purpose was to identify which techniques could link the pressure-time series to the physical phenomena observed in gas-solid fluidized beds.

Literature indicates that the analysis of pressure fluctuation signals from time-series can be performed using several techniques. These analysis techniques can be classified into three predominant categories: time domain methods, frequency domain (spectral analysis) methods and state space (chaos analysis) methods (van Ommen, et al., 2011).

2.2.1 Time Domain Analysis

2.2.1.1 Standard Deviation or Variance

Analysis in the time domain represents the simplest approach. A widely adopted time domain analysis technique is through the standard deviation or variance (viz. second order statistical moment) which is obtained from the amplitude of pressure fluctuation signals. This technique involves investigating the relationship between the standard deviation, which represents an alternative measure of the amplitude of pressure fluctuation signals, and the superficial gas velocity. The typical behaviour of the relationship between these two variables can be seen in Figure 2.3 under Section 2.1.7.

A change in trend of the standard deviation helps to identify a change in fluidization regime (van Ommen, et al., 2011). According to Sobrino et al. (2008), the change in standard deviation can be used to obtain the minimum fluidization velocity or as an on-line mechanism to identify de-fluidization in industrial fluidized bed vessels. In addition, the standard deviation technique can be used to demarcate the transition from the bubbling to the turbulent regime (Bi, et al., 2000). The transition begins at the critical velocity, u_c and ends at the terminal velocity, u_k .

In the work of Andreux et al. (2005), it was found that the maximum in standard deviation might over predict the superficial gas velocity at which the transition from the bubbling to turbulent regime actually occurs. In addition, the strong dependence of the standard deviation of the pressure signals on the superficial gas velocity creates a doubt as to whether this technique would be applicable in industry, where the gas velocity is rarely constant.

2.2.1.2 Additional Time Domain Methods

In addition to the standard deviation technique, there exist several other less popular methods for analysis of pressure fluctuation signals in the time domain. These methods include: the average cycle time as well as the use of autoregressive (AR) models (van Ommen, et al., 2011).

The average cycle time can be calculated easily by observing the number of times a pressure signal passes its average value. This method functions well for data obtained from models while poor results are displayed for experimental data points. The reason behind this is that average cycle time has a strong sensitivity to noise and high frequency pressure fluctuations lead to the

signal repeatedly crossing the average, as in the case for experimental data (Briens & Briens, 2002). Like the standard deviation technique, a change in the pattern of the average cycle time represents a change in fluidization regime.

A major downfall of the standard deviation and average cycle time techniques is that these methods represent an indirect measure of the hydrodynamic behaviour of the bed. Furthermore since amplitude is the only factor considered, this can be misleading. In the work of Johnsson et al. (2000), it was found that a major drawback of using the amplitude of the pressure fluctuation to classify the different regimes lies in the fact that no information is provided on the time-scale. In addition, the amplitude of the pressure signals is dependent on three factors: the flow dynamics, distribution of particles in the fluidized bed and the changes in the average suspension density. The relationship between these three factors is not yet known and as a result, it makes it difficult to draw definite conclusions about the hydrodynamic behaviour of the fluidized bed.

The AR model technique involves developing a model for the time-series of stochastic pressure fluctuations in a fluidized bed system. The pressure fluctuation signal is assumed to be an output of a linear time-invariant system which is typically moulded by a forcing function which represents the fluidization behaviour (bubble formation at the distributor as well bubble eruption at the bed surface). The aim is to prove that there exists a clear relationship between mechanical systems of a particular degree (mechanical oscillators) and the fluidized bed behaviour. The problem arises in that it is difficult to understand the hydrodynamic behaviour of a fluidized bed which effectively results in a lack of understanding of the stochastic nature of the input signal which generates the pressure signal. Further work is required of this technique, for the true nature to be appreciated.

2.2.2 Frequency Domain Analysis

The analysis of fluctuations in pressure signals in the frequency domain through Fourier analysis is commonly employed by researchers in order to identify and monitor the various fluidization regimes. Power spectral density analysis comprises the investigation of the changes in power spectra as a result of the changes in the dynamic behaviour of a system, which is used predominantly to provide a quantitative description of the fluidization regimes in a fluidized bed system. This is done by evaluating the narrowing and broadening of the power spectra as well as observing the dominant frequency component present in the spectra. According to Johnsson et

al. (2000), the predominant fluidized bed frequency of pressure fluctuation is generally below 10 Hz. As a result, sampling with a frequency of 20 Hz to obtain dominant frequencies from the Fast Fourier Transform (FFT), is frequently considered sufficient.

The FFT represents a mathematical tool that is used to determine the power spectral density analysis by converting a signal which is a function of time into a signal which is a function of frequency. The FFT functions by decomposing an N point time domain signal into N time domain signals each composed of a single point. The N frequency spectra corresponding to the N time domain signals are thereafter calculated and the N spectra are combined into a single frequency spectrum (Alberto, et al., 2004).

The Fourier Transform of a function x_t in the finite time interval of 0 to T is given by:

$$X(f, T) = \int_0^T x(t) e^{-j2\pi ft} dt \quad (2-15)$$

The time of sampling is defined as $t_n = n\Delta t$ which relies on the assumption that x_t is sampled at N equally spaced points at a distance of Δt . It is generally suitable to begin with $n = 0$ and this effectively leads to:

$$x_n = x(n\Delta t) \quad n = 0, 1, 2, 3 \dots, N - 1 \quad (2-16)$$

For arbitrary values of frequency, f , the discrete version of Equation (2-15) is defined as:

$$X(f, T) = \Delta t \sum_{n=0}^{N-1} x_n \exp[-j2\pi fn\Delta t] \quad (2-17)$$

The discrete frequency values commonly employed in the calculation of $X(f, t)$ are given by:

$$f_k = \frac{k}{T} = \frac{k}{N\Delta t} \quad k = 0, 1, 2, 3 \dots, N - 1 \quad (2-18)$$

The transformed values supply the Fourier components that are defined for Equation (2-19). This occurs at the frequencies that are obtained from Equation (2-18).

$$X_k = \frac{X(f_k)}{\Delta t} = \sum_{n=0}^{N-1} x_n \exp \left[-j \frac{2\pi kn}{N} \right] \quad k = 0, 1, 2, 3 \dots, N-1 \quad (2-19)$$

The FFT algorithm is able to calculate the amounts of X_k that will appear to larger or smaller amplitude, in agreement with the characteristic of the system that is analysed (Alberto, et al., 2004). However, the results obtained from Equation (2-19) can only be represented up to $k = \frac{N}{2}$ as a consequence of the Nyquist frequency which occurs at this point.

An application of the FFT technique in literature can be seen in Figure 2.5 below. This method functions by displaying the graphical relationship of the amplitude of pressure fluctuations, as obtained from the FFT, against the dominant frequency component.

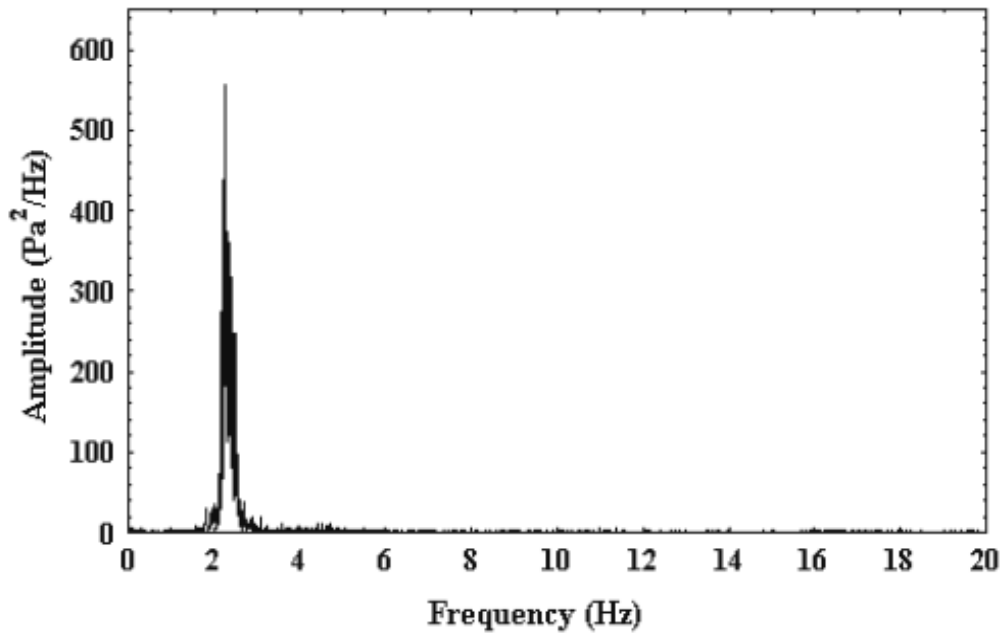


Figure 2.5 Power Spectrum of the single bubbling regime for sand particles with a 727 μm diameter, bed height 11 cm and column I.D 11.15 cm; Alberto, et al. (2004)

The benefit of using the FFT to understand the dynamics of a fluidized bed is that this technique is a more accurate and improved representation than the amplitude analysis method from the time domain. Johnsson et al. (1995) studied the hydrodynamic behaviour of fluidized bed vessels comprising of different geometries. It was found that in vessels in which a change in fluidization regime occurred, there was a pronounced shift in the dominant frequency component. Moreover, for no change in fluidization regime, there was a minimum change in the

peak frequency during an increase in superficial gas velocity. In addition, all fluidized bed vessels displayed a maximum in the amplitude of the pressure fluctuation signals. Johnsson et al. (1995) concluded that the maximum in amplitude was mainly due to the redistribution of the bed particles from the freeboard side to the cyclone side hence amplitude analysis needs to be exercised with caution.

The downfall of analysis in the frequency domain through the FFT is that the interpretation of the power spectra can be subjective. Due to different observation methods, different researchers may have varying opinions on the dominant frequency component. In addition, the shape of the power spectra is dependent on a number of factors. These include the number of samples, the sampling frequency together with the number of spectra that is averaged. In order to improve on this technique, for a fixed number of samples, a trade-off has been developed between the statistical significance and the frequency resolution of the power spectrum.

2.2.3 State Space Domain

Analysis of the pressure fluctuation signal in the state space domain is used to complement the work performed in the previously mentioned methods i.e. time domain and frequency domain. The application of analysis in the state space domain has increased since the latter 1990s and this approach is best suited for non-linear data analysis (van Ommen, et al., 2011). The key reason for the rise in this analysis technique is largely due to the manner in which this method handles the hydrodynamics of the fluidized bed. Instead of focussing on the movement of all individual solid particles in a fluidized bed, this technique places emphasis on the temporal spatial patterns that are generated within the bed by projecting all the variables influencing the system into a multidimensional space, known as the state space. The collection of the various states of the fluidized bed system is referred to as the ‘attractor’ which represents the dynamic evolution of the system (Johnsson, et al., 2000). Techniques for analysis in the state space domain rely on the formulation of the attractor and the fact that all the variables governing the system exist in a single measured parameter, the pressure fluctuation.

Analysis of pressure time-series data to characterize the attractor is widely expressed through the correlation dimension and Kolmogorov entropy and/or the Lyapunov exponents. The correlation dimension is a characteristic which indicates the degrees of freedom of the system while the latter two characteristics represent a measure of the predictability of the system as well as the sensitivity to the initial conditions (Johnsson, et al., 2000). The Kolmogorov entropy

relies on the idea of following two points situated on the attractor that are closer than a chosen (small) length scale. This occurs until the distance between the points has grown above that of the chosen length scale, with the time lapse being measured. The shorter the time required for the initially nearby points to diverge, the greater the Kolmogorov entropy (van Ommen, et al., 2011). Linear systems have been proved to be predictable with Kolmogorov entropy of zero while random systems are unpredictable with infinite Kolmogorov entropy.

In the work of van der Schaaf et al. (2004), it was found that there exists a directly proportional relationship between the power spectral density and the Kolmogorov entropy. This was also investigated by Zhao et al. (2001) and supported by several researchers including Villa Briongos et al. (2006, 2007) and van Ommen et al. (2011). The proportional relationship between the Kolmogorov entropy and dominant frequency from the power spectra was confirmed for the bubbling, slugging and circulating fluidized bed systems. Generally, analysis in the frequency domain is preferred over the correlation dimension and Kolmogorov entropy. The main reason behind this is due to an easier calculation procedure as well as the ease at which analysis in the frequency domain can be associated with the physical phenomena occurring in the fluidized bed system. Moreover, the dominant frequency as obtained from the power spectra does not depend on calculation parameters whereas the Kolmogorov entropy and correlation dimension do.

The Lyapunov exponents represent the local rate of convergence or divergence between two adjacent points on the attractor. For a chaotic system, at least one of the Lyapunov exponents must be positive which quantifies the 'sensitivity to initial conditions' (Scala, 2013). A major downfall of calculating the Lyapunov exponents from experimental data is the formulation of false results when the dimension of the reconstructed state space is greater than the dimension of the actual state space. In addition, the benefit of using this characteristic is questionable with more readily accessible alternatives being available. In the work of van Ommen et al. (2011), it was found that determining the Lyapunov exponents provide little added value as compared to the Kolmogorov entropy. This was further supported by Scale (2013), Guo et al. (2003) and van der Stappen (1996). It is for this reason that the method of using Lyapunov exponents is seldom used in order to understand the dynamics of a fluidized bed system (Scala, 2013).

3

CHAPTER 3

EQUIPMENT DESCRIPTION

Chapter 3 aims to describe in detail the experimental apparatus used in this work to obtain pressure fluctuation data in order to understand the hydrodynamic behaviour of gas-solid fluidized beds. The primary experimental aspects covered in this chapter include:

1. Gas-solid fluidized bed apparatus.
2. Flow measurement and control.
3. Pressure measurement and control.
4. Data capture and description of the software interface.

3.1 The Gas-Solid Fluidized Bed Apparatus

The gas-solid fluidized bed apparatus employed in this work has been successfully used by several researchers for many years. These include van Ommen et al. (2010), Johnsson et al. (2000), Alberto et al. (2004) and Fan et al. (1981). The key components for the experimental apparatus remain the same for most researchers. However, slight differences occur in the choice of pressure transmitter as well as some fluidized bed columns having a cyclone present to redistribute entrained particles. In this work, a high frequency pressure transmitter was employed and a cyclone was not required as the fluidized bed column was sufficiently tall.

The gas-solid fluidized bed system comprised of the following:

- Three cylindrical fluidized bed vessels constructed with Perspex.
 - Fluidized bed 1 (Internal diameter of 5 cm and height of 200 cm).
 - Fluidized bed 2 (Internal diameter of 11 cm and height of 153 cm).
 - Fluidized bed 3 (Internal diameter of 29 cm and height of 507.5 cm).
- Air distributor.
- Three rotameters.
- A single air compressor.
- DC power supply.
- WIKA model P30 pressure transmitter.
- WIKA model 2500 digital pressure gauge.
- Data acquisition system.

Figure 3.1 shows the setup of the experimental equipment. The key features included the rotameters for flow measurement and control, the three fluidized bed columns and the WIKA model P30 pressure transmitter.

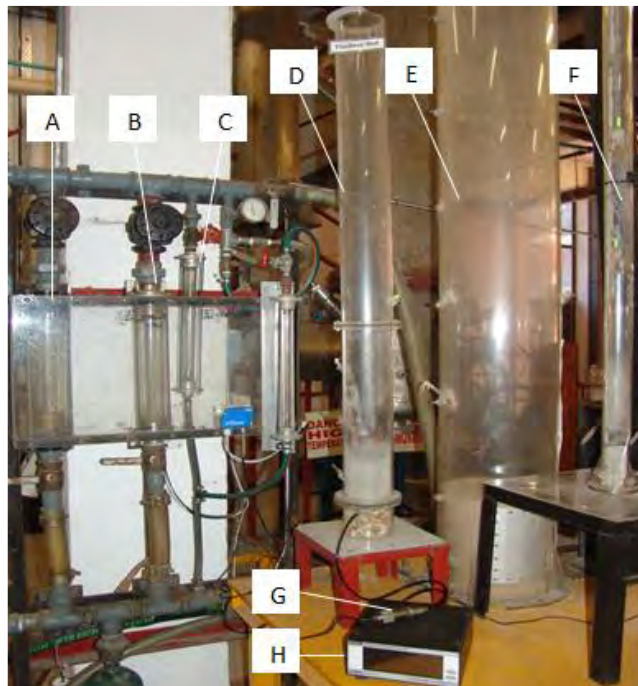


Figure 3.1 Experimental Setup of the Fluidized Bed System

A – Rotameter 1; **B** – Rotameter 2; **C** – Rotameter 3; **D** – Fluidized Bed 2 (I.D 11 cm; total height 153 cm); **E** – Fluidized Bed 3 (I.D 29 cm; total height 507.5 cm); **F** – Fluidized Bed 1 (I.D 5 cm; total height 200 cm); **G** – WIKA model P30 pressure transmitter; **H** – WIKA model 2500 digital pressure gauge

A schematic of the experimental set-up can be seen in Figure 3.2 below. The schematic includes a single fluidized bed column. Although three vessels of different sizes were present, the schematic is an adequate representation of the experimental set-up as only a single column was used at a time.

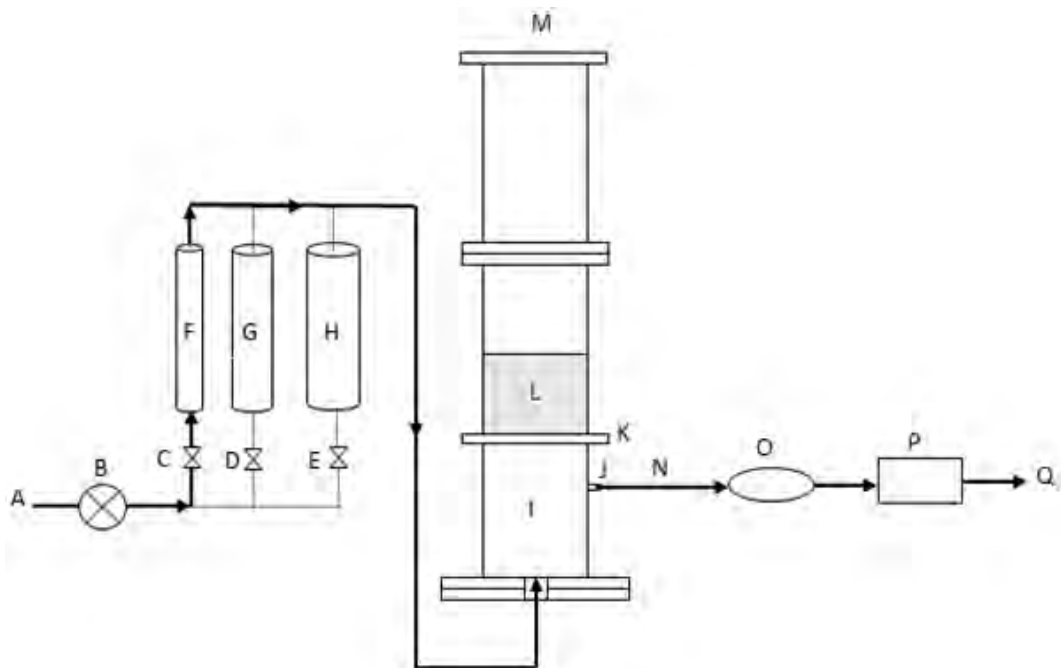


Figure 3.2 Schematic representation of the experimental gas-solid fluidized bed apparatus

A – Air inlet from compressor; **B** – Gate valve; **C, D, E** – Stop valves; **F, G, H** – rotameters; **I** – Plenum chamber; **J** – Pressure measurement point; **K** – Air distributor; **L** – Solid particles; **M** – Fluidized bed column; **N** – Pressure probe; **O** – WIKA model P30 pressure transmitter; **P** – Data acquisition board; **Q** – Pressure signal sent to computer system

3.1.1 Fluidized Bed Column

The fluidized bed column represents a vessel in which the fluidization of solid particles occurs upon contact with a fluidizing medium. In this dissertation, three fluidized bed columns, with

size and geometry described above, were employed. Each column was used independently to each other with varying material and particle bed height. As mentioned above, all three columns were cylindrical in geometry and fabricated with Perspex which was highly transparent. This allowed for the visual observation of the fluidization state as well as visualization of the movement of the solid particles in the bed. The main components of the fluidized bed column include: the bed region, the distributor plate and the plenum chamber.

3.1.2 The Bed Region

The bed region represents the segment of the fluidized bed column in which the solid particles are contained. In this research, three different materials (sand, plastic beads and FCC) were placed in the bed region of each fluidization column at various bed heights. The movement of the solid particles and fluidization behaviour was thereafter analysed.

3.1.3 The Distributor Plate

The aeration plate or distributor plate plays a critical role in the fluidization behaviour of a gas-solid fluidized bed. The function of the distributor plate is to ensure uniform distribution of the fluidizing medium (air) into the bed region of the fluidized bed column. All three fluidized bed columns employed a perforated plate as the distributor type. This was in agreement with the work of Geldart and Baeyens (1985), Kunii and Levenspiel (1991) and Alberto et al. (2004) which comprised of holes of 1 mm in diameter and a total free area of 2.5 %. The position of the perforated distributor plate for each fluidization column was as follows:

- Fluidized bed 1 – 15 cm above column base.
- Fluidized bed 2 – 11 cm above column base.
- Fluidized bed 3 – 9 cm above column base.

3.1.4 The Plenum Chamber

The plenum chamber represents the part of the fluidized bed that is positioned directly below the distributor plate. The packing material for the fluidized bed is contained in this region as well the pressure measurement points in all three fluidization vessels. The packing material allowed for better distribution of the air in the fluidized bed. The fluidizing medium, which was

air, was allowed to enter the plenum chamber at the bottom via the main air supply system. The air supply system consisted of a compressor and three rotameters which allowed for the control of the air flow rate into the fluidized bed column.

3.1.5 Flow measurement and Control

Largely due to ease of availability, the fluidizing gas was compressed air obtained from the buildings air supply system. A gate valve was present to control the flow of air into the fluidized bed system. The superficial gas velocity of the air entering the plenum chamber was then determined with one of three rotameters positioned after the gate valve. The three rotameters consisted of different sizes and the selection of which rotameter to apply was strongly influenced by the choice of the fluidized bed column. The rotameters had already been calibrated at room temperature and 140 kPa. The calibration equations to obtain the flow rate in $\frac{L}{min}$ were given as follows:

$$\text{Rotameter 1 (small size)} = 5.4 R + 10.83 \quad (3-1)$$

$$\text{Rotameter 2 (medium size)} = 37.4 R + 94.6 \quad (3-2)$$

$$\text{Rotameter 3 (large size)} = 98.0 R + 285.3 \quad (3-3)$$

where R represents the experimental rotameter reading.

3.1.6 Pressure measurement and Control

The pressure in the fluidized bed was measured in the plenum chamber through the use of a WIKA model P30 pressure transmitter. This transmitter was capable of operating at significantly high frequencies while being able to measure pressure fluctuation signals in the range of 0 to 160 kPa. Polyethylene tubes with an internal diameter of 3 mm were used to connect the pressure transmitter to the measurement point on the plenum chamber in the fluidized bed column. The length of each segment of the polyethylene tubes was shorter than 60 cm as recommended by van Ommen et al. (2000) who studied the response characteristics of probe-transducer systems for pressure measurements in gas-solid fluidized beds. The pressure measurement point for each fluidization column was as follows:

- Fluidized bed 1 – positioned 3 cm below the distributor plate.
- Fluidized bed 2 – positioned 3.5 cm below the distributor plate.
- Fluidized bed 3 – positioned 3.5 cm below the distributor plate.

It was imperative that the pressure measurement point be positioned below the air distributor plate. This was to avoid any penetration of solids into the pressure probe which may result in damage to the transmitter. The pressure measurement precision was estimated at $\pm 0.05\%$.

The WIKA model 2500 digital pressure gauge was used to determine the minimum and maximum pressure fluctuation signals in the fluidized bed. This was to verify the measurements provided by the WIKA model P30 pressure transmitter. The pressure measurement precision was estimated at $\pm 0.003\%$. A description of the data acquisition process and monitoring software can be identified in Appendix C.

4

CHAPTER 4

EXPERIMENTAL PROCEDURE

This chapter will focus on the experimental methods and procedures employed when operating the gas-solid fluidized bed apparatus discussed in Chapter 3. The following sections will be investigated:

1. Particle selection and characterization.
2. Preparation of the experimental equipment.
3. Operation of the experimental equipment.
4. Processing of pressure fluctuation signals.

4.1 Particle Selection and Characterization

4.1.1 Particle Selection

The key component of this research was to investigate the fluidization behaviour of various solid particles in different sized fluidized bed columns. The state of fluidization for a single column is strongly influenced by the properties of the solid particles. These include density, particle size as well as particle geometry. This makes it essential to carefully select the particles for the fluidized bed as different materials tend to behave differently. Geldart Group A and

Geldart Group B materials represent the most widely used particles for fluidized bed applications.

Due to the low cost and ease of availability, sand particles are often used in laboratory experiments to represent the fluidization behaviour of Group B materials. This helps to improve the understanding of the fluidization behaviour of similar materials, from the same Geldart Group, which are known to fluidize easily. Another commonly used material is spent FCC which is classified as Geldart Group A. These particles are employed in fluid catalytic processes in industry.

This research has focussed on studying the state of fluidization for three different materials from different Geldart Groups, namely: spent FCC (Geldart Group A), sand particles (Geldart Group B) and plastic beads (Geldart Group D). Measurements were not undertaken for Geldart Group C materials largely due to these materials not being suitable for fluidization.

4.1.2 Particle Characterization

Particle characterization represents a critical parameter for the fluidization behaviour of a gas-solid fluidized bed. Particle characterization tests include: size distribution, density, shape as well as voidage. This represents a portion of fluidization that is often studied separately as preliminary tests. Since the focus of this work was to investigate the fluidization behaviour of selected Geldart Groups in different fluidized bed vessels, characterization tests were only undertaken to determine particle size and particle density. The particle characterization procedures were conducted three times and an average was then taken. The results presented are the average values.

4.1.2.1 Particle density

The density for the various materials that were utilised in this work was determined by making use of a displacement test method through the use of a pycnometer. The density of sand and FCC was determined through the water displacement technique while the density of the plastic beads was obtained by using 1-butanol in place of water for the displacement technique. It was observed that plastic beads floated in water and to reduce the possibility of error, an alcohol had to be utilised. The choice of 1-butanol as the alcohol was largely due to it being readily available as well as having a low volatility. This meant that the alcohol would not evaporate as

fast as the lighter alcohols (methanol, ethanol and 1-propanol). The accuracy of density determination through the displacement method required precise measurements of mass and volume. Mass measurements were undertaken using the OHAUS digital mass balance with precision of ± 0.01 mg. The procedure for the determination of the density of the solid particles is indicated below:

1. The mass of a dry, empty pycnometer m_0 was determined.
2. A sample of the experimental material was then filled into the pycnometer and the mass of the pycnometer and solid particles, m_1 was measured.
3. The liquid (distilled water or 1-butanol) was then filled up to the mark on the pycnometer and the total mass, m_T was measured.
4. The temperature of the liquid was obtained by making use of a mercury thermometer and this ensured precise density measurements for the liquid as density varies with temperature.
5. The mass of the liquid was determined by, $m_l = m_T - m_1$. Similarly, the mass of the solid particles was determined by $m_p = m_1 - m_0$.
6. The volume of liquid was determined by $V_l = \frac{m_l}{\rho_l}$ while the density used was taken at the temperature of the liquid. The volume of solid was thereafter determined by taking the difference between the total pycnometer volume and liquid volume, $V_p = V_{pycnometer} - V_l$.
7. The density of solid particles was thereafter determined using the equation,
$$\rho_p = \frac{m_p}{V_p}.$$

4.1.2.2 Particle size

Particle size distribution was determined through the use of a Shimadzu SALD-3101 Laser Diffraction Particle Size Analyser. This method relies on the solid particles being exposed to laser light with the particle size distribution being determined from the light intensity

distribution pattern of the diffracted light emitted from the particles. The light intensity of the diffracted light is known to be directly proportional to the particle size. The Shimadzu SALD-3101 Laser Diffraction Particle Size Analyser used in this work was capable of measuring particle sizes over an extensive range of diameters from 0.05 to 3000 μm . The physical properties of the materials (spent FCC, sand and plastic beads) employed in this work can be seen in Table 4.1.

Table 4.1 Physical characteristics of solid particles

Material	Particle density (g/cm^3)	Particle diameter (μm)	Geldart Classification
Spent FCC	1.38	80	A
Sand	2.60	300	B
Plastic beads	0.93	2280	D

4.2 Preparation of the Experimental Equipment

4.2.1 Cleaning of the Gas-Solid Fluidized Bed Apparatus

The gas-solid fluidized bed column was thoroughly cleaned prior to experimental measurements being conducted. Cleaning of the apparatus was essential as any impurities or dust particles in the fluidized bed system may have an influence on the pressure fluctuation signals. In addition, cleaning of the fluidized bed column improved the transparency and ensured that the fluidization state could be clearly identified. The cleaning process involved spraying water through the column while wiping the outside with a wet cloth. The column was then allowed sufficient time to dry after which the fluidized bed was ready for use.

4.2.2 Detection of penetration of solid particles through distributor plate

The movement of solid particles from the bed region, through the distributor plate, to the plenum chamber was undesirable. This condition may have an adverse effect on the measurement of the pressure fluctuation as well as result in damage to the pressure transmitter. This was due to the solid particles entering and blocking the tubes connecting the pressure transmitter to the fluidized bed system. Therefore, it was vital that the experimental apparatus be operated without any penetration of the solid particles through the distributor plate. The plenum

chamber for all three fluidized bed columns was transparent and as a result, prior to the experiments being performed for each material, an observation was performed on whether the solid particles were penetrating through the distributor plate or not. Penetration through the distributor plate did not occur for sand (all three fluidized beds) and plastic beads (only employed in 11 cm I.D fluidized bed). However, due to the small size, spent FCC was observed to move through the distributor to the plenum chamber in the 11 cm I.D fluidized bed. In order to prevent this from occurring, a fine wire mesh with size of $50\ \mu\text{m}$ was placed above the distributor plate.

4.3 Operation of the Experimental Equipment

Operation of the gas-solid fluidized bed apparatus (discussed in Section 3.1) was performed at ambient conditions. In each experiment, the solid particles under investigation were filled in the clean fluidized bed to the desired bed height. In order to improve accuracy, the bed height was measured at eight points around the column using a measuring tape and an average was thereafter taken. The WIKA model P30 pressure transmitter was then connected from the data acquisition board to the pressure measurement point in the plenum chamber. The gate valve and stop valves were thereafter opened and compressed air was allowed to enter the system. Depending on the size of the fluidized bed, a suitable rotameter was selected in order to regulate the air flow rate. It was important that the pressure upstream the rotameters was maintained at 140 kPa. This was due to the rotameters being calibrated at this pressure. In addition, the compressor supply pressure was monitored throughout each experimental run. Minimal fluctuations, which did not have a significant impact on the results, were identified.

The air flow rate was then varied until a particular state of fluidization was visually identified in the fluidized bed. The superficial air velocity was determined by using the selected rotameter calibration equation and dividing the calibrated volumetric flow rate, Q by the cross-sectional area, A of the fluidized bed. Once a state of fluidization was observed, the experiment was controlled by using Easy Com 2011 Windows. The sampling time was specified as $2\ \text{ms}$ (corresponding to a sampling frequency of $500\ \text{Hz}$) and the total measurement time was set at $30\ \text{minutes}$. The pressure fluctuation signals were then recorded and stored on a computer for further processing. With the purpose of ensuring greater accuracy, three experimental runs were conducted for each condition investigated. The operational conditions for the experimental work can be seen in Table 4.2. Predicted superficial gas velocities were used as a guide for the operation conditions of the fluidized bed. However, largely due to the uncertainty and lack of

reliable predictive models, operation conditions were selected based on the bed behaviour that was observed.

Table 4.2 Operational Conditions of Gas-Solid Fluidized System

Column Diameter (cm)	Material	Bed Height (cm)	Gas velocity (m/s)	Fluidization Regime
5	Sand	8	0.46 / 0.73	Slugging / Turbulent
		30	0.37 / 0.55	Slugging / Turbulent
11	Spent FCC	11	1.36	Bubbling
		21	1.70	Bubbling
	Sand	11	0.59 / 1.02 / 1.88	Bubbling/ Slugging/ Turbulent
		16	0.59 / 0.93/ 1.79	Bubbling/ Slugging/ Turbulent
11	Plastic Beads	21	0.59/ 0.84/ 1.19	Bubbling/ Slugging/ Turbulent
		11	0.84 / 2.56	Bubbling / Slugging
	16	0.84 / 2.05	Bubbling / Slugging	
	21	0.84 / 1.70	Bubbling / Slugging	
29	Sand	28	0.84 / 1.62	Bubbling / Slugging
		32	0.25	Bubbling
		83	0.19	Bubbling

4.4 Processing of Pressure Fluctuation Signals

In order to ensure high precision in the statistical analysis, the experimental data was analysed by dividing each run into eight overlapping data segments comprising of 6126 data points. The FFT of each segment (with a total of 49 008 data points) was then determined through the use of MATLAB. MATLAB is a computer software programme which has a built in function that allows for calculations of the Fourier Transform to be performed with ease. The software results were then exported to Microsoft Excel where the data was sorted with the aim of identifying the dominant frequency for each data segment. An average dominant frequency was then taken by using the twenty-four data segments over the three runs.

5

CHAPTER 5

RESULTS AND DISCUSSION

This chapter presents the results for the gas-solid fluidized bed systems investigated in this work. The reliability of the experimental results is largely dependent on the accuracy and precision of the measurement of the pressure fluctuation signals. In an attempt to ensure accurate experimental results as well as correct operation of the gas-solid fluidized bed system, measured pressure fluctuation data were analysed and compared against literature data for spent FCC in an 11 cm I.D column with a bed height of 20.5 cm. The choice of this material was largely due to reliable literature data being available for verification. In addition, spent FCC is a material which is difficult to acquire. Hence a comparison using this material will provide a good representation on the accuracy of the experimental apparatus and procedures.

Analysis of pressure fluctuation data for spent FCC (bed height of 11 and 21 cm), sand (bed height of 11 and 21 cm) and plastic beads (bed height of 11 and 28 cm) in the time domain are also presented in this chapter.

New data for the analysis of pressure fluctuation signals in the frequency domain for different fluidized bed columns (5, 11 and 29 cm I.D) are also included. The systems under investigation were as follows: I.D 5 cm (sand – bed height of 8 and 30 cm), I.D 11 cm (spent FCC - bed

height of 11, 16 and 21 cm; sand - bed height of 11, 16 and 21 cm and plastic beads – bed height of 11, 16, 21 and 28 cm) as well as I.D 29 cm (sand- bed height of 32 and 83 cm).

5.1 Comparison to Literature Data

As mentioned above, the reliability of the experimental measurements is strongly influenced by the implementation of correct procedures and operation of the gas-solid fluidized bed apparatus. Since the main focus of this dissertation was on analysis in the frequency domain, the comparison between experimental and literature data was made in this domain. For analysis in the frequency domain, the distinguishing feature is the identification of a peak frequency observed in the power spectra generated from the FFT. The physical properties of the fluidizing material in conjunction with the operating conditions play a vital role in the position of the peak frequency component. As a result, careful consideration had to be given when comparing experimental data to literature data.

The literature data was taken from Alberto et al. (2004). The comparison was made with spent FCC as the bed material with experimental properties (Geldart Group A, $\rho_p = 1.37 \text{ g/cm}^3$, $d_p = 80 \text{ }\mu\text{m}$) similar to that employed in literature (Geldart Group A, $\rho_p = 1.38 \text{ g/cm}^3$, $d_p = 92 \text{ }\mu\text{m}$). In addition, the experimental operating conditions (11 cm I.D column and 21 cm bed height) were kept close to the literature conditions (11.12 cm I.D column and 20.5 cm bed height).

The experimental and literature results can be seen in Figures 5.1 and 5.2 below. The dominant frequency from experimental measurements was determined as 4.04 Hz while the literature value for the same conditions was given as approximately 4 Hz. It can be concluded that the experimental data is in close agreement with the literature data with slight differences attributed to minor differences in particle size as well as the bed height.

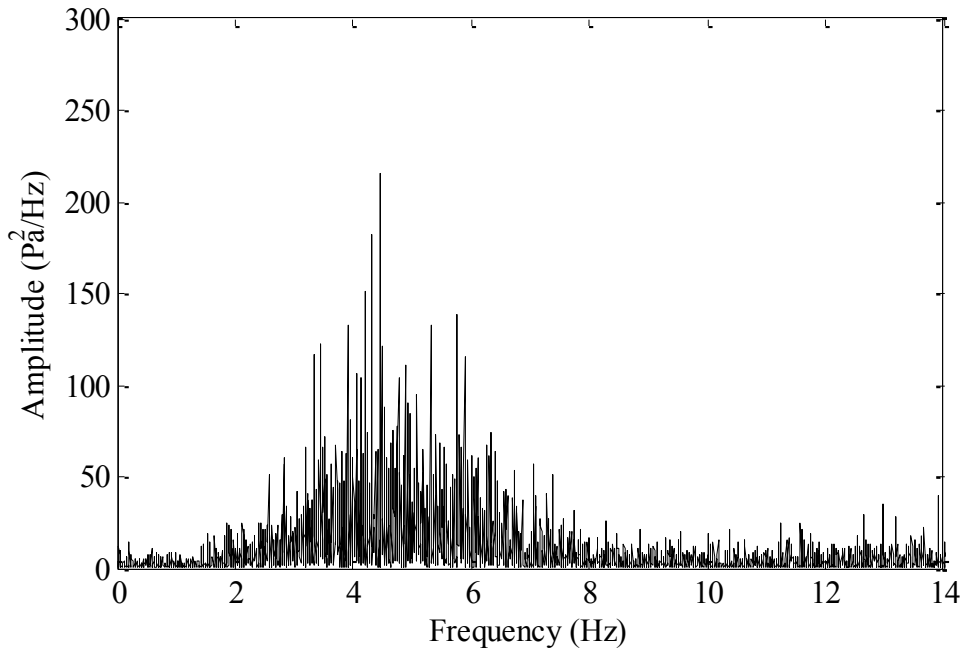


Figure 5.1 Power spectrum of the bubbling regime for FCC with 80 μm, bed height 21 cm and column I.D 11 cm; Experimental

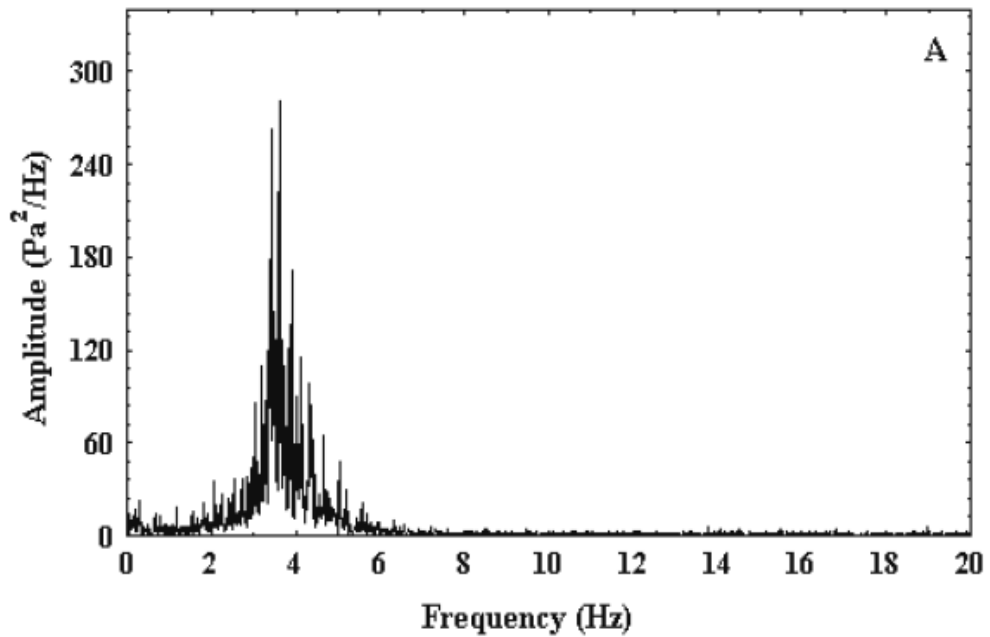


Figure 5.2 Power spectrum of the bubbling regime for FCC with 92 μm, bed height 20.5 cm and column I.D 11.15 cm; Alberto et al. (2004)

5.2 Analysis in the time domain

Analysis in the time domain represents the simplest analysis technique and this is achieved by plotting a sequence of pressure fluctuation signals at various instances of time. It is always beneficial to inspect the signal in the time domain by analysing the time-pressure behaviour before further processing can occur. This is done to identify any abnormalities which may be due to the fluidized bed behaviour as well as problems with the data acquisition system. As mentioned in Section 2.2.1.1, the standard deviation technique represents the widely adopted method for analysis in the time domain.

5.2.1 Time-pressure behaviour

The time-pressure behaviour was analysed for all materials in the 11 cm I.D fluidized bed column with a time sequence of 10 s. The fluidization regimes were identified visually by varying the superficial gas velocity of the air entering the fluidized bed column. The bubbling regime was identified by the formation of a large number of bubbles which originated at the distributor and exploded at the bed surface. The slugging regime was identified by the presence of large bubbles which were approximately similar in size to the diameter of the column while the turbulent regime was observed by the disappearance of the upper bed surface as well as rapid, turbulent motion of particle clusters being apparent.

The time-pressure behaviour for the bubbling regime with Geldart Group A material (spent FCC) at two bed heights (11 and 21 cm) is presented in Figure 5.3. It can be seen that the pressure fluctuation signals for both bed heights is complex and irregular. This profile is largely due to the presence of multiple bubbles, comprising of different sizes, which moved through the fluidized bed at different velocities. In addition, the pressure fluctuation signals at an increased bed height are observed to display higher amplitude than the signals at a lower bed height. The main reason for this is that an increase in bed height allowed for more bubbles to be produced. This effectively resulted in an increase in the pressure fluctuation signals as indicated by the greater amplitude.

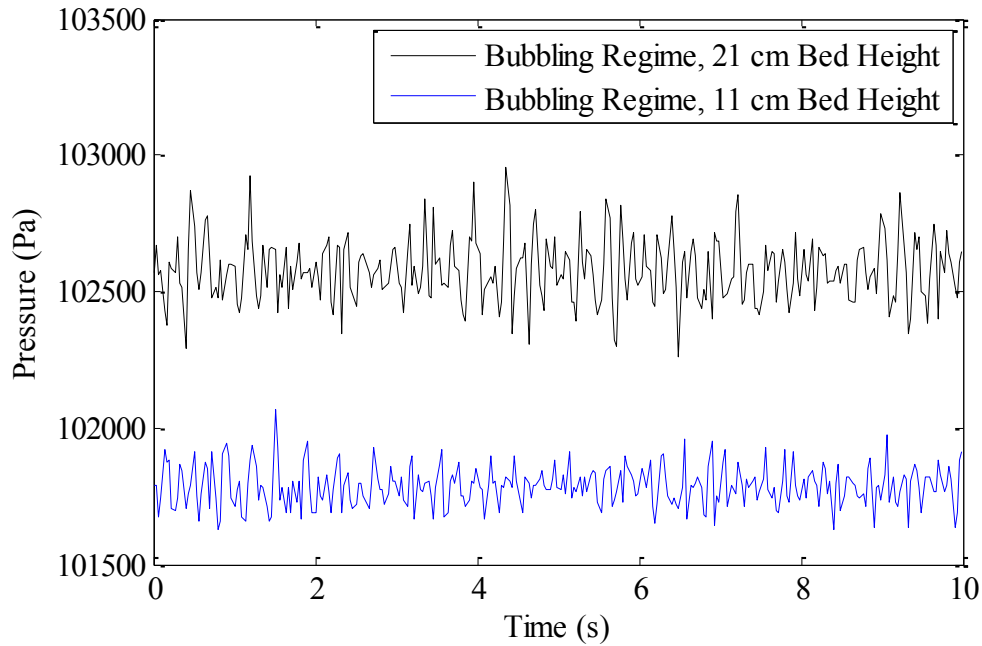


Figure 5.3 Time sequences of the pressure fluctuation signals measured in the bubbling regime using spent FCC in the 11 cm I.D column at the indicated bed heights

The time-pressure behaviour for Geldart Group B particles (sand) at a bed height of 11 can be observed in Figure 5.4. The sand particles were observed to fluidize very easily with the bubbling, slugging and turbulent regimes identified in the fluidized bed. As seen in Figure 5.4, the bubbling regime displayed a rapid, irregular pressure fluctuation signal. This was due to numerous bubbles of varying sizes. In comparison with the slugging regime, the differences were difficult to observe.

The main difference between the two regimes lied in the amplitude of the pressure fluctuation which was marginally greater for the slugging regime. This was due to the formation of larger bubbles or slugs which led to an increase in the pressure fluctuation signals that eventually led to a higher amplitude. The turbulent regime showed the greatest increase in the pressure fluctuation signal. In addition, there was a decrease in the periodicity of the pressure fluctuation. This was a result of the vigorous contact that occurred between the gas and solid in the fluidized bed due to the high gas velocity. The vigorous contact increased the friction on the walls of the fluidized bed column. This then led to an increase in the pressure drop which resulted in higher amplitude pressure fluctuations. As observed in the time-series profile, differentiating between the three fluidization regimes was difficult with the amplitude being the main defining factor.

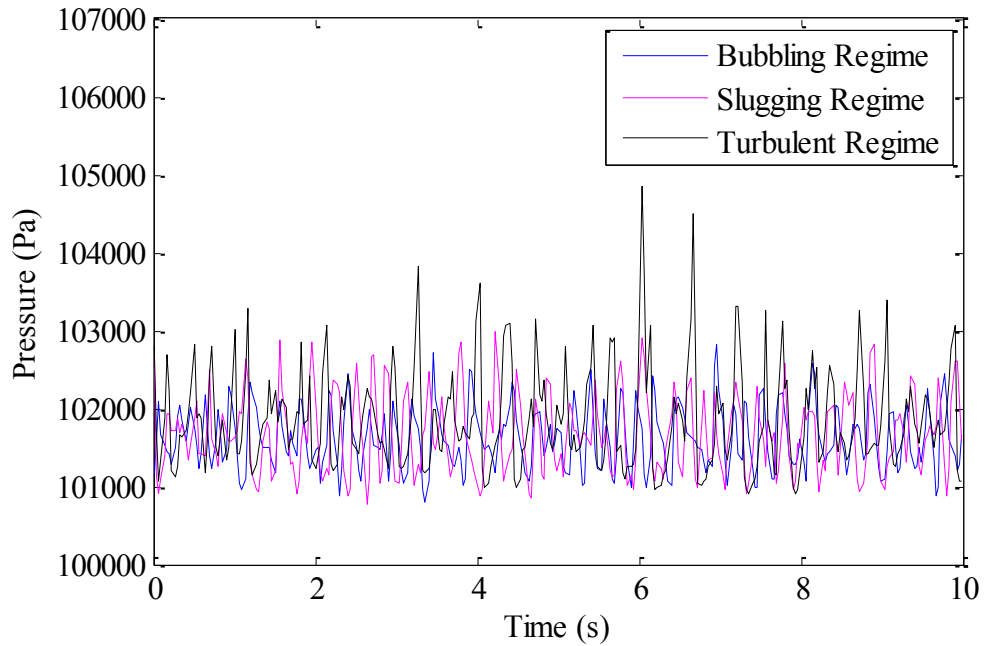


Figure 5.4 Time sequences of the pressure fluctuation signals measured in various regimes using sand in the 11 cm I.D column at a bed height of 11 cm

The time sequences of the pressure fluctuation signals for the same material at an increased bed height of 21 cm are presented by Figure 5.5. In comparison with a bed height of 11 cm, it could be noted that all three regimes displayed similar time-pressure behaviour with the only significant difference being in the amplitude of the pressure fluctuation. This was significantly greater at a higher bed height. This could be due to more time being allowed for the interaction and formation of bubbles in the fluidized bed. In addition, the pressure is higher at an increased bed height and as a result, the pressure fluctuations due to the bursting of bubbles at the bed surface, is greater. As before, it was extremely difficult to definitely distinguish between the regimes due to similar time-pressure behaviour.

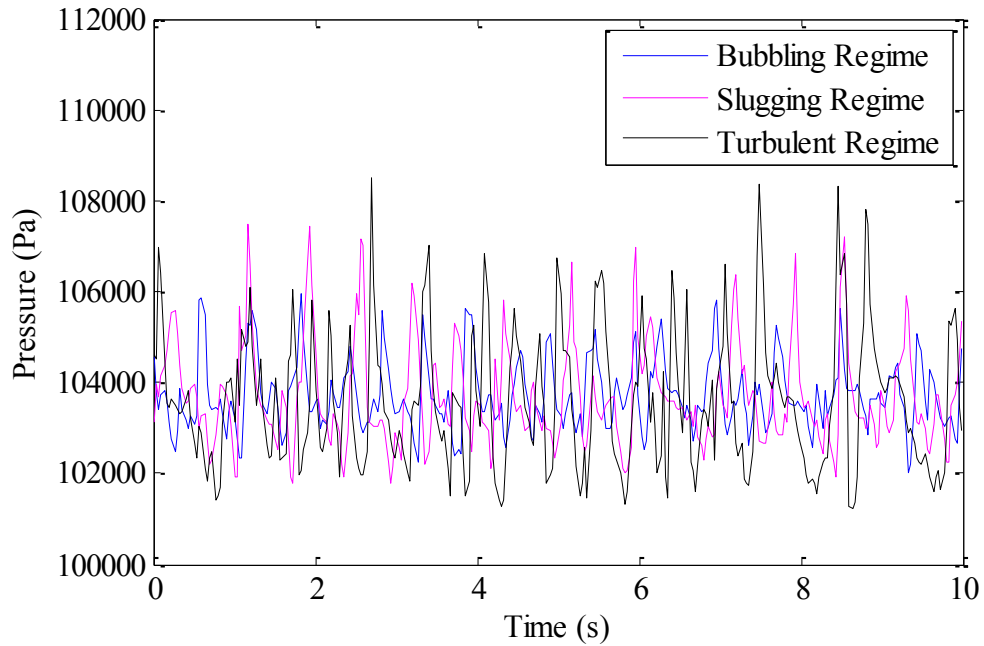


Figure 5.5 Time sequences of the pressure fluctuation signals measured in various regimes using sand in the 11 cm I.D column at a bed height of 21 cm

The time-series behaviour for the Geldart Group D particles (plastic beads) for the static bed, bubbling and slugging fluidization states at a bed height of 11 and 28 cm are presented by Figures 5.6 and 5.7 below. It could be seen that the time-pressure profile, at both bed heights, followed the same trend as the Geldart Group A and B particles as described above. In accordance with literature, the static bed displayed a constant pressure fluctuation signal irrespective of the time scale. This was observed for both bed heights at very low gas velocities (0.5 – 0.64 m/s). This behaviour could be described by the fact that the solid particles remained stationary in the fixed bed regime while the fluidizing gas passed through the void spaces between the particles. As a result, the pressure fluctuation signals were minimal.

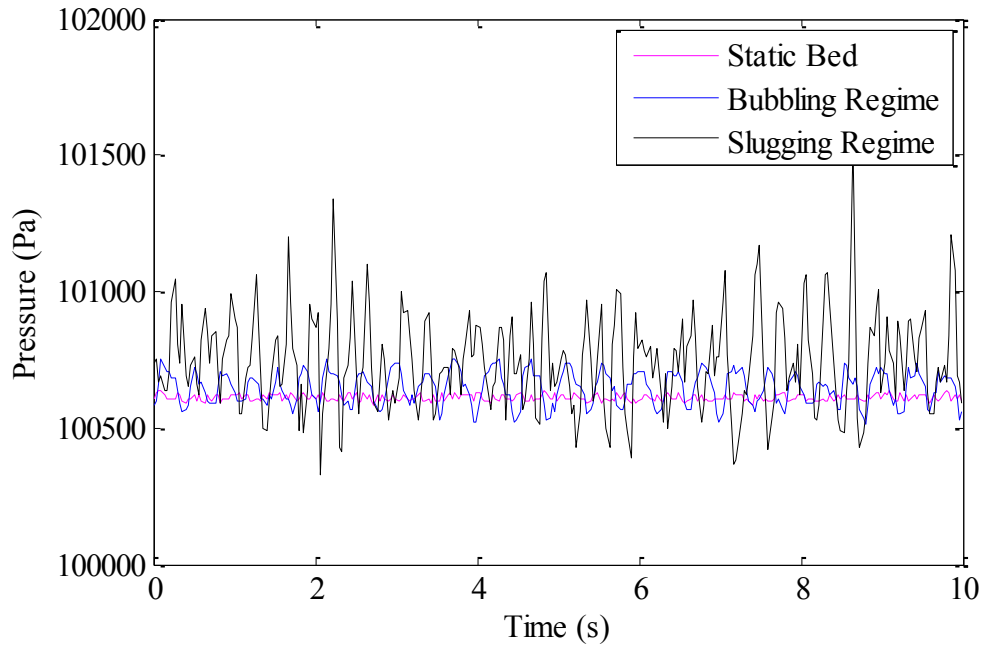


Figure 5.6 Time sequences of the pressure fluctuation signals measured in the indicated regimes using plastic beads in the 11 cm I.D column at a bed height of 11 cm

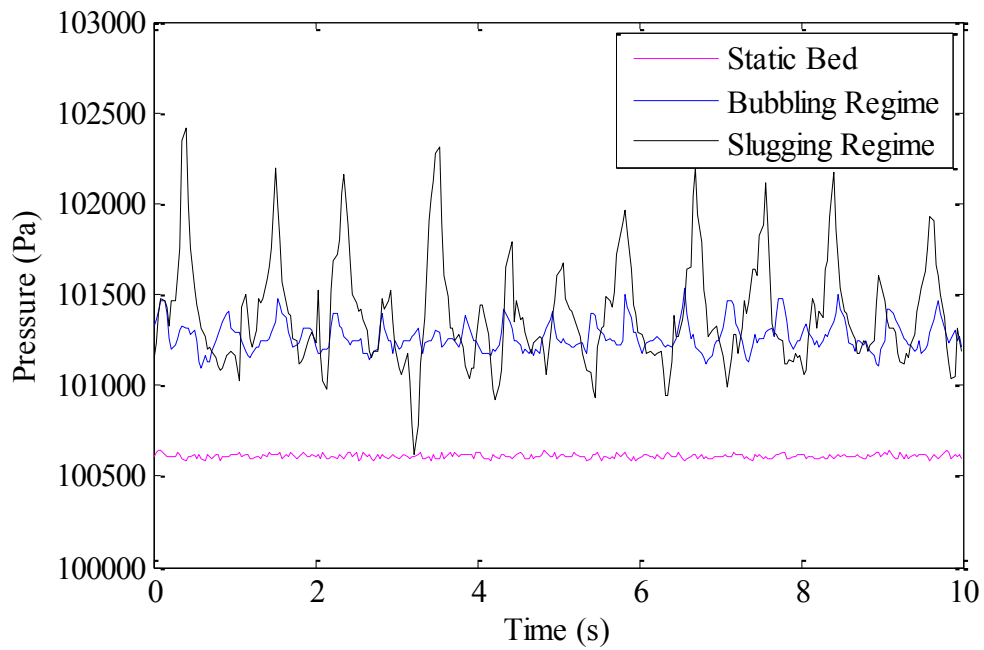


Figure 5.7 Time sequences of the pressure fluctuation signals measured in the indicated regimes using plastic beads in the 11 cm I.D column at a bed height of 28 cm

Although the time-pressure behaviour displayed differences in the pressure fluctuation signals for the various fluidization states, it should be noted that this analysis technique represents a subjective technique for distinguishing between fluidization states. This is due to the fact that the different fluidization states can easily be confused as in the case of Johnsson et al. (2000) in which similar time-pressure behaviour was verified for the turbulent and pneumatic transport regimes. This is largely because amplitude and signal variation profiles are the only two factors considered in this analysis technique.

5.2.2 Standard Deviation or Variance

5.2.2.1 Experimental regime transition velocity

In an attempt to show typical results from employing the standard deviation technique, the standard deviation of the pressure fluctuation at various superficial gas velocities for the Geldart Group B material is presented in Figure 5.8. These results were for the 11 cm I.D column with a static bed height of 11 cm. The experimental measurements were repeated three times and the average pressure fluctuation was then determined for each superficial gas velocity. The transition from the bubbling to the turbulent regime is defined as the superficial gas velocity (u_c) at which the amplitude of the standard deviation of the pressure fluctuation is at a maximum. For this work, the maximum in the standard deviation was determined to be approximately 1.10 m/s.

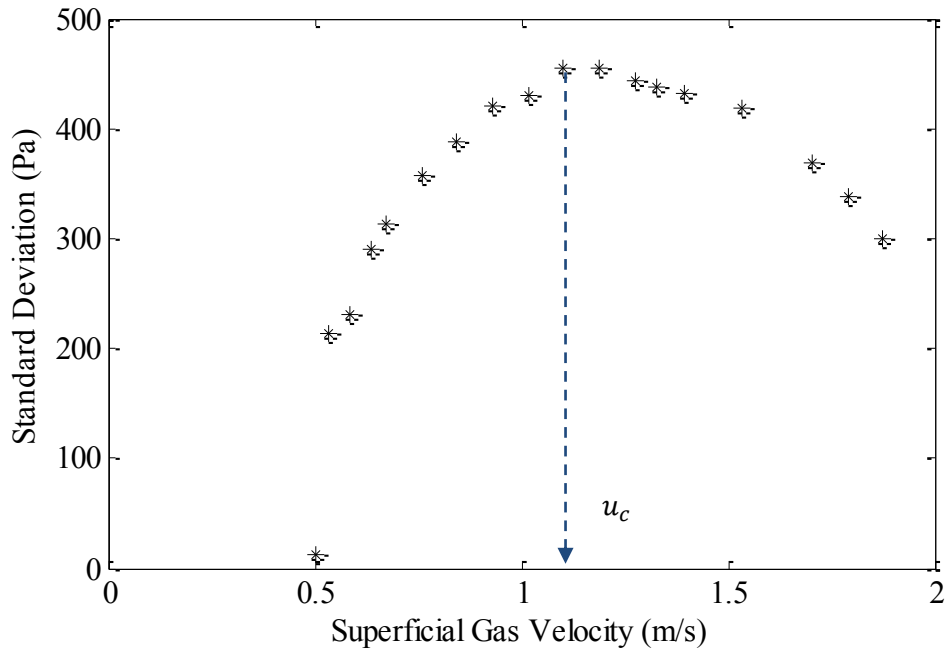


Figure 5.8 Standard deviation of pressure fluctuation as a function of superficial gas velocity for sand particles at a bed height of 11 cm

It could be seen that the standard deviation technique did provide an indication on the behaviour of the fluidization regime transition i.e. from the bubbling to turbulent regime. However, largely due to the strong dependence on the superficial gas velocity, there are doubts as to whether this method could be applied in industry where operating conditions such as the superficial gas velocity are known to fluctuate. In addition, this method relies on characterizing fluidization regimes solely by amplitude which provides no information on the time scale of the system. Finally, the use of the standard deviation technique should be applied with care as differences in standard deviation can be a result of a number of different factors with not all of them representing a change of regime.

5.2.2.2 Prediction of the regime transition velocity

As described in Section 2.1.7, there exist several correlations for the prediction of the transition velocity from the bubbling to turbulent regime. These results can be seen in Table 5.1. The best correlations for Geldart Group B materials were selected from the work of Arnaldos and Casal (1996). It was found that the experimental value for the transition velocity (1.10 m/s) agreed reasonably well with the predicted values. However, caution needs to be taken when using correlations as most of them have been proposed sometime back. Furthermore, with the

exception of the correlation developed by Cai et al. (1989), the correlations do not consider the diameter of the column. This factor significantly influences the ability to achieve a particular fluidization regime and as a result, the predicted values for the transition velocity may be misleading.

Table 5.1 Correlations and predictions for u_c using sand in the 11 cm I.D column and a bed height of 11 cm

Author	Equation	Predicted Value (m/s)
Bi and Grace (1995)	$Re_c = 0.565 Ar^{0.461}$	1.06
Cai et al. (1989)	$u_c = (gd_p)^{0.5} \left[\frac{0.211}{D_t^{0.27}} + \frac{2.42 \times 10^{-3}}{D_t^{1.27}} \right] \left[\frac{D_t(\rho_p - \rho_g)}{d_p \rho_g} \right]^{0.27}$	0.90
Jin et al. (1986)	$u_c = (gd_p)^{0.5} \left[\frac{(KD_f)(\rho_p - \rho_g)}{d_p \rho_g} \right]^{0.27}$ $KD_f = 0.00367 \text{ (for free bed)}$	0.85
Lee and Kim (1990)	$Re_c = 0.7 Ar^{0.485}$	1.58
Nakajima et al. (1991)	$Re_c = 0.633 Ar^{0.467}$	1.24

5.3 Analysis in the frequency domain

Analysis in the time domain did reveal differences in the time-pressure behaviour for the different contact regimes investigated. However, it should be noted that the profile observed for regimes such as the bubbling and slugging appeared to be fairly similar with the differentiating factor being the amplitude and signal variation profile. Confusion of the different fluidization regimes can occur easily and this creates a doubt on the reliability of this analysis technique. The primary function of analysis of pressure fluctuation signals in the time domain is to validate

whether fluidization has occurred or not. This resulted in the search of more objective techniques in order to establish differences in the dynamics of each fluidization state. This was achieved by analysis of the pressure fluctuation signals in the frequency domain using power spectral analysis.

The transformation of the pressure fluctuation signal from the time domain to the frequency domain was achieved by the FFT. This was implemented on the software package, MATLAB which had a built-in, *fft* function. The MATLAB code for a single run with the eight segments can be seen in Appendix B. The power spectra represented the behaviour of the pressure fluctuation signals in the frequency domain with the dominant frequency defined as the frequency component at which the highest peak was observed. A significant contribution of this dissertation lies in the fact that analysis in the frequency domain was employed in three fluidized bed columns having internal diameters of 5, 11 and 29 cm. The results for each system are presented below.

5.3.1 Fluidized bed 1 (Internal diameter of 5 cm and height of 200 cm)

5.3.1.1 Sand Particles

The power spectra for the Geldart Group B materials in the 5 cm I.D fluidized bed column are presented in this section. In order to observe the influence of the bed height of the material on the dominant frequency, two bed heights of 8 and 30 cm were investigated. Due to the small column diameter, the only regimes achieved with the sand particles were the slugging and turbulent regimes respectively. As mentioned in Section 5.2.1, the slugging regime was verified by the presence of large bubbles or slugs which originated at the bottom of the fluidized bed and exploded on the surface. The turbulent regime was identified by the loss of the upper bed surface with turbulent particle clusters being observed in the column. Visual identification of fluidization behaviour is widely adopted and this can be seen in the work of van Ommen et al. (2011), Alberto et al. (2003) as well as Johnsson et al. (2000).

Figure 5.9 represents the power spectrum, as obtained from the FFT, for the slugging regime for sand particles at a bed height of 8 cm. Inspection of the spectrum revealed several high amplitude peaks with a single frequency component of higher amplitude standing out. This was defined as the dominant frequency and for the operating conditions employed, it was determined as approximately 2.45 Hz. Figure 5.10 represents the turbulent regime under the

same conditions. The dominant frequency was found to be 1.93 Hz. In addition to the higher amplitude for the turbulent regime, it can be seen that there was a clear difference between the dominant frequencies for both fluidization regimes.

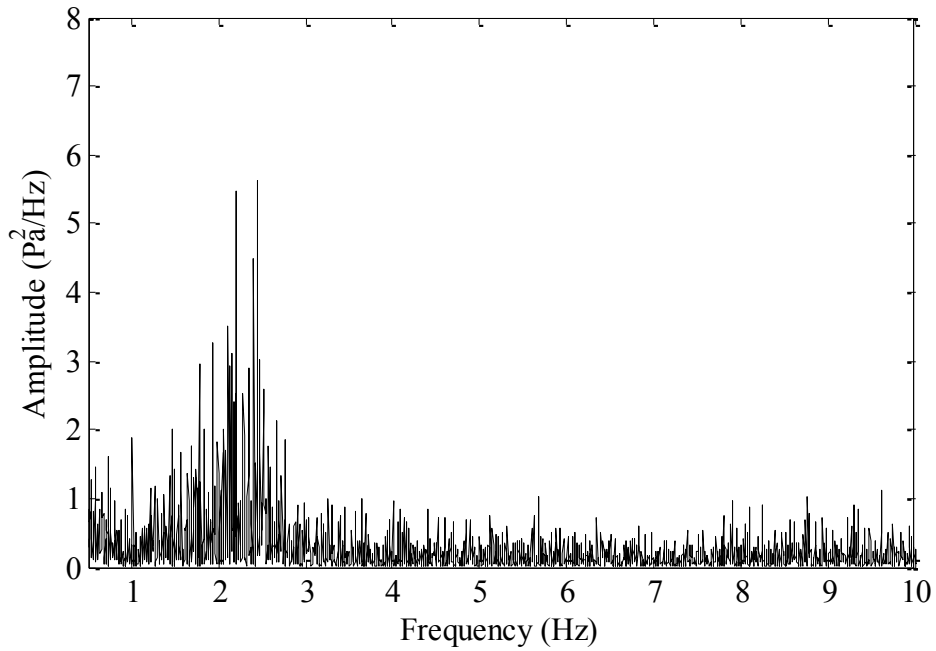


Figure 5.9 Power spectrum of the slugging regime of sand particles in the 5 cm I.D column with a bed height of 8 cm

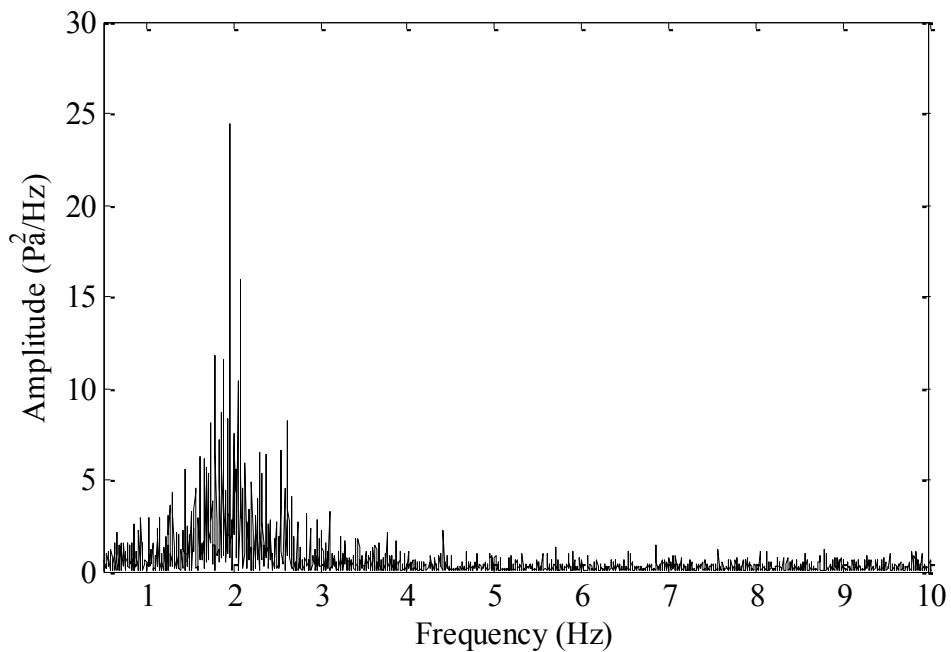


Figure 5.10 Power spectrum of the turbulent regime of sand particles in the 5 cm I.D column with a bed height of 8 cm

When the bed height was increased to 30 cm, it was found that the same two regimes (slugging and turbulent) could be identified in the fluidized bed column. However, it was noted that it was easier to identify each fluidization state as the behaviour was more evident in the column at the higher bed height. This was better illustrated in the power spectrum which could be seen to be narrow and distinct for both regimes at the bed height of 30 cm. Furthermore, the dominant frequency was clearly identified at the higher bed height.

The power spectrum for the slugging regime at a bed height of 30 cm is shown in Figure 5.11 below. For these operating conditions, the peak frequency was evaluated as 1.34 Hz. It could be seen that the increase in material bed height had an influence on the dominant frequency as there was a noticeable shift in the dominant frequency for the same regime. The power spectrum for turbulent conditions at the higher bed height is presented in Figure 5.12. In this instance, the dominant frequency was determined as 0.77 Hz. This was considerably less than the dominant frequency for the turbulent regime at a bed height of 8 cm, which was found to be 1.93 Hz.

The amplitude of the power spectrum for both regimes at a bed height of 30 cm were seen to be significantly greater than that which was seen previously for the lower bed height. The main reason for this was due to the occurrence of more bubbles or slugs (slugging regime) as well as increased turbulence and particle mixing (turbulent regime) at a higher bed height. This behaviour increased the pressure fluctuation signals which effectively resulted in a higher amplitude in the power spectrum.

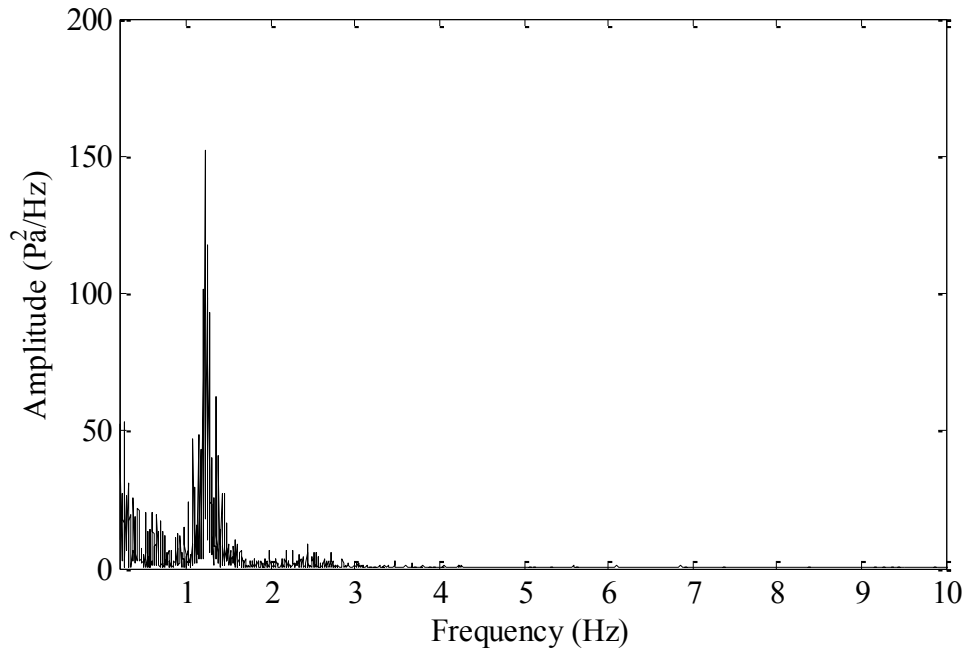


Figure 5.11 Power spectrum of the slugging regime of sand particles in the 5 cm I.D column with a bed height of 30 cm

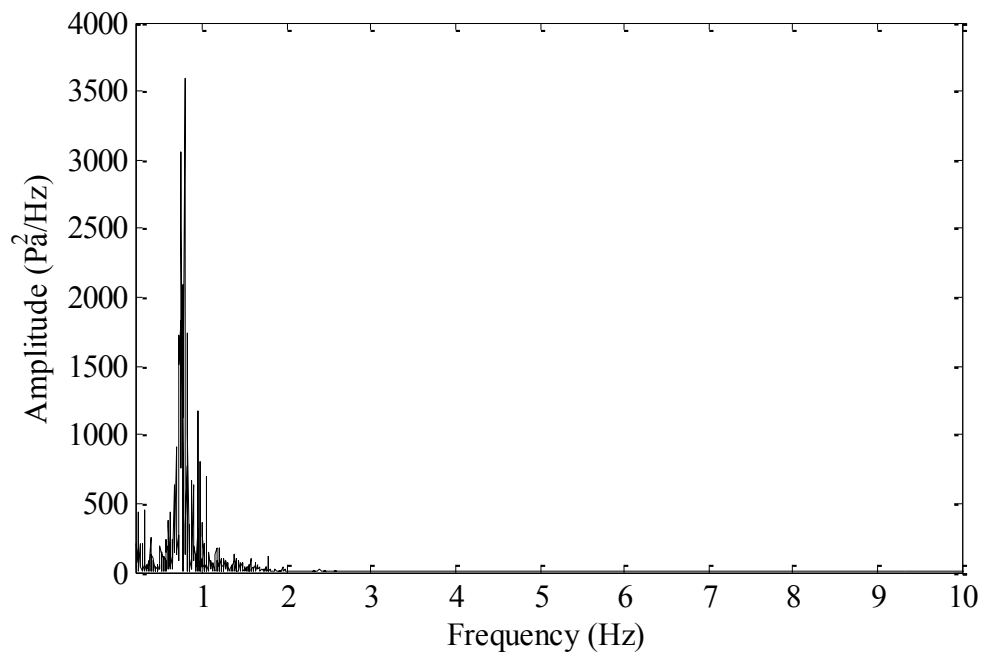


Figure 5.12 Power spectrum of the turbulent regime of sand particles in the 5 cm I.D column with a bed height of 30 cm

5.3.1.2 Other Materials

The Geldart Group A and D materials were employed in the 5 cm I.D fluidized bed column. However, it was found that for both materials, a dominant frequency could not be identified. This was irrespective of the superficial gas velocity and material bed height. The Geldart Group A particles were observed to undergo a noticeable bed expansion with no bubbling present. This behaviour would be suggestive of particulate fluidization. For the Geldart Group D particles, the reason for the lack of a dominant frequency may be due to the large particle sizes. This effectively resulted in a low ratio of the column diameter to particle diameter which meant that good fluidization could not be achieved.

5.3.2 Fluidized bed 2 (Internal diameter of 11 cm and height of 153 cm)

5.3.2.1 Sand Particles

In order to understand the hydrodynamic behaviour in different fluidized bed columns, experimental measurements were thereafter conducted in a column with internal diameter of 11 cm and total height of 153 cm. Due to the material being readily available as well as possessing the ability to fluidize easily, sand particles were first employed in this column. As observed previously in the 5 cm I.D column, the sand particles were once again found to display excellent fluidization behaviour. This behaviour was typical for Geldart Group B materials which are known to fluidize easily. It was further observed that three fluidization regimes could be achieved with the sand particles in the 11 cm I.D column. This was true for all bed heights (11, 16 and 21 cm).

The bubbling regime was identified at low superficial gas velocities while the slugging and turbulent regimes were seen at higher gas velocities. The results for the bed heights of 11 and 21 cm are presented in this section with the results for a bed height of 16 cm presented in Appendix A. This was done to prevent any repetition with a comparison of the two extreme conditions providing an adequate representation on the trend of the dominant frequency. An increase in bed height resulted in a distinct shift in the dominant frequency and this indicated the great potential of using this technique for identification of different fluidization regimes in industry.

Figure 5.13 represents the power spectrum for the bubbling regime of sand particles at a bed height of 11 cm. It could be seen that the resulting spectrum was broad with a dominant

frequency clearly evident. This suggested the presence of important frequency components in the dynamics of fluidization for the bubbling regime. The power spectrum was produced from the pressure fluctuation in the fluidized bed, which occurred due to the formation of air bubbles which rose through the bed. The formation of a wide spectrum, with evidence of a dominant frequency, suggested the presence of multiple bubbles of varying sizes with one size being present in larger numbers. This led to one particular bubble being noticeable when compared to others, as indicated by the dominant frequency. As shown in Figure 5.13, the dominant frequency was almost positioned at the centre of the spectrum with a value of approximately 4.07 Hz.

The power spectrum characteristic for the slugging regime at a bed height of 11 cm is presented in Figure 5.14. The dominant frequency was identified at approximately 2.63 Hz. Experimental measurements indicated the presence of large bubbles which practically occupied the entire diameter of the fluidized bed. In comparison with the slugging behaviour that was observed for the sand particles in the 5 cm I.D column, it was found that the slugs in the 11 cm I.D column exhibited a less frequent occurrence with a greater distance between successive slugs as they approached the surface. In addition, the dominant frequency for the slugging regime in 11 cm I.D column was found to differ from the values identified in the 5 cm I.D column. This meant that column diameter and bed height have an influence on the dominant frequency component.

The turbulent fluidization state was apparent at sufficiently high gas velocities. This regime was characterized by irregular, short-lived voids which moved through the bed in a rapid stirring movement. Furthermore, it was observed that it was difficult to identify the bed surface. The turbulent motion of the sand particles in the fluidized bed had a significant influence on the pressure fluctuation signals which could be seen in the spectra where a number of high amplitude peaks were visible. However, as before, a single frequency component stood out from the rest and from the power spectrum in Figure 5.15, the dominant frequency was positioned at 2.44 Hz. This was marginally smaller than the dominant frequency that was observed for the slugging regime, which had a value of 2.63 Hz. However, despite several repeated measurements, the same dominant frequencies were obtained for both regimes. Hence, it could be stated that the fluidization regime did have an influence on the dominant frequencies as there was a slight but visible shift from the slugging to the turbulent regime.

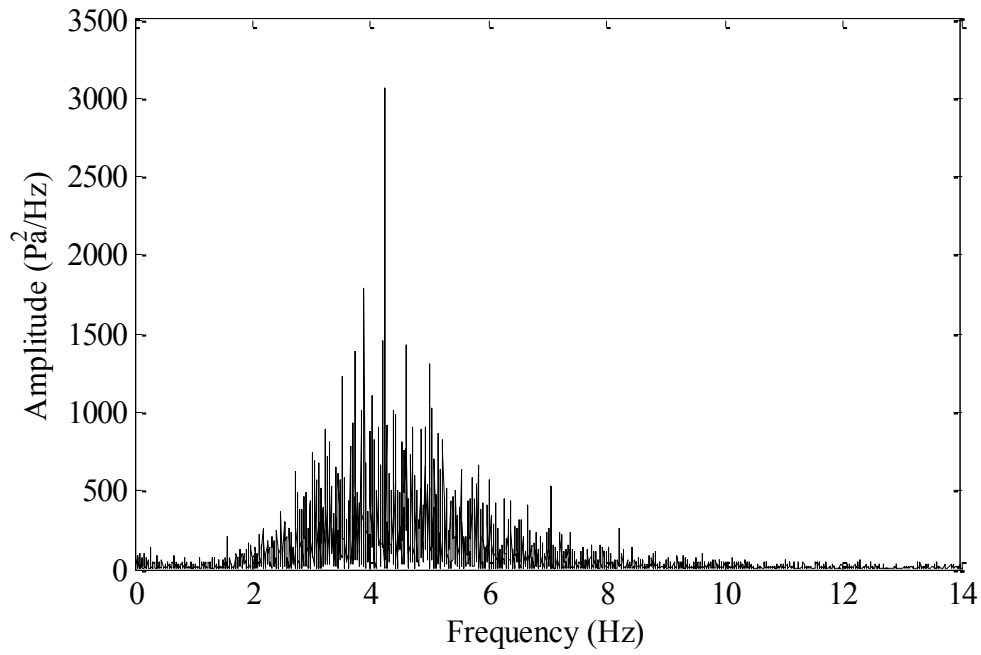


Figure 5.13 Power spectrum of the bubbling regime of sand particles in the 11 cm I.D column with a bed height of 11 cm

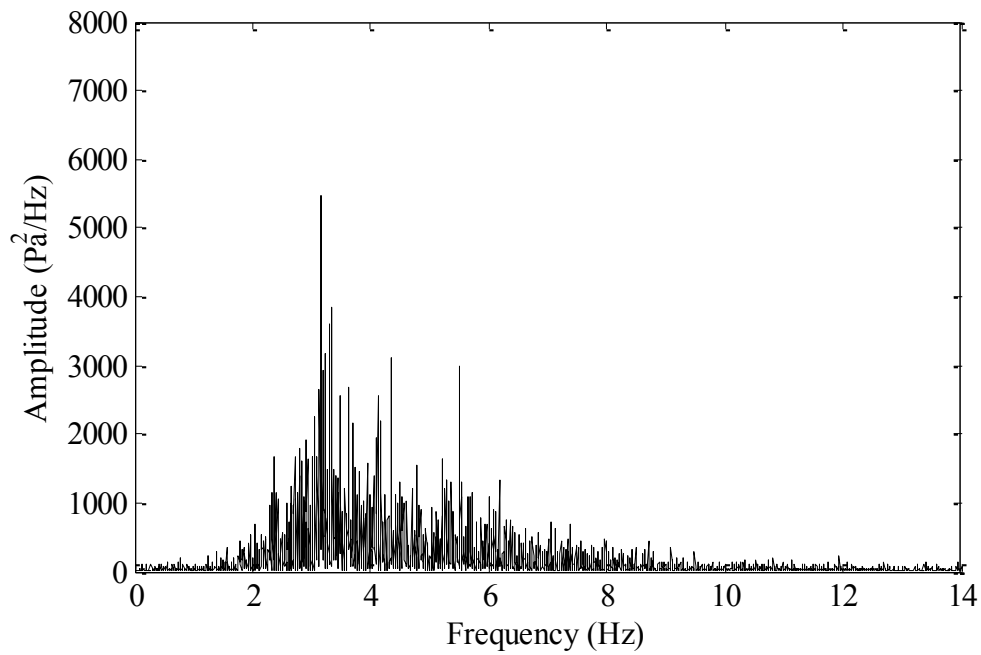


Figure 5.14 Power spectrum of the slugging regime of sand particles in the 11 cm I.D column with a bed height of 11 cm

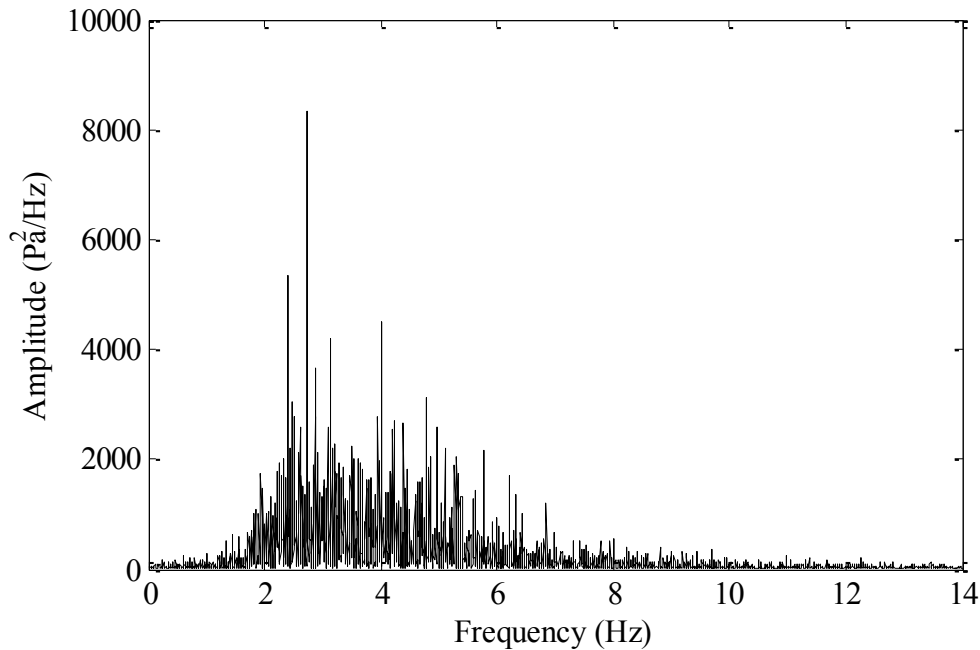


Figure 5.15 Power spectrum of the turbulent regime of sand particles in the 11 cm I.D column with a bed height of 11 cm

In an attempt to further improve the understanding of the influence of the bed height on the power spectra, the static bed height of the sand particles was increased from 11 to 21 cm. The power spectra for the three fluidization regimes are presented in Figures 5.16, 5.17 and 5.18 below. In comparison to the power spectra at the bed height of 11 cm, it was instantly seen that the spectra produced at an increased bed height was much more distinct with a narrow spectra clearly evident. This was apparent for all three regimes. This behaviour was in accordance to the work of Johnsson et al. (2000) who established that an increase in bed height resulted in a spectra with higher amplitude and more distinct peaks.

Figure 5.16 represents the power spectrum for the bubbling regime at a bed height of 21 cm. In this instance, the dominant frequency was determined as 1.74 Hz. The amplitude of the power spectrum, at a bed height of 21 cm, could be seen to be significantly larger than the amplitude at a bed height of 11 cm. The primary reason for the narrower spectra, with a higher amplitude, was due to the fact that an increased bed height led to the bubbles being more concentrated with more coalescence towards the centre of the bed. This effectively resulted in more time being allowed for the interaction of the bubbles which then meant a higher energy content as observed by the higher amplitude peaks.

In the case of the slugging regime as presented in Figure 5.17, the dominant frequency was approximately 1.13 Hz. The increase in bed height displayed the same trend as seen before, with a distinct shift in the dominant frequency. In addition, the bubbling and slugging regimes could be clearly distinguished based on the dominant frequency.

As observed in Figure 5.18, the dominant frequency for the turbulent regime at a bed height of 21 cm was found to be 0.98 Hz. Once again, these results appeared to be close to the dominant frequency of the slugging regime. However, it should be noted that several repeat measurements were performed. In addition, the turbulent regime displayed the largest amplitude peak from all investigated regimes. Experimental observations further revealed the presence of large, irregular shaped voids in the fluidized bed and this is a characteristic of turbulent conditions.

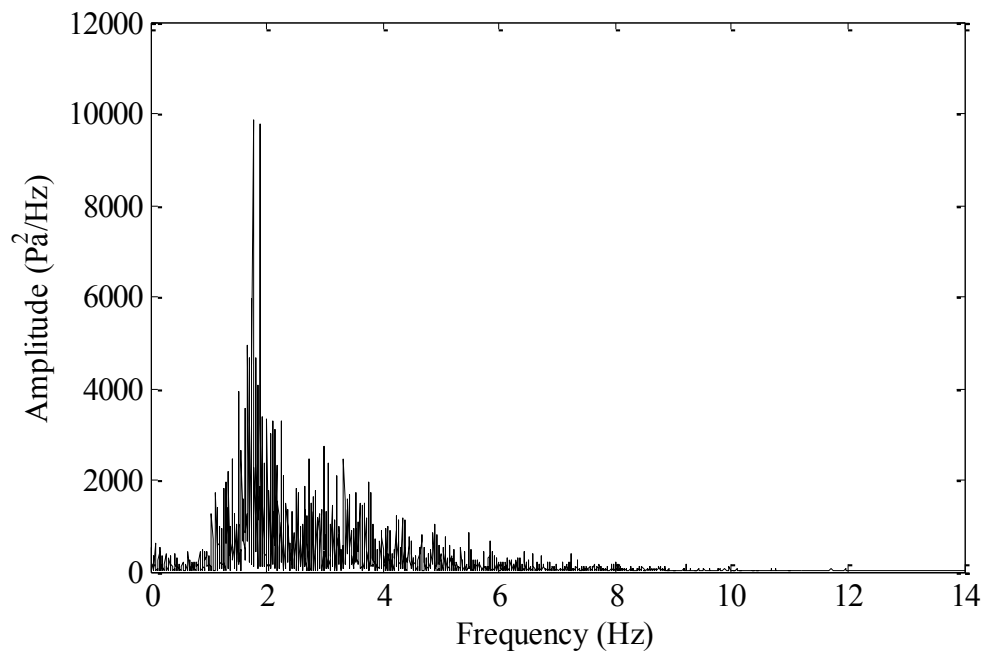


Figure 5.16 Power spectrum of the bubbling regime of sand particles in the 11 cm I.D column with a bed height of 21 cm

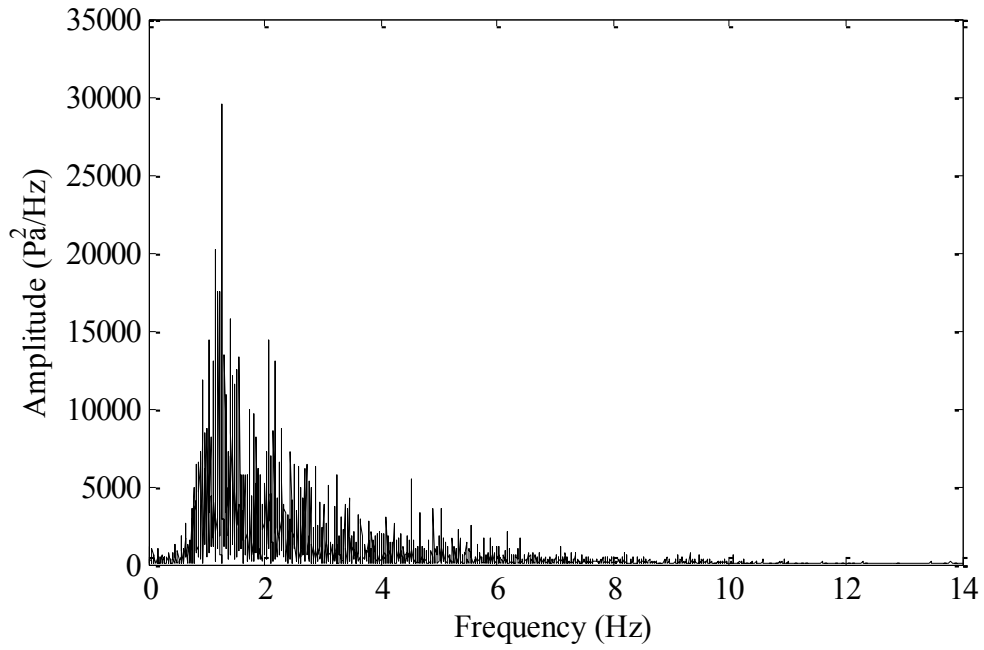


Figure 5.17 Power spectrum of the slugging regime of sand particles in the 11 cm I.D column with a bed height of 21 cm

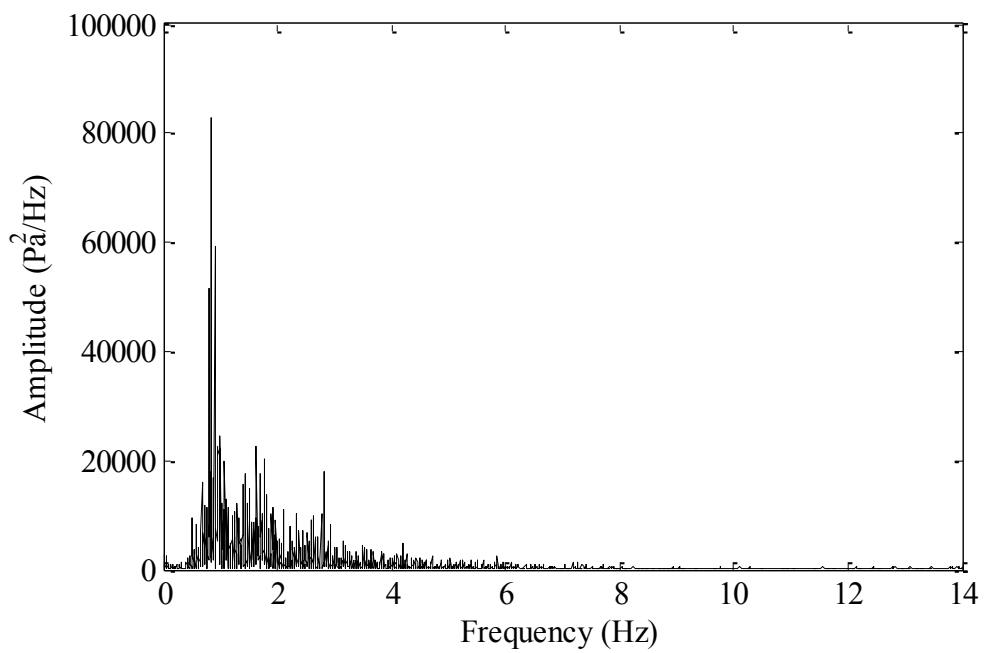


Figure 5.18 Power spectrum of the turbulent regime of sand particles in the 11 cm I.D column with a bed height of 21 cm

5.3.2.2 Plastic Beads

In order to understand the dynamic behaviour of different materials in a fluidized bed column, plastic beads were thereafter used in the 11 cm I.D column. As seen in Section 4.1.2.2, plastic beads were classified as Geldart Group D materials. It was found that only the bubbling and slugging regimes could be identified in this fluidized bed column. This was observed at all bed heights (11, 16, 21 and 28 cm). The power spectra results for the plastic beads at a bed height of 11 and 21 cm are presented in this section with the remaining results displayed in Appendix A. It was desired to produce spectra such as those seen here which are characterized as being narrow with clear evidence of a dominant frequency being present.

Figure 5.19 displays the power spectrum results for the bubbling regime for the plastic beads at a bed height of 11 cm. Under these operating conditions, the dominant frequency was observed to be around 2.54 Hz. Experimental observations indicated that bubbling occurred at a higher superficial gas velocity as compared to when sand particles were used. Furthermore, bubbling was also observed to occur at approximately 4 to 5 cm above the distributor plate which was in agreement with the behaviour of Geldart Group D particles.

For the slugging regime under the same conditions, the dominant frequency was determined as approximately 1.83 Hz. The power spectrum for the slugging regime is presented in Figure 5.20. It could be seen that the two regimes could clearly be differentiated based on the dominant frequency component. Analysis of both spectra revealed the same trend that was identified before. There was a visible shift in the dominant frequency from the bubbling to slugging regime and the amplitude of the spectra was greater for the slugging regime. This implied a change in the dynamics of the system as well as the formation of larger gas voids (roughly the size of the diameter of the column) in the slugging regime.

Under the operating conditions, the turbulent regime could not be achieved due the requirement of excessive gas velocities as well as the column height being a restricting factor. In order to operate in the turbulent regime, either a taller column was required or a cyclone was necessary in order to ensure that entrained material could be circulated back to the bed. However, this was not implemented on the 11 cm I.D column as there were doubts as to whether the column could support a cyclone.

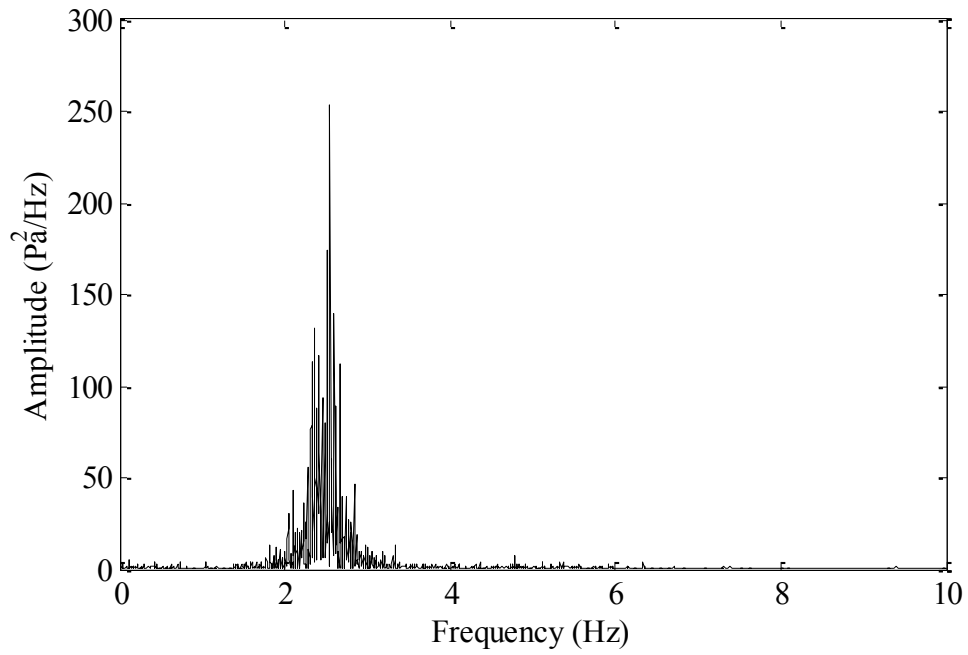


Figure 5.19 Power spectrum of the bubbling regime of plastic beads in the 11 cm I.D column with a bed height of 11 cm

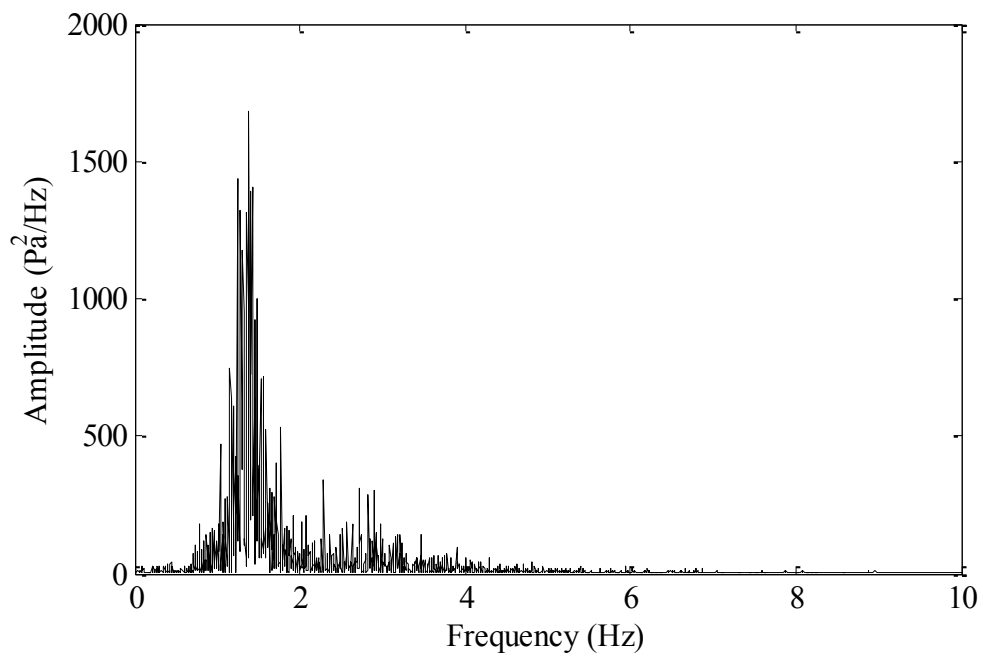


Figure 5.20 Power spectrum of the slugging regime of plastic beads in the 11 cm I.D column with a bed height of 11 cm

An increase in bed height led to the spectra represented in Figures 5.21 and 5.22 for the bubbling and slugging regimes respectively. Figure 5.21 shows the power spectrum for the bubbling regime for the plastic beads at a bed height of 21 cm. In this instance, the dominant frequency was identified at approximately 1.36 Hz. As observed previously, the amplitude of the spectra for the bubbling regime was smaller than the amplitude of the spectra from the slugging regime. This was in accordance to the work of van Ommen et al. (2011) who found that the gas voids formed in the bubbling regime were much smaller than the voids formed in the slugging regime. This implied that in the bubbling regime, a smaller number of particles were moved during their ascent which effectively resulted in less movement at the bed surface and a smaller amplitude. The dominant frequency for the slugging regime, as seen in Figure 5.22, was evaluated as approximately 1.14 Hz. It could be seen that there was a distinct shift in the dominant frequency for both regimes at the increased bed height.

Results for the bed heights of 16 and 28 cm exhibited the same trend with the dominant frequency becoming smaller as the bed height was increased. This can be seen in Appendix A. The dominant frequencies for the bubbling and slugging regimes were verified at 2.11 and 1.35 Hz for a bed height of 16 cm while a bed height of 28 cm indicated dominant frequencies of 1.17 and 0.81 Hz respectively.

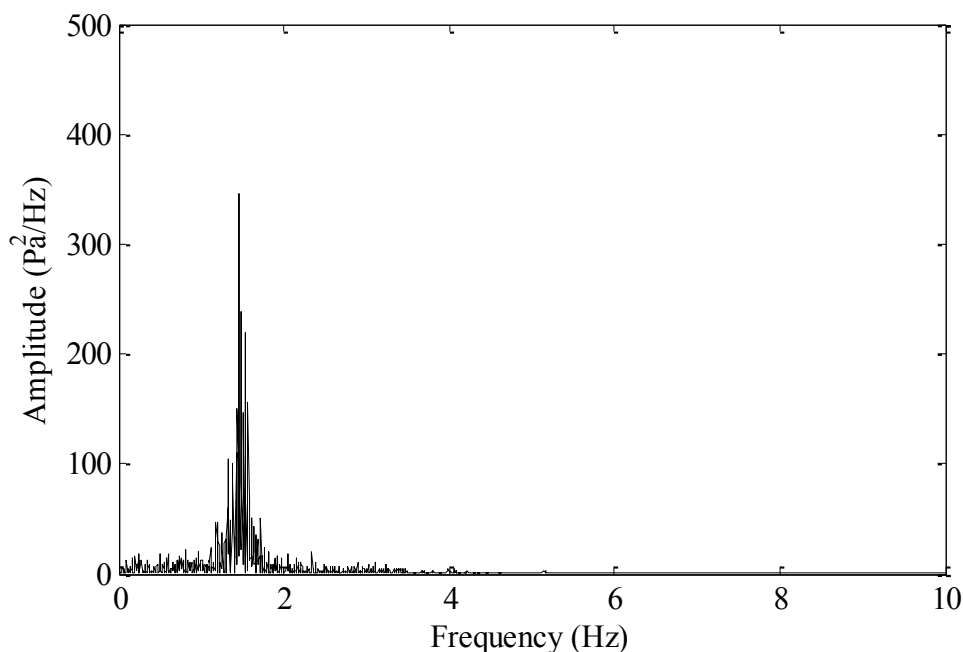


Figure 5.21 Power spectrum of the bubbling regime of plastic beads in the 11 cm I.D column with a bed height of 21 cm

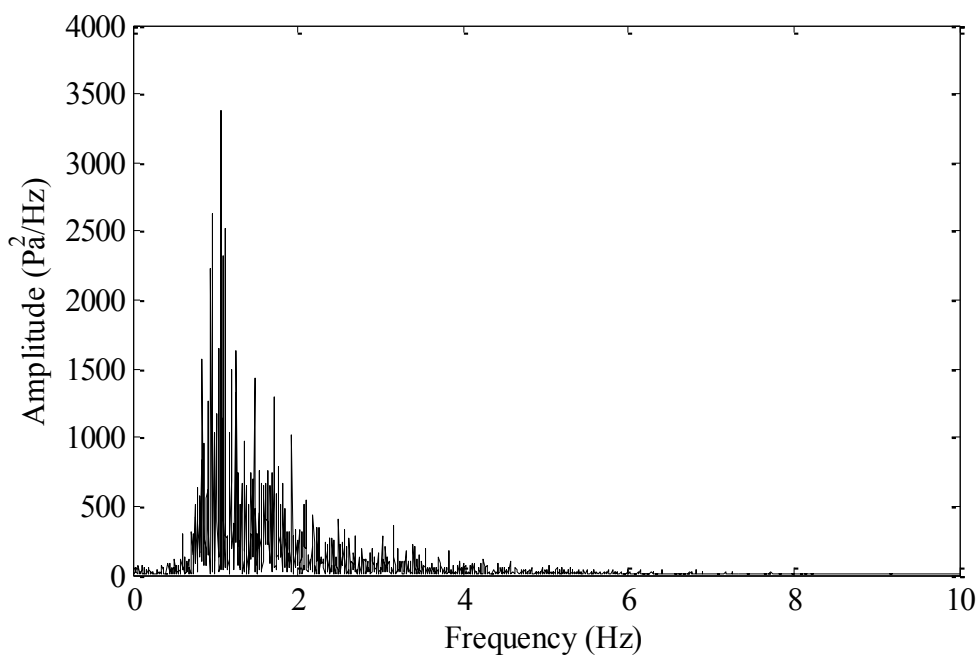


Figure 5.22 Power spectrum of the slugging regime of plastic beads in the 11 cm I.D column with a bed height of 21 cm

5.3.2.3 Spent FCC

As mentioned in Section 4.1.1, spent FCC plays a vital role in fluid catalytic processes in industry. As a result, experimental measurements using this material will provide essential information which could assist in improving the understanding of the behaviour of these materials. However, analysis in the frequency domain using spent FCC is not often performed and this is largely due to the difficulty in obtaining the material from industry. In this work, spent FCC was obtained from Sasol Ltd. Spent FCC represents Geldart Group A particles and the behaviour for these particles in the 11 cm I.D column is presented below.

It was found that the spent FCC particles fluidized very differently from the sand particles and plastic beads. Fluidization was observed to occur at very low superficial gas velocities with a noticeable bed expansion identified prior to the formation of bubbles. With an increase in gas velocity, bubbles that formed and split frequently were observed. These characteristics are typical for Geldart Group A powders.

Experimental measurements further revealed that the only regime that could be achieved was the bubbling regime. Higher gas velocities merely resulted in loss of material due to entrainment. In addition, at higher gas velocities, the catalyst particles were observed to stick to the walls of the column due to static charges. Figure 5.23 represents the power spectrum for the bubbling regime at a bed height of 11 cm. An important characteristic was evident from the power spectra. This was the presence of a frequency component of higher amplitude which was almost located at the centre of the spectrum. This information is significant as it means that pressure fluctuation signals from industry can be used to identify different fluidization states. The dominant frequency under these conditions was determined as 7.47 Hz.

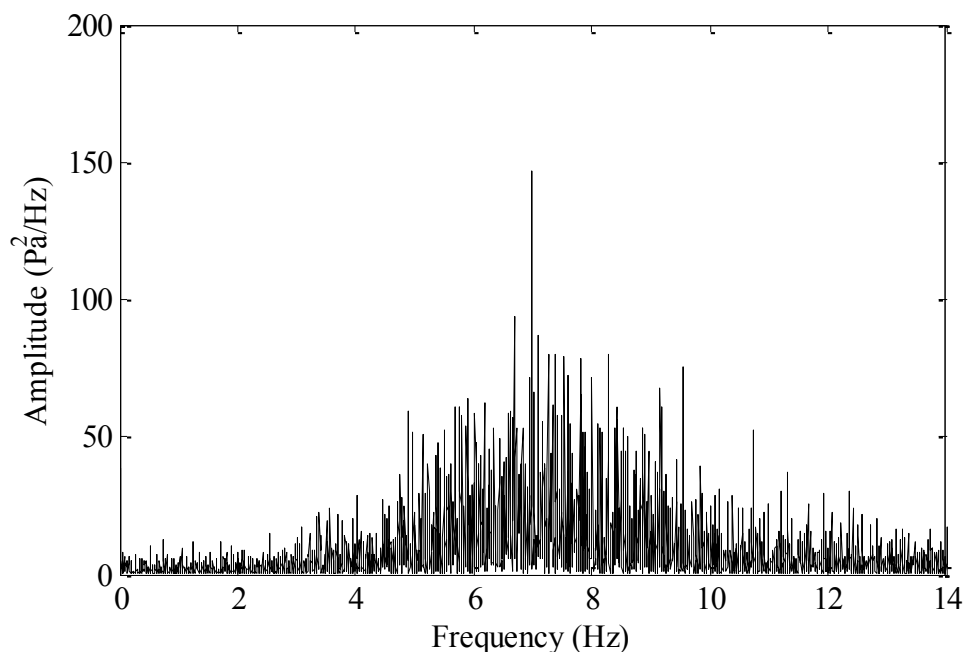


Figure 5.23 Power spectrum of the bubbling regime of spent FCC in the 11 cm I.D column with a bed height of 11 cm

An increase in bed height had the same influence that was observed for the sand particles and plastic beads. There was a distinct shift in the dominant frequency with the amplitude being greater at a higher bed height. Figure 5.24 shows the power spectrum profile for the bubbling regime using spent FCC at a bed height of 16 cm. It could be seen that the dominant frequency was less than the peak frequency that was observed at a bed height of 11 cm. The dominant frequency under these conditions was found to be approximately 5.22 Hz.

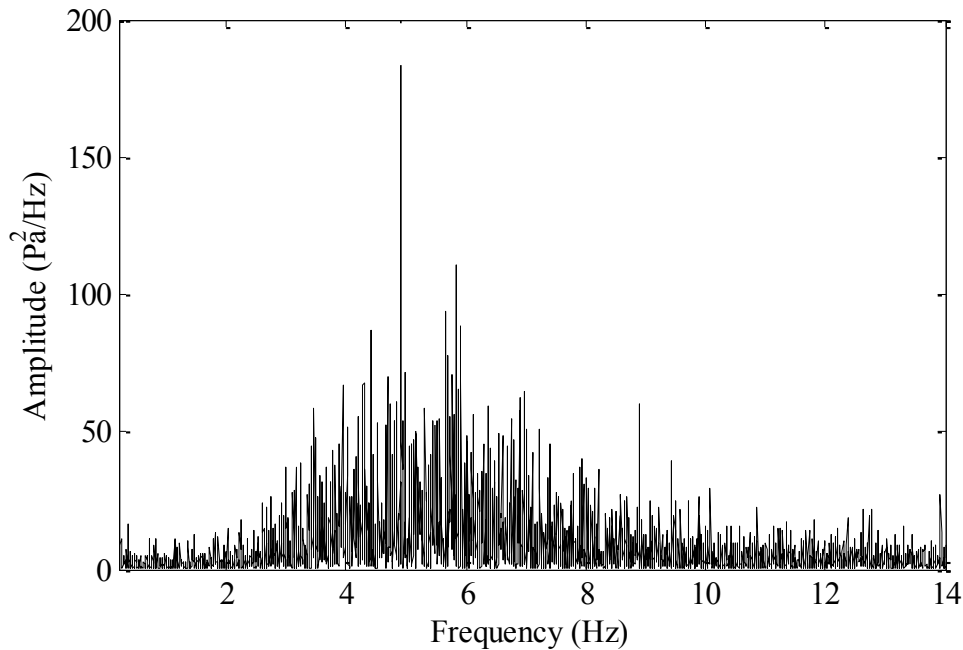


Figure 5.24 Power spectrum of the bubbling regime of spent FCC in the 11 cm I.D column with a bed height of 16 cm

5.3.3 Fluidized bed 3 (Internal diameter of 29 cm and height of 507.5 cm)

An important contribution of this dissertation was to focus on the fluidization behaviour in different fluidized bed columns. The behaviour in the 5 and 11 cm I.D columns have been presented previously and this section will focus on the power spectra results for the 29 cm I.D column. The presence of a dominant frequency in this large column could provide important information on the potential of using this technique in industrial applications in which fluidized beds are large in size.

5.3.3.1 Sand Particles

The power spectra profile for the sand particles in the 29 cm I.D fluidized bed column are presented below. Like before, in order to determine the effect of the bed height on the dominant frequency, two bed heights of 32 and 80 cm were investigated. The pressure fluctuation signals were observed to be significant (close to 160 kPa) in the 29 cm I.D column and largely due to limitations in the pressure transmitter (operating range of 0 to 160 kPa), the bubbling regime was the only regime achieved in this column.

Figure 5.25 represents the profile for the sand particles at a bed height of 32 cm. An important observation on the clear evidence of a single dominant frequency can be made. In this instance, the dominant frequency was observed to occur at a very low frequency of approximately 0.0363 Hz. Experimental observations indicated that the fluidized bed behaved like a typical bubbling bed. Formation of multiple bubbles of small sizes were seen as well as uniform bubble distribution throughout the bed.

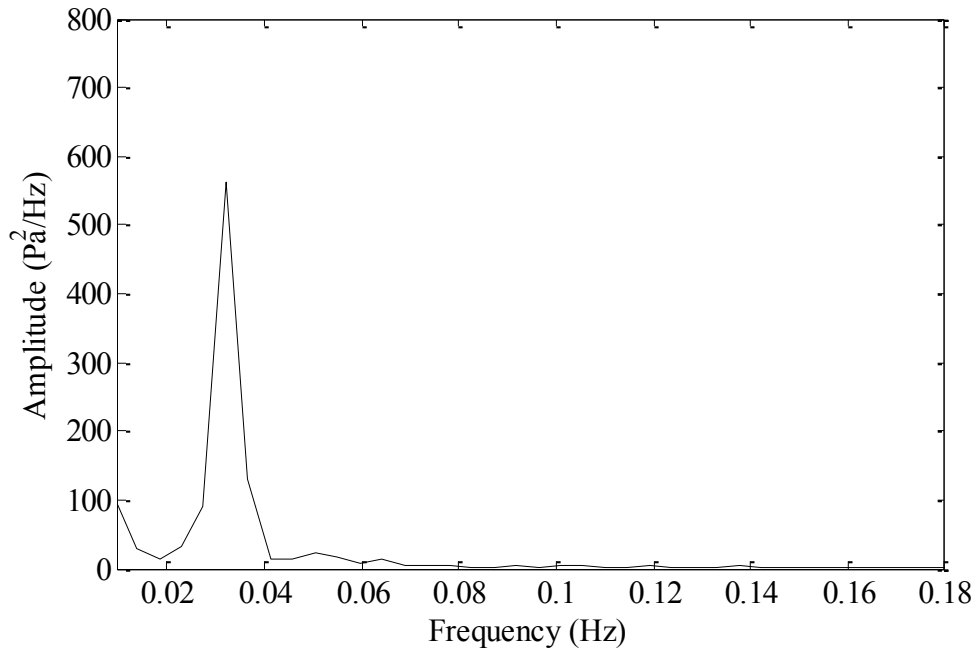


Figure 5.25 Power spectrum of the bubbling regime of sand particles in the 29 cm I.D column with a bed height of 32 cm

Figure 5.26 represents the power spectrum of the sand particles for the bubbling regime at a bed height of 80 cm. The dominant frequency was found to be marginally smaller at approximately 0.0264 Hz. This behaviour did follow the trend that was seen for all materials thus far with the dominant frequency being smaller at higher bed heights. However, additional frequency components were identified in the power spectra at a bed height of 80 cm. These peaks were evident at frequencies of approximately 0.06 and 0.085 Hz respectively. The dominant frequency represents the frequency of the bulk of the bubbles whereas the smaller frequency peaks could be due to single particles being present in minor numbers.

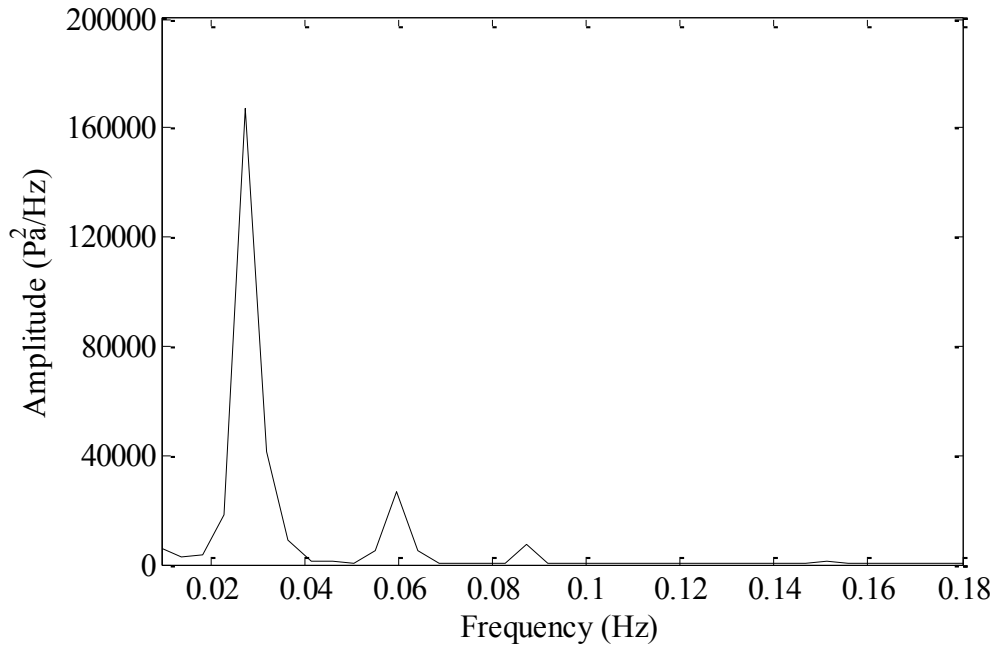


Figure 5.26 Power spectrum of the bubbling regime of sand particles in the 29 cm I.D column with a bed height of 80 cm

5.3.3.2 Other Materials

The Geldart Group A and D particles could not be employed in the 29 cm I.D fluidized bed column. This was due to the restriction on the WIKA model P30 pressure transmitter, which was only capable of operating in the pressure range of 0 to 160 kPa as well as the lack of sufficient material for experimental measurements to be conducted in the 29 cm I.D column.

5.3.4 Summary of frequency domain analysis

In an attempt to provide a clearer indication on the trend that was observed in each fluidized bed column, the dominant frequencies were compared against the aspect ratio and a summary of the results is presented in this section. As mentioned in Section 2.1.2, the aspect ratio is defined as the ratio of the bed height to the column diameter (L/D). As a result, an understanding of the dominant frequency trend at different aspect ratios improves our knowledge on the dynamics of a fluidized bed. Ideally, the relationship between dominant frequencies and aspect ratio should be independent of column diameter as it is a ratio that is being considered. However, experimental results indicated that there was a significant difference in the relationship between

dominant frequencies and aspect ratios for different fluidized bed columns. This implied that the dynamics in the different columns were greatly different with the results being column specific. Figure 5.27 represents the relationship between dominant frequency and L/D ratio for the slugging and turbulent regimes in the 5 cm I.D column. The trend that was seen was that an increase in the L/D ratio resulted in a distinct drop in the dominant frequency. This was valid for both fluidization regimes. In industry, a high L/D ratio is not actually desired as this would mean a greater amount of material is required and this would increase the operating costs quite significantly. The reason for the choice of high ratios in the 5 cm I.D column was largely due to the small column diameter and the difficulty in achieving and observing the different fluidization states i.e. the regimes were more apparent at higher bed heights which corresponded to a higher L/D ratio.

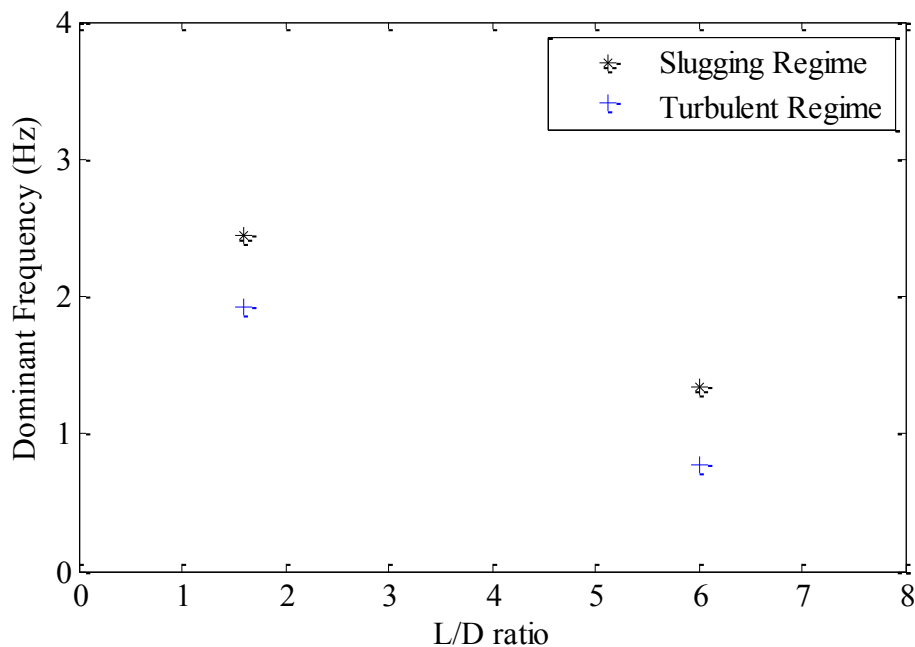


Figure 5.27 Summary of the relationship between dominant frequency and L/D ratio for the indicated regimes using sand in the 5 cm I.D column

The trend in the 11 cm I.D column for sand, plastic beads and spent FCC is presented below. Figure 5.28 displays the relationship between the dominant frequency and L/D ratio for the sand particles. Three fluidization regimes i.e. the bubbling, slugging and turbulent regimes were achieved in the 11 cm I.D column. For all regimes, it could be seen that the same trend that was observed previously was present. The relationship between dominant frequency and L/D ratio appeared to be linear but more experimental measurements would be required to obtain a better

understanding on this relationship. In addition, for a specific L/D ratio, it was clear that there was a decrease in dominant frequency from the bubbling to the slugging to the turbulent regime.

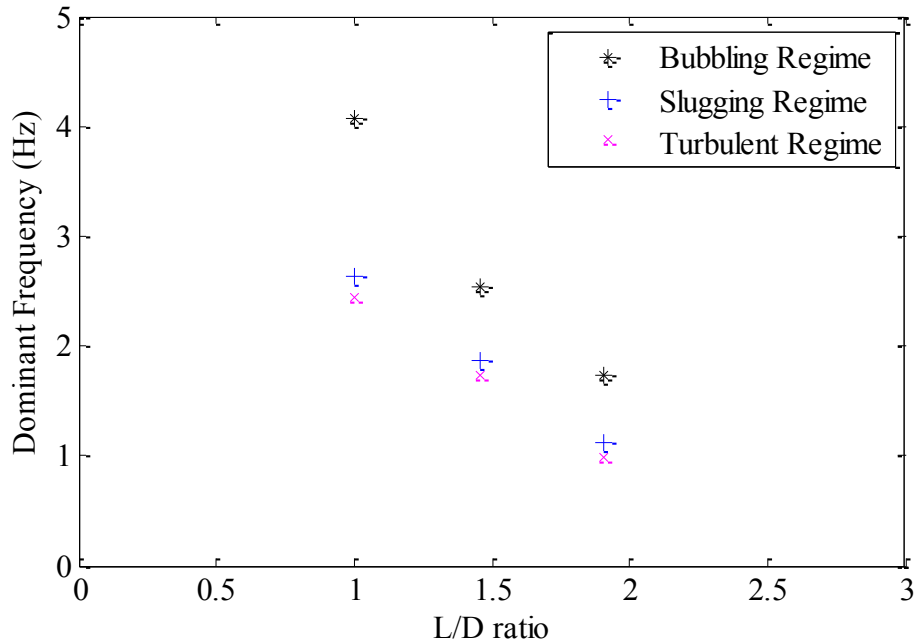


Figure 5.28 Summary of the relationship between dominant frequency and L/D ratio for the indicated regimes using sand in the 11 cm I.D column

For the plastic beads in the 11 cm I.D column, the relationship trend is presented in Figure 5.29. As mentioned previously, the bubbling and slugging regimes were the only regimes identified in the 11 cm I.D column. The behaviour pattern for the plastic beads followed that which was observed for the sand particles in both columns i.e. there was a noticeable decrease in dominant frequency for both regimes with increasing L/D ratio. Furthermore, the dominant frequency for the slugging regime was lower than the peak frequency of the bubbling regime. This was in agreement with the relationship trend that was identified thus far.

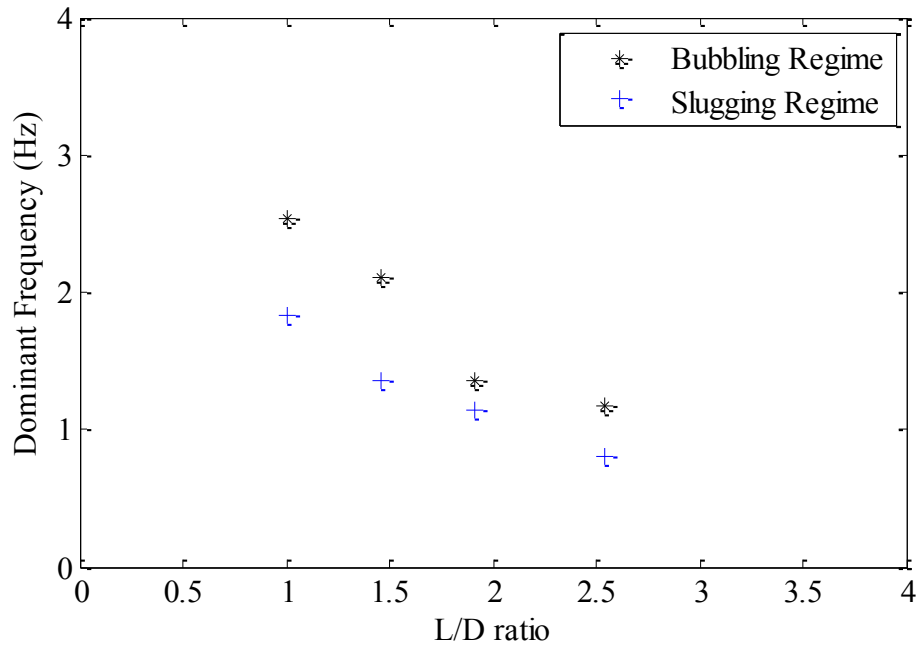


Figure 5.29 Summary of the relationship between dominant frequency and L/D ratio for the indicated regimes using plastic beads in the 11 cm I.D column

The relationship between the dominant frequency and L/D ratio for the catalyst in the 11 cm I.D column is shown in Figure 5.30 below. As mentioned in Section 5.3.2.3, the bubbling regime was the only regime that could be achieved in this column. This was due to entrainment as well as the particles sticking to the walls of the column at higher gas velocities. From Figure 5.30, it could be seen that the spent catalyst also exhibited the same trend with the dominant frequency occurring at a lower value with increasing L/D ratio. This could prove to be beneficial as the potential for predicting the dominant frequency for catalyst particles for a particular fluidization state may actually be possible. In order to improve the accuracy and reliability, more data points would be required. This would further provide a more definite indication on the graphical relationship that exists between the dominant frequency and L/D ratio.

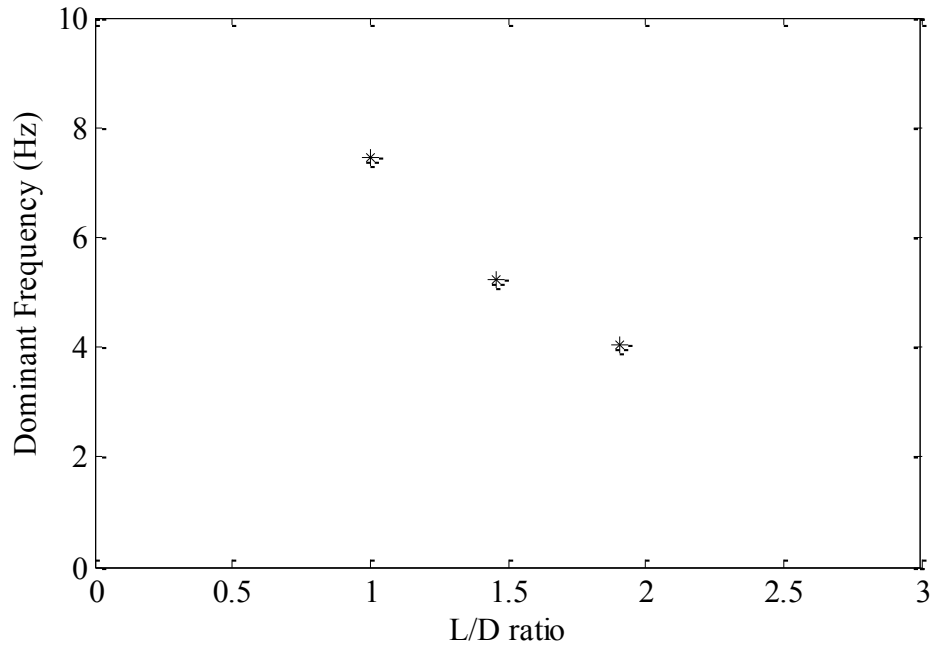


Figure 5.30 Summary of the relationship between dominant frequency and L/D ratio for the bubbling regime using spent FCC in the 11 cm I.D column

Figure 5.31 below represents the relationship between the dominant frequency and L/D ratio for the sand particles in the 29 cm I.D column. As mentioned previously, due to restrictions on the WIKA model P30 pressure transmitter, the bubbling regime was the only regime that could be achieved in the 29 cm I.D column. The relationship between the dominant frequency and L/D ratio in the 29 cm I.D column was in agreement with the trend that was observed for all materials in the previous two columns. In addition, the dominant frequency for the same regime at a similar L/D ratio indicated large differences between the three columns. This would imply that the relationship trend would be column specific. Hence, by determining the relationship between the dominant frequency and L/D ratio for a specific column, the conditions for the different regimes may be predicted. This could prove to be a useful tool in the understanding of the dynamic behaviour of various materials in fluidized bed systems.

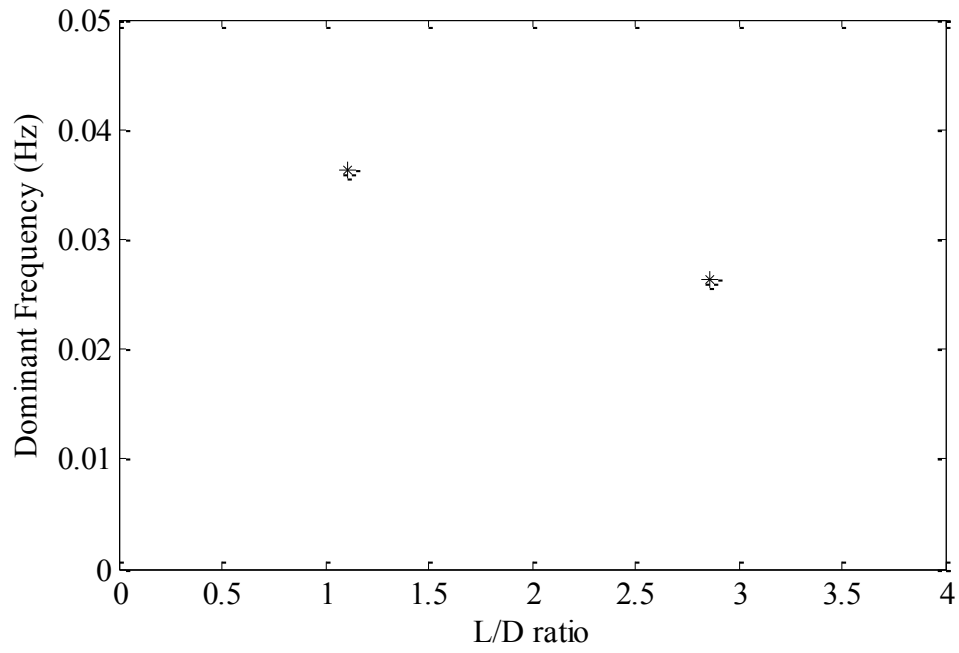


Figure 5.31 Summary of the relationship between dominant frequency and L/D ratio for the bubbling regime using sand particles in the 29 cm I.D column

6

CHAPTER 6

CONCLUSION

This dissertation was concerned with the time-series analysis of pressure fluctuation signals in gas-solid fluidized beds. This also included evaluating the suitability of using pressure fluctuation as a diagnostic tool to evaluate fluidized bed performance through identification of the different fluidization regimes. Analysis of the pressure fluctuation signals in the time domain was investigated. However, the main focus was to assess the viability of analysis of the pressure fluctuation in the frequency domain through the use of the FFT for different materials in different fluidized bed columns at various bed heights

The pressure fluctuation data was measured using a similar setup to the well-developed gas-solid fluidized bed apparatus employed by several researchers including van Ommen et al. (2010), Johnsson et al. (2000), Alberto et al. (2004) and Fan et al. (1981). Minor modifications included the use of three different fluidized bed columns as well as the use of a high frequency pressure transmitter which was capable of measuring pressure fluctuation signals in the range of 0 to 160 kPa. In order to validate correct operation of experimental equipment as well as procedures employed in this work, spectral analysis through the FFT, for the spent catalyst particles in the 11 cm I.D column at a bed height of 20.5 cm, served as a test system. There was excellent agreement between the experimental data and literature data of Alberto et al. (2004).

Analysis of pressure fluctuation data in the time domain often represents the simplest approach for the identification of the different fluidization regimes. Analysis in the time domain was conducted in the 11 cm I.D column at different bed heights with the Geldart Group A, B and D particles. The time-pressure behaviour for all regimes were observed to be very similar and differentiation between fluidization regimes was difficult to identify. This was evident for all materials with the only significant difference being in the amplitude and signal variation profile. Analysis using the standard deviation technique for the Geldart Group B particles revealed that this method was suitable to predict the regime transition from the bubbling to turbulent fluidization state. In addition, the transition velocity obtained from the standard deviation technique was found to be in close agreement with predicted values.

Analysis of the pressure fluctuation signals through the FFT and frequency domain analysis was proven to be a viable technique for identifying and distinguishing between fluidization regimes. The dependence between fluidizing behaviour and process variables, which included bed characteristics and fluidizing medium characteristics, was successfully identified. Analysis in the frequency domain was investigated in three different fluidized bed columns at various bed heights. In the 5 cm I.D column, the Geldart Group A and D particles did not indicate a dominant frequency regardless of the superficial gas velocity or material bed height. The Group A particles exhibited particulate fluidization behaviour while the behaviour of the Group D particles was attributed to the large particle diameter as well as the low column diameter to particle diameter ratio. The slugging and turbulent regimes for the Group B particles could clearly be distinguished based on a distinct peak frequency.

Results in the 11 cm I.D fluidized bed showed that all three Geldart Groups could undergo fluidization. For the Geldart Group A particles, the bubbling regime was successfully identified and distinguished at different bed heights. Group A particles were observed to fluidize very differently from the other two materials with a visible bed expansion seen prior to bubbling. Geldart Group B particles exhibited excellent fluidization behaviour with dominant frequencies clearly evident for the bubbling, slugging and turbulent regimes. For the Group D particles, dominant frequencies for the bubbling and slugging regimes were identified and eminent at different bed heights. It was further evident that the choice of material had a significant impact on the fluidizing behaviour and more so, the dominant frequency. This was apparent as different materials showed different dominant frequencies for the same fluidization regimes. This was valid for all bed heights.

Results from the 29 cm I.D column revealed that only the Geldart Group B particles could undergo fluidization. Measurements could not be performed with the Group A and D particles and this was due to lack of sufficient material as well as restrictions on the operating range of the WIKA model P30 pressure transmitter. Once again, the Geldart Group B particles displayed excellent fluidization behaviour with the bubbling regime clearly visible. Measurements were conducted at two bed heights of 32 and 80 cm with a single, distinct peak frequency evident.

Analysis in the frequency domain further revealed that factors such as particle properties as well as column properties, which included column diameter and bed height, had a significant influence on the dynamics of the bed. This was identified by the change in the amplitude of the pressure fluctuation signals together with a shift in the dominant frequency as the operating conditions were varied. The relationship between dominant frequency and the L/D ratio was found to be inversely proportional with an increase in the L/D ratio leading to a decrease in the dominant frequency. This trend was observed for all particles and all regimes. It was further observed that the relationship between these two variables were column specific as there were large differences in dominant frequency for the same regime with identical particles at similar L/D ratios.

The use of high frequency pressure measurements provides the added advantage in that it is not limited to academic research. Industrial application is definitely viable as these pressure sensors can be employed in a robust and cost effective way. This implies that spectral analysis in conjunction with an understanding of the relationship between dominant frequency and L/D ratio could play an important role in understanding the hydrodynamic nature of a system which could prove to be an important diagnostic tool for identification of different fluidization regimes in industry.

7

CHAPTER 7

RECOMMENDATIONS

In order to obtain superior quality experimental results, improvements for the efficiency and operation of the gas-solid fluidized bed apparatus are required. In addition, careful consideration needs to be taken on the troubleshooting and monitoring of the operation of the apparatus. Therefore, the following recommendations are proposed below:

1. Future work investigating the effect of bed material and bed height should be conducted in a fluidized bed with a larger diameter. This will provide information on the influence of the column diameter on fluidization behaviour. Furthermore, a comparison with this work will provide information on the possibility of scale-up as well as issues that might be encountered.
2. Other analysis techniques such as methods for analysis in the state space domain should be employed. This will complement the work obtained in the time domain and frequency domain. It will further ensure a comparison between measurements in the time domain, frequency domain and state space domain.

REFERENCES

- Abdullah, M. Z., Husain, Z. & Yin Pong, S. L., 2003. Analysis of cold flow fluidization test results for various biomass fuels. *Biomass and Bioenergy*, 24(6), pp. 487-494.
- Alberto, C., Felipe, S. & Rocha, S. C. S., 2004. Time Series Analysis of Pressure Fluctuation in Gas-solid Fluidized Beds. *Brazilian Journal of Chemical Engineering*, 21(03), pp. 497-507.
- Andreux, R., Gauthier, T., Chaouki, J. & Simonin, O., 2005. New description of fluidization regimes. *American Institute of Chemical Engineers*, Volume 51, pp. 1125-1130.
- Arnaldos, J. & Casal, J., 1996. Prediction of transition velocities and hydrodynamical regimes in fluidized beds. *Powder Technology*, Volume 86, pp. 285-298.
- Baeyens, J. & Geldart, D., 1974. An Investigation into Slugging Fluidized Beds. *Chemical Engineering Science*, Volume 29, p. 255.
- Basu, P., 2006. *Combustion and gasification in fluidized beds*. Nova Scotia: CRC Press.
- Benyahia, F. & O'Neill, K. E., 2005. Enhanced Voidage Correlations for Packed Beds of Various Particle Shapes and Sizes. *Particulate Science & Technology*, Volume 23, pp. 169-177.
- Bi, H. T., 2007. A critical review of the complex pressure fluctuation phenomenon in gas-solids fluidized beds. *Chemical Engineering Science*, Volume 62, pp. 3473-3493.
- Bi, H. T., Ellis, N., Abba, I. A. & Grace, J. R., 2000. A state-of-the-are review of gas-solid turbulent fluidization. *Chemical Engineering Science*, Volume 55, pp. 4789-4825.
- Bi, H. T. & Grace, J. R., 1995. Regime transitions affecting gas-solids suspensions and fluidized beds. *Transactions of the Institution of Chemical Engineers*, Volume 73, pp. 154-161.
- Bi, H. T., Grace, J. R. & Lim, K. S., 1995. Transition from bubbling to turbulent fluidization. *Industrial and Engineering Chemistry Research*, Volume 34, pp. 4003-4008.

- Bourgeois, P. & Grenier, P., 1968. The ratio of terminal velocity to minimum fluidising velocity for spherical particles. *The Canadian Journal of Chemical Engineering*, Volume 46, pp. 325-328.
- Briens, L. A. & Briens, C. L., 2002. Cycle detection and characterization in chemical engineering. *American Institute of Chemical Engineers*, Volume 48, pp. 970-980.
- Briens, L. A. & Ellis, N., 2005. Hydrodynamics of three-phase fluidized bed systems examined by statistical, fractal, chaos and wavelet analysis methods. *Chemical Engineering Science*, Volume 60, pp. 6094-6106.
- Briangos, J. V., Aragon, J. M. & Palancar, M. C., 2007. Phase space structure and multi-resolution analysis of gas-solid fluidized bed hydrodynamics: Part II: Dynamic Analysis. *Chemical Engineering Science*, Volume 62, pp. 2865-2879.
- Cai, P., Chen, S. P., Jin, Z. Q. & Wang, Z. W., 1989. Effect of operating temperature and pressure on the transition from bubbling to turbulent fluidization. *American Institute of Chemical Engineers*, 85(270), pp. 37-43.
- Chitester, D. C., Kornosky, R. M., Fan, L. & Danko, J. P., 1984. Characteristics of fluidization at high pressure. *Chemical Engineering Science*, Volume 39, pp. 253-261.
- Crowe, C. T., 2006. *Multiphase Flow Handbook*. Boca Raton, FL: CRC Press.
- Croxford, A. J. & Gilbertson, M. A., 2011. Pressure fluctuations in bubbling gas-fluidized beds. *Chemical Engineering Science*, Volume 66, pp. 3569-3578.
- Fan, L. T., Ho, T. C. & Hiraoka, S., 1981. Pressure FLuctuations in a Fluidized Bed. *American Institute of Chemical Engineers*, Volume 27, p. 388.
- Geldart, D., 1973. Types of gas fluidization. *Powder Technology*, 7(5), pp. 285-292.
- Geldart, D., 1986. *Gas Fluidization Technology*. Chichester: John Wiley & Sons Ltd.

- Geldart, D. & Baeyens, J., 1985. The Design of Distributors for Gas-Fluidized Beds. *Powder Technology*, Volume 42, p. 67.
- Grace, J. R., 1982. Fluidized bed hydrodynamics. In: G. Hestroni, ed. *Handbook of Multiphase Systems*. Washington,DC: Hemisphere, pp. 25-30.
- Guevara, D. E., 2010. *Bed height and material density effects on fluidized bed hydrodynamics, Master of Science in Engineering (Chemical Engineering) Thesis*, Iowa State University, Ames,Iowa.
- Guo, Q. J., Yue, G. X., Suda, T. & Sato, J., 2003. Flow characteristics in a bubbling fluidized bed at elevated temperature. *Chemical Engineering & Processing*, Volume 42, pp. 439-447.
- Gyan, R., Ntunka, M. G. & Carsky, M., 2014. Time-series analysis of pressure fluctuations in gas-solid fluidized beds. *The South African Journal of Chemical Engineers*, 19(3), pp. 9-21.
- Hartman, M., Trnka, O. & Svoboda, K., 2009. Use of Pressure Fluctuations to Determine Online the Regime of Gas-Solids Suspensions from Incipient Fluidization to Transport. *Institute of Chemical Process Fundamentals*, Volume 48, pp. 6830-6835.
- Hilal, N., Ghannam, M. T. & Anabtawi, M. Z., 2001. Effect of bed diameter, Distributor and Inserts on Minimum Fluidization Velocity. *Chemical Engineering Technology*, 24(2), pp. 161-165.
- Jin, Y., Yu, Z. Q., Wang, Z. W. & Cai, P., 1986. *A criterion for transition from bubbling to turbulent fluidization*. New York: Engineering Foundation.
- Johnsson, F., Svensson, A., Andersson, S. & Leckner, B., 1995. Fluidization regimes in boilers. In: *Fluidization VIII*. New York: Tours, pp. 129-136.
- Johnsson, F. et al., 2000. Characterization of Fluidization Regimes by Time-Series Analysis of Pressure Fluctuations. *International Journal of Multiphase Flow*, Volume 26, p. 663.
- Kumar, A., Gupta, A. K. & Kumar, A., 2014. Momentum Transfer in Fluidized Bed. *International Journal of Engineering and Technical Research*, 2(11), pp. 299-303.

- Kunii, D. & Levenspiel, O., 1991. *Fluidization Engineering*. New York: John Wiley & Sons.
- Lee, G. S. & Kim, S. D., 1990. Bed expansion characteristics and transition velocity in turbulent fluidized beds. *Powder Technology*, Volume 62, pp. 207-215.
- Liao, L., 2013. *Influence of Particle Shape and Bed Height on Fluidization*, Master of Science in Engineering (Chemical Engineering) Thesis, University of Florida, Gainesville, Florida.
- Lim, C. N., Gilbertson, M. A. & Harrison, A. J. L., 2007. Bubble distribution and behaviour in bubbling fluidised beds. *Chemical Engineering Science*, Volume 62, pp. 56-69.
- Nakajima, M. et al., 1991. Bubble fraction and voidage in an emulsion phase in the transition to a turbulent fluidized bed. In: P. Basu, M. Horio & M. Hasatani, eds. *Circulating Fluidized Bed*. Oxford: Pergamon Press, pp. 79-84.
- Pell, M., 1990. *Gas Fluidization*. 7th ed. New York: Elsevier Science Publishers.
- Ramos, G. C., Garcia, R. M., Prieto, J. J. & Guardiola, J. S., 2002. Minimum fluidization velocities for gas-solid 2D beds. *Chemical Engineering and Processing*, 41(9), pp. 761-764.
- Reina, J., Velo, E. & Puigjaner, L., 2000. Predicting the minimum fluidization velocity of polydisperse mixtures of scrap-wood particles. *Powder Technology*, Volume 111, pp. 245-251.
- Sadeghbeigi, R., 2000. *Fluid Catalytic Cracking Handbook*. 2nd ed. Texas: Gulf Publishing.
- Sasic, S., Leckner, B. & Johnsson, F., 2007. Characterization of fluid dynamics of fluidized beds by analysis of pressure fluctuations. *Progress in Energy and Combustion Science*, 33(5), pp. 453-496.
- Scala, F., 2013. *Fluidized bed technologies for near-zero emission combustion and gasification*. 2nd ed. Cambridge: Woodhead Publishing.
- Singh, R. K. & Roy, G. K., 2008. Prediction of minimum slugging velocity, bubbling bed index and range of bubbling fluidization in cylindrical and non-cylindrical gas-solid fluidized beds. *Indian Journal of Chemical Technology*, Volume 15, pp. 85-89.

- Sobrino, C., Sanchez-Delgado, S., Garcia-Hernando, N. & de Vega, M., 2008. Standard deviation of absolute and differential pressure fluctuations in fluidized beds of group B particles. *Chemical Engineering Research and Design*, Volume 86, pp. 1236-1242.
- Stewart, P. S. B. & Davidson, J. F., 1967. Slug flow in fluidized beds. *Powder Technology*, 61(1), pp. 61-80.
- van der Schaaf, J. et al., 2004. Similarity between chaos analysis and frequency analysis of pressure. *Chemical Engineering Science*, Volume 59, pp. 1829-1840.
- van der Stappen, M. L. M., 1996. *Chaotic Hydrodynamics of Fluidized Beds, Doctor of Philosophy in Engineering (Chemical Engineering) Thesis*, Delft University Press, Delft, Netherlands.
- van Ommen, J. R. et al., 2011. Time-series analysis of pressure fluctuations in gas-solid fluidized beds-a review. *International Journal of Multiphase Flow*, 37(5), pp. 403-428.
- van Ommen, J. R., Schouten, J. C., van der Stappen, M. L. M. & van der Bleek, C. M., 2000. Response characteristics of probe-transducer systems for pressure measurements in gas-solid fluidized beds: how to prevent pitfalls in dynamic pressure measurements. *Powder Technology*, Volume 113, p. 217.
- Verloop, J. & Heertjes, P. M., 1974. Periodic Pressure Fluctuations in Fluidized Beds. *Chemical Engineering Science*, Volume 29, pp. 1035-1042.
- Villa Briongos, J., Aragón, J. M. & Palancar, M. C., 2006. Phase space structure and multi-resolution analysis of gas–solid fluidized bed hydrodynamics: part I – the EMD approach. *Chemical Engineering Science*, Volume 61, pp. 6969-6980.
- Villa Briongos, J., Aragón, J. M. & Palancar, M. C., 2007. Phase space structure and multi-resolution analysis of gas–solid fluidized bed hydrodynamics: part II: dynamic analysis. *Chemical Engineering Science*, Volume 62, pp. 2865-2879.
- Wen, C. Y. & Yu, Y. H., 1966. A generalized method for predicting the minimum fluidization velocity. *American Institute of Chemical Engineers*, Volume 12, pp. 610-612.

Wiens, J. S., 2010. *Experimental and Modeling Study of a Cold-Flow Fluid Catalytic Cracking Unit Stripper*, Doctor of Philosophy in Engineering (Chemical Engineering) Thesis, University of Saskatchewan, Saskatoon, Canada.

Yang, W. C., 1976. *Proceedings of the Pneumotransport 3*. Bedford, BHRA Fluid Engineering, pp. 28-40.

Yang, W. C., 2003. Bubbling Fluidized Beds. In: W. C. Yang, ed. *Handbook of Fluidization and Fluid-Particle Systems*. 1st ed. New York: Marcel Dekker, pp. 53-112.

Yates, J. G., 1983. *Fundamentals of Fluidized-Bed Chemical Processes*. London: Butterworths.

Zhao, G. B., Chen, J. Z. & Yang, Y. R., 2001. Predictive model and deterministic mechanism in a bubbling fluidized bed. *American Institute of Chemical Engineers*, Volume 47, pp. 1524-1532.

APPENDIX A

ADDITIONAL FREQUENCY DOMAIN RESULTS

The results presented in this section are based on analysis in the frequency domain through the use of the FFT. These results are based on Fluidized Bed 2 with internal diameter of 11 cm and total height of 153 cm. In an attempt to understand the influence of the bed height on the dominant frequency, experimental measurements were conducted at several bed heights. In order to ensure comparison, results for two bed heights for each material was presented in Chapter 5 with the remaining results being presented below.

Sand Particles

The sand particles behaved as typical Geldart Group B materials which are known to fluidize easily. The multiple bubbling, slugging and turbulent regimes were identified for the 11 cm I.D column at a bed height of 16 cm. Figure A.1 represents the bubbling regime which was found to display a dominant frequency of approximately 2.53 Hz. The broad spectra was a consequence of multiple bubbles being present in the fluidized bed. In the case of the slugging regime, the dominant frequency was observed to shift to around 1.87 Hz. The power spectra for the slugging regime is represented by Figure A.2. For the turbulent regime, as observed in Figure A.3, the dominant frequency was estimated at 1.73 Hz. It was found that the behaviour displayed at a bed height of 16 cm followed the trend of the results presented in Section 5.3.2.1.

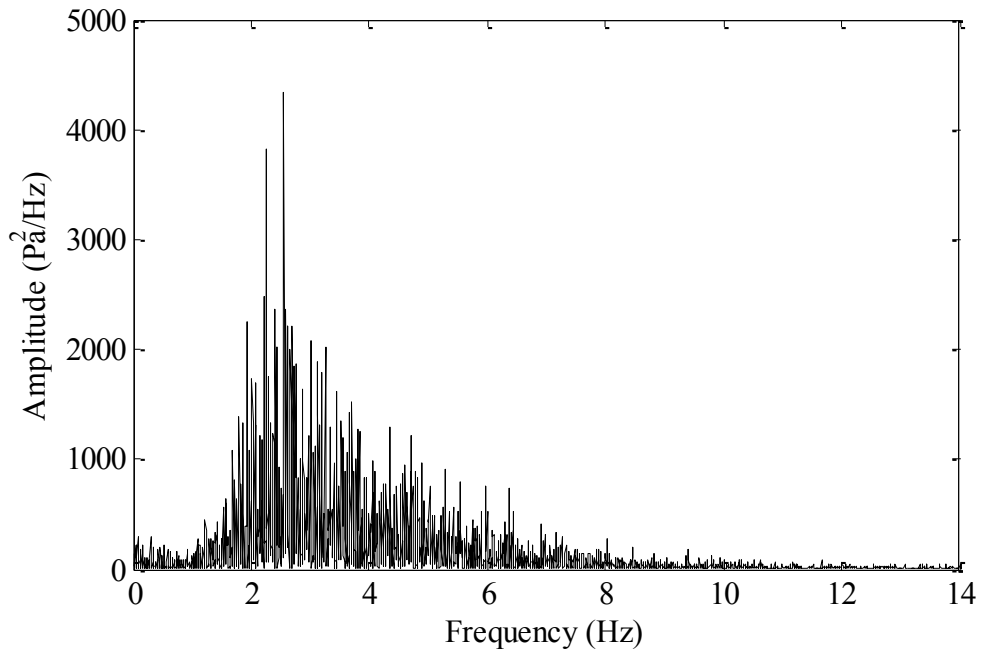


Figure A.1 Power spectra of the bubbling regime of sand particles in the 11 cm I.D column with a bed height of 16 cm

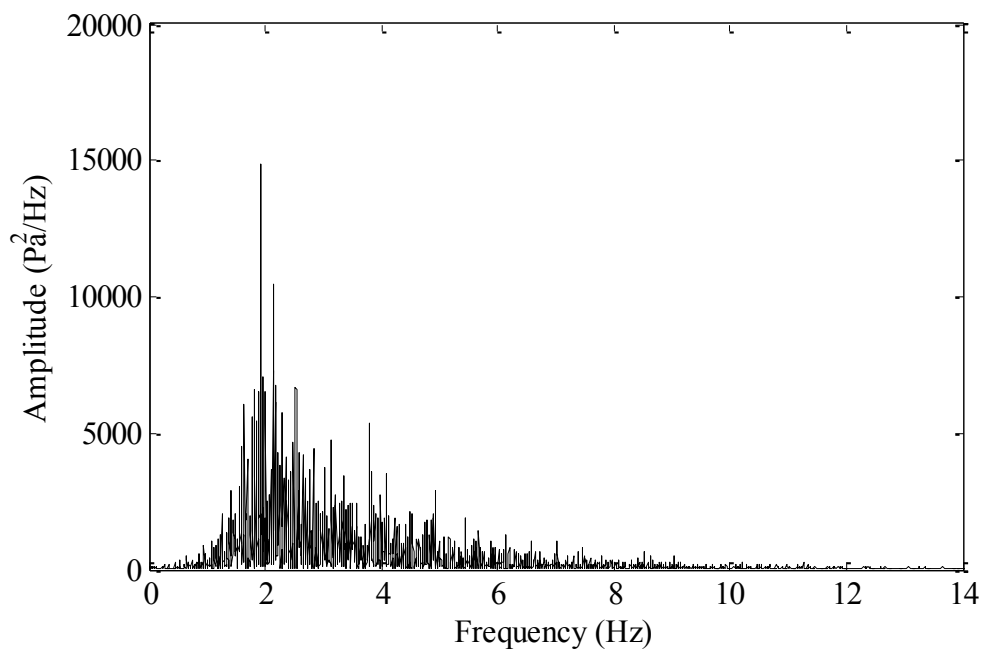


Figure A.2 Power spectra of the slugging regime of sand particles in the 11 cm I.D column with a bed height of 16 cm

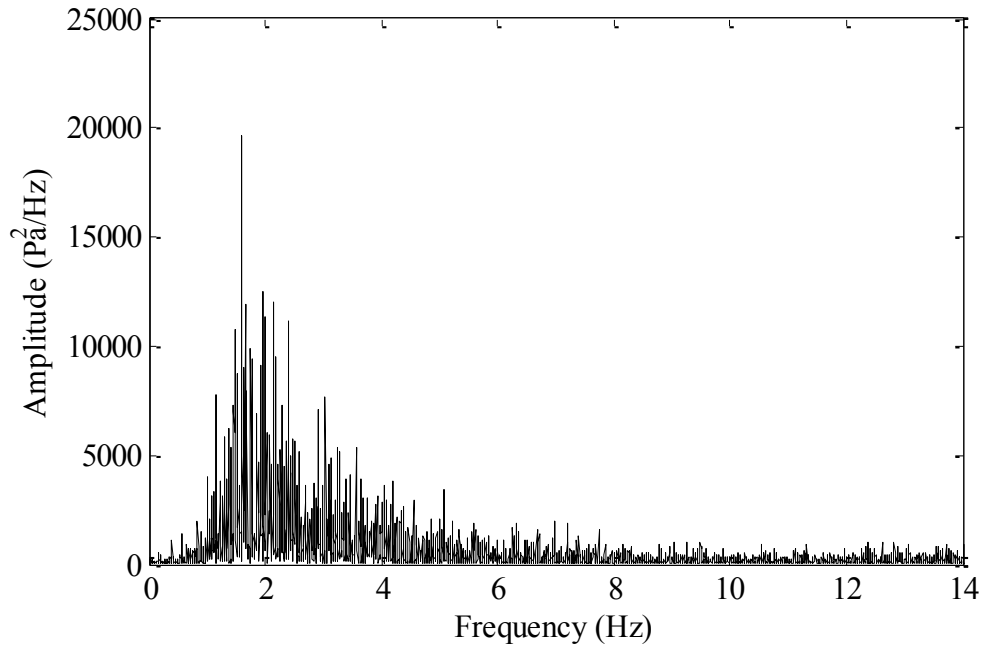


Figure A.3 Power spectra of the turbulent regime of sand particles in the 11 cm I.D column with a bed height of 16 cm

Plastic Beads

The plastic beads exhibited typical Geldart Group D material behaviour with fluidization only taking place at higher gas velocities. In addition, bubble formation was observed to occur 4 to 5 cm above the distributor plate. For plastic beads, experimental measurements were conducted at four different bed heights with the results of 11 and 21 cm displayed in Section 5.3.2.2. In order to prevent repetition of results, the two extreme conditions were compared in Section 5.3.2.2 with the additional results (bed heights of 16 and 28 cm) being presented in this section.

The power spectra for the bubbling and slugging regime at a bed height of 16 cm is shown in Figures A.4 and A.5 below. As seen in Figure A.4, the dominant frequency for the bubbling regime was 2.11 Hz. The dominant frequency for the slugging regime was found to be approximately 1.35 Hz, as represented by Figure A.5.

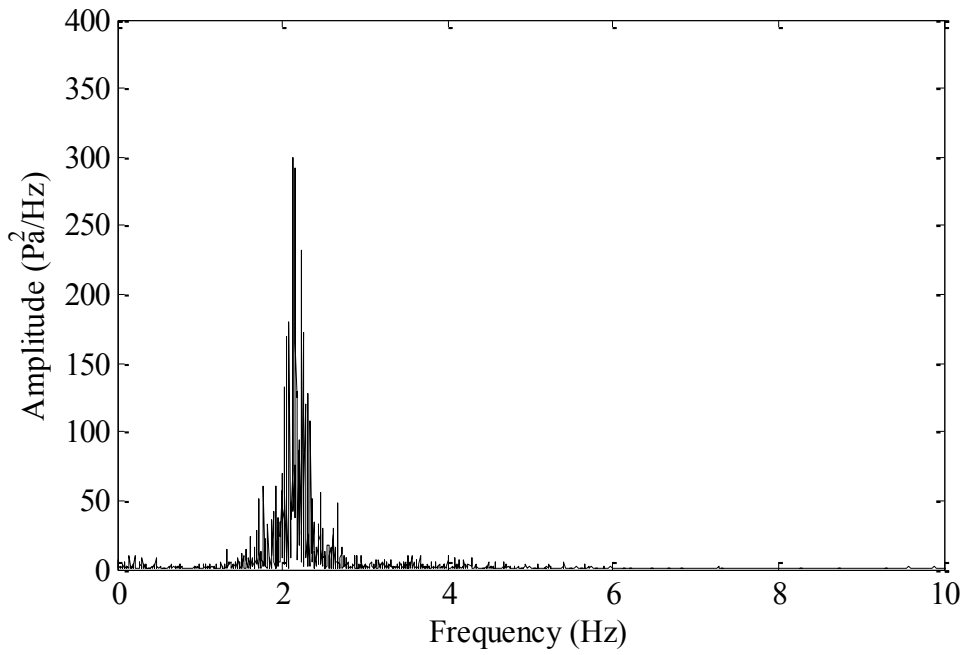


Figure A.4 Power spectra of the bubbling regime of plastic beads in the 11 cm I.D column with a bed height of 16 cm

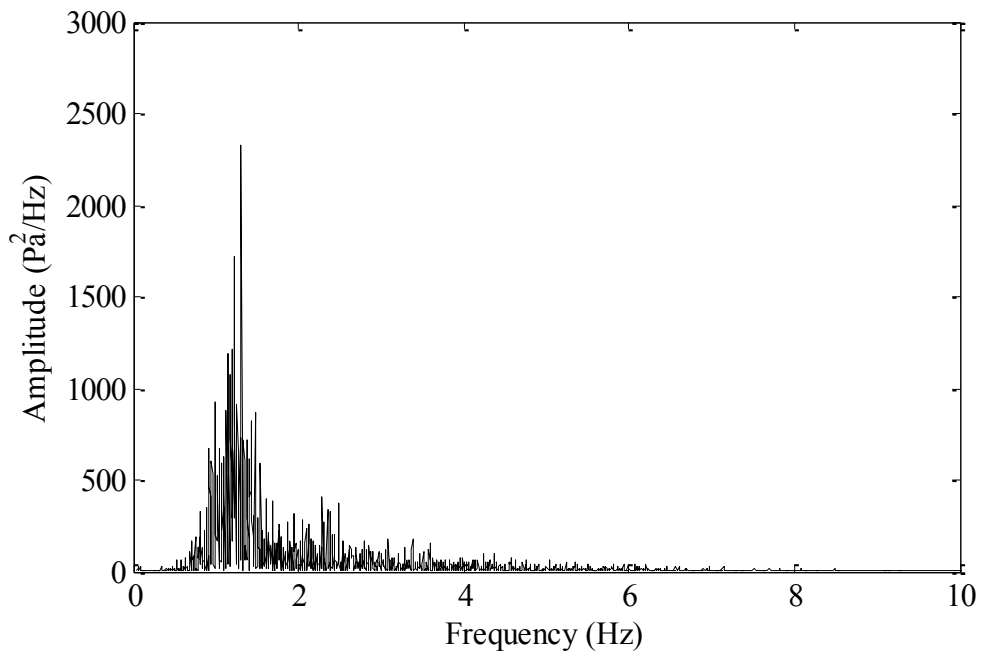


Figure A.5 Power spectra of the slugging regime of plastic beads in the 11 cm I.D column with a bed height of 16 cm

For a bed height of 28 cm, the resulting power spectra for the bubbling and slugging regimes is shown in Figures A.6 and A.7 below. Figure A.6 represents the bubbling regime which displayed a dominant frequency of approximately 1.17 Hz. The dominant frequency for the slugging regime was identified as 0.81 Hz, as represented in Figure A.7.

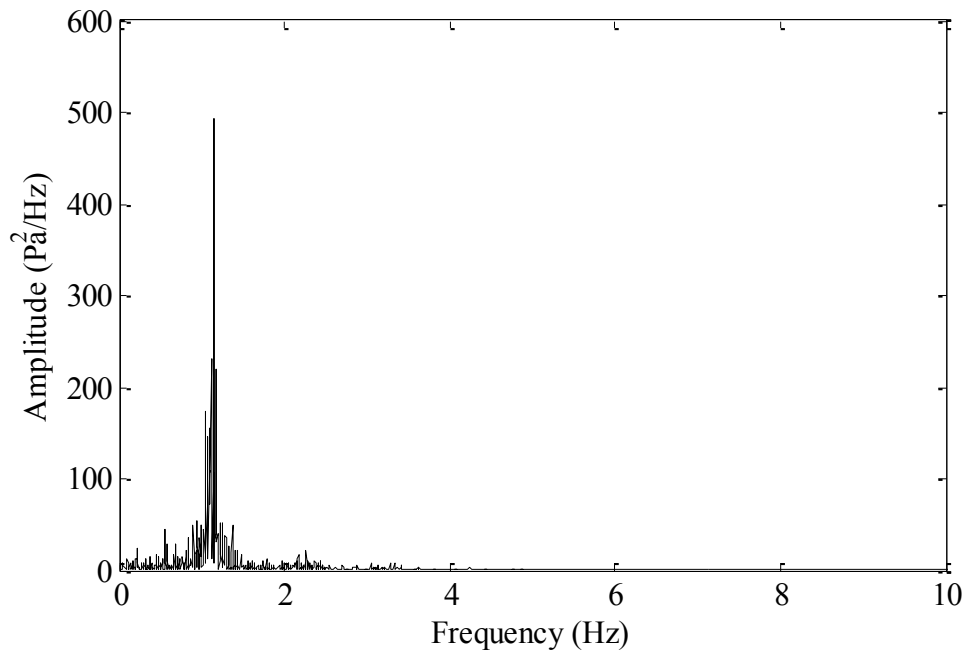


Figure A.6 Power spectra of the bubbling regime of plastic beads in the 11 cm I.D column with a bed height of 28 cm

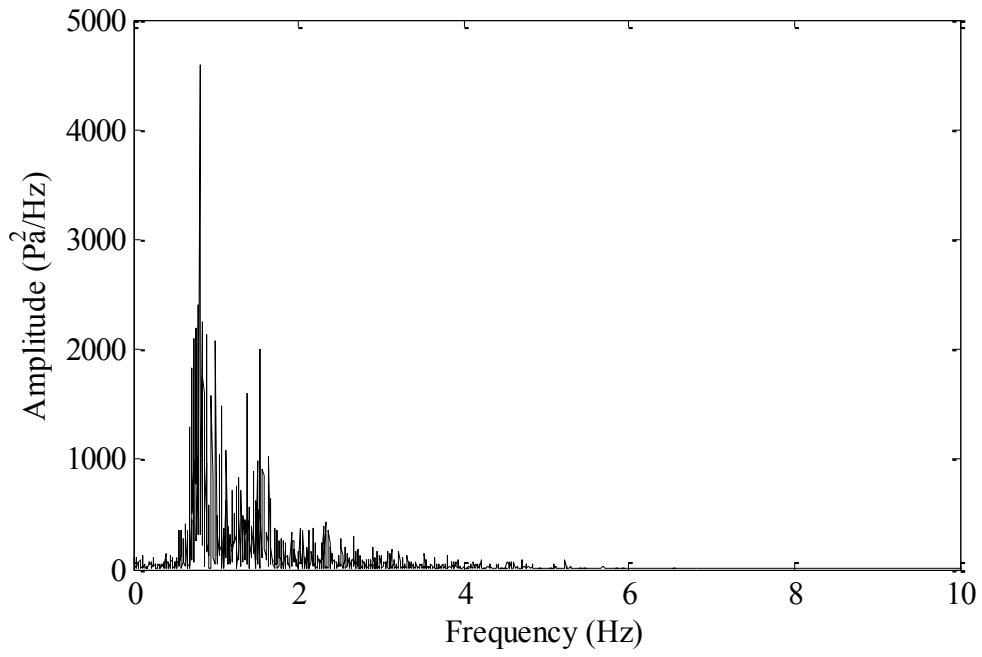


Figure A.7 Power spectra of the slugging regime of plastic beads in the 11 cm I.D column with a bed height of 28 cm

APPENDIX B

MATLAB CODE FOR IMPLEMENTATION OF THE FFT

Analysis in the frequency-domain was accomplished by transforming the time-pressure signals, obtained from experimental measurements, into the frequency domain. This was successfully achieved by implementing the FFT algorithm via a built-in function on the MATLAB software package. The simulation code for the bubbling regime for sand particles at a bed height of 11 cm in the 11 cm I.D fluidized bed column is presented below. The code represents a single run which was broken up into eight segments. The same code was used for additional runs and new operating conditions with the Excel File being changed to account for new experimental data.

```
% Initialize workspace

clear
clc

% Specifying Microsoft Excel Document containing experimental data

ExcelfileS = 'F:\ID11 0.5 Lmin 11cm-1.xlsx' ;
ExcelsheetS = '0.5 Lmin';

% Specifying number of data points, interval time and frequency
calculation

N1 =6123 ;
T = 218;
freq = [1:N1/2-1]/T

% Reading experimental data and implementing the Fast Fourier
Transform for each segment

Data_Range1 = 'A3:A6126';
pressure1 = xlsread(ExcelfileS ,ExcelsheetS, Data_Range1);
Pressure_Pa1 = pressure1*10^3;
p1 = abs(fft(Pressure_Pa1))/(N1/2);
p1=p1(2:N1/2).^2 ;

Data_Range2 = 'A6127:A12250';
pressure2 = xlsread(ExcelfileS ,ExcelsheetS, Data_Range2);
Pressure_Pa2 = pressure2*10^3;
p2 = abs(fft(Pressure_Pa2))/(N1/2);
p2=p2(2:N1/2).^2;

Data_Range3 = 'A12251:A18374';
pressure3 = xlsread(ExcelfileS ,ExcelsheetS, Data_Range3);
Pressure_Pa3 = pressure3*10^3;
p3 = abs(fft(Pressure_Pa3))/(N1/2);
```

```

p3=p3(2:N1/2).^2;

Data_Range4 = 'A18375:A24498';
pressure4 = xlsread(ExcelfileS ,ExcelsheetS, Data_Range4);
Pressure_Pa4 = pressure4*10^3;
p4 = abs(fft(Pressure_Pa4))/(N1/2);
p4=p4(2:N1/2).^2;

Data_Range5 = 'A24499:A30622';
pressure5 = xlsread(ExcelfileS ,ExcelsheetS, Data_Range5);
Pressure_Pa5 = pressure5*10^3;
p5 = abs(fft(Pressure_Pa5))/(N1/2);
p5=p5(2:N1/2).^2;

Data_Range6 = 'A30623:A36746';
pressure6 = xlsread(ExcelfileS ,ExcelsheetS, Data_Range6);
Pressure_Pa6 = pressure6*10^3;
p6 = abs(fft(Pressure_Pa6))/(N1/2);
p6=p6(2:N1/2).^2;

Data_Range7 = 'A36747:A42870';
pressure7 = xlsread(ExcelfileS ,ExcelsheetS, Data_Range7);
Pressure_Pa7 = pressure7*10^3;
p7 = abs(fft(Pressure_Pa7))/(N1/2);
p7=p7(2:N1/2).^2;

Data_Range8 = 'A42871:A47634';
pressure8 = xlsread(ExcelfileS ,ExcelsheetS, Data_Range8);
Pressure_Pa8 = pressure8*10^3;
p8 = abs(fft(Pressure_Pa8))/(N1/2);
p8=p8(2:N1/2).^2;

% Plotting the power spectrum for each data segment

figure
subplot(4,2,1)
plot(freq, p1,'k')
axis([0 14 0 4000])
set(get(gcf,'CurrentAxes'),'FontName','Times New Roman','FontSize',10.5)
xlabel('Frequency (Hz)')
set(get(gcf,'CurrentAxes'),'FontName','Times New Roman','FontSize',10.5)
ylabel('Amplitude (Pa^2/Hz)')

subplot(4,2,2)
plot(freq, p2,'k')
axis([0 14 0 4000])
set(get(gcf,'CurrentAxes'),'FontName','Times New Roman','FontSize',10.5)
xlabel('Frequency (Hz)')
set(get(gcf,'CurrentAxes'),'FontName','Times New Roman','FontSize',10.5)
ylabel('Amplitude (Pa^2/Hz)')

```

```

subplot(4,2,3)
plot(freq, p3,'k')
axis([0 14 0 4000])
set(get(gcf,'CurrentAxes'),'FontName','Times New Roman','FontSize',10.5)
xlabel('Frequency (Hz)')
set(get(gcf,'CurrentAxes'),'FontName','Times New Roman','FontSize',10.5)
ylabel('Amplitude (Pa^2/Hz)')

subplot(4,2,4)
plot(freq, p4,'k')
axis([0 14 0 4000])
set(get(gcf,'CurrentAxes'),'FontName','Times New Roman','FontSize',10.5)
xlabel('Frequency (Hz)')
set(get(gcf,'CurrentAxes'),'FontName','Times New Roman','FontSize',10.5)
ylabel('Amplitude (Pa^2/Hz)')

subplot(4,2,5)
plot(freq, p5,'k')
axis([0 14 0 4000])
set(get(gcf,'CurrentAxes'),'FontName','Times New Roman','FontSize',10.5)
xlabel('Frequency (Hz)')
set(get(gcf,'CurrentAxes'),'FontName','Times New Roman','FontSize',10.5)
ylabel('Amplitude (Pa^2/Hz)')

subplot(4,2,6)
plot(freq, p6,'k')
axis([0 14 0 4000])
set(get(gcf,'CurrentAxes'),'FontName','Times New Roman','FontSize',10.5)
xlabel('Frequency (Hz)')
set(get(gcf,'CurrentAxes'),'FontName','Times New Roman','FontSize',10.5)
ylabel('Amplitude (Pa^2/Hz)')

subplot(4,2,7)
plot(freq, p7,'k')
axis([0 14 0 4000])
set(get(gcf,'CurrentAxes'),'FontName','Times New Roman','FontSize',10.5)
xlabel('Frequency (Hz)')
set(get(gcf,'CurrentAxes'),'FontName','Times New Roman','FontSize',10.5)
ylabel('Amplitude (Pa^2/Hz)')

subplot(4,2,8)
plot(freq, p8,'k')
axis([0 14 0 4000])
set(get(gcf,'CurrentAxes'),'FontName','Times New Roman','FontSize',10.5)
xlabel('Frequency (Hz)')
set(get(gcf,'CurrentAxes'),'FontName','Times New Roman','FontSize',10.5)

```

```
ylabel('Amplitude (Pa^2/Hz)')
```

Exporting the FFT results to Microsoft Excel for analysis and determination of the dominant frequency

```
d = xlswrite ('F:\triale.xlsx',freq,'Sheet1','A2');
s = xlswrite ('F:\triale.xlsx',pf,'Sheet1','B2');
d = xlswrite ('F:\triale.xlsx',freq,'Sheet1','D2');
s = xlswrite ('F:\triale.xlsx',p2,'Sheet1','E2');
d = xlswrite ('F:\triale.xlsx',freq,'Sheet1','G2');
s = xlswrite ('F:\triale.xlsx',p3,'Sheet1','H2');
d = xlswrite ('F:\triale.xlsx',freq,'Sheet1','J2');
s = xlswrite ('F:\triale.xlsx',p4,'Sheet1','K2');
d = xlswrite ('F:\triale.xlsx',freq,'Sheet1','M2');
s = xlswrite ('F:\triale.xlsx',p5,'Sheet1','N2');
d = xlswrite ('F:\triale.xlsx',freq,'Sheet1','P2');
s = xlswrite ('F:\triale.xlsx',p6,'Sheet1','Q2');
d = xlswrite ('F:\triale.xlsx',freq,'Sheet1','S2');
s = xlswrite ('F:\triale.xlsx',p7,'Sheet1','T2');
d = xlswrite ('F:\triale.xlsx',freq,'Sheet1','V2');
s = xlswrite ('F:\triale.xlsx',p8,'Sheet1','W2');
```

APPENDIX C

DATA CAPTURE AND DESCRIPTION OF SOFTWARE INTERFACE

The pressure fluctuation signal from the gas-solid fluidized bed was then conveyed from the WIKA model P30 pressure transmitter to a data acquisition system where further processing occurred. The software package that was used to control and measure the pressure fluctuation was Easy Com 2011 Windows. There were two main interfaces on the software: the instrument interface and the data logger interface. One interface allowed for the selection of the pressure transmitter and defined the input variables (instrument interface) while the other served as an output interface (data display and pressure fluctuation graph). The data logger interface also allowed for the control of the pressure transmitter by specifying when to start and end data logging, unit selection as well as the measuring rate.

Figure C.1 is a representation of the main window which appeared when the software was first opened. On this window were the following options: add instrument (1), remove instrument (2), communication (3), instrument list (4) and working pane (5). Add instrument (1) allowed the selected instrument (WIKA model P30 pressure transmitter) to be connected to the instrument list, while remove instrument (2) removed the selected instrument from the instrument list. Communication (3) indicated whether the connection to the instrument was established or disconnected. The instrument list (4) displayed all connected instruments while the working pane (5) contained all the necessary functions required to set the instrument as well as displayed the results.

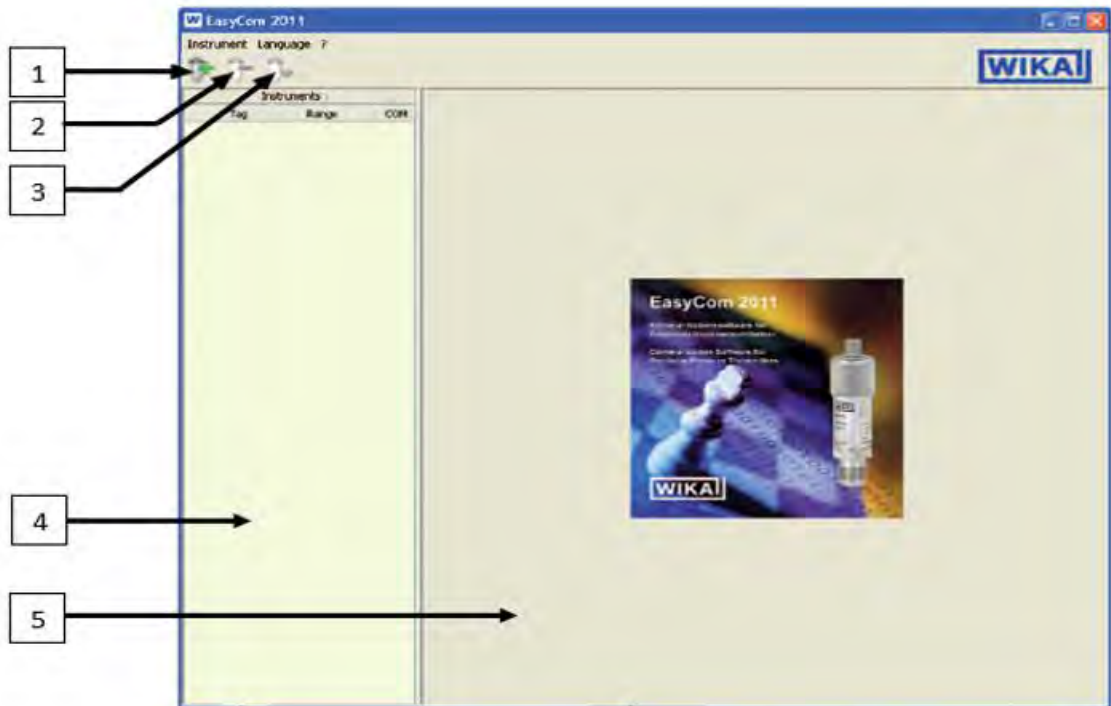


Figure C.1 Main window configuration

1 – Add instrument; 2 – Remove instrument; 3 – Communication; 4 – Instrument list;
5 – Working pane

Once the WIKA model P30 pressure transmitter had been successfully connected, an instrument menu (6) and Data logger (7) menu appeared in the working pane. The instrument menu contained three functions (8) (information, adjustment and settings). This can be seen in Figure C.2. The functions (8) provided information on the properties of the connected instrument (Information) as well as allowed for the input variables to be defined and adjusted (Adjustment and Settings). The adjustment function allowed for the adjustment of the span of the connected instrument while the settings function allowed the user to specify the operating mode and the measured variable.

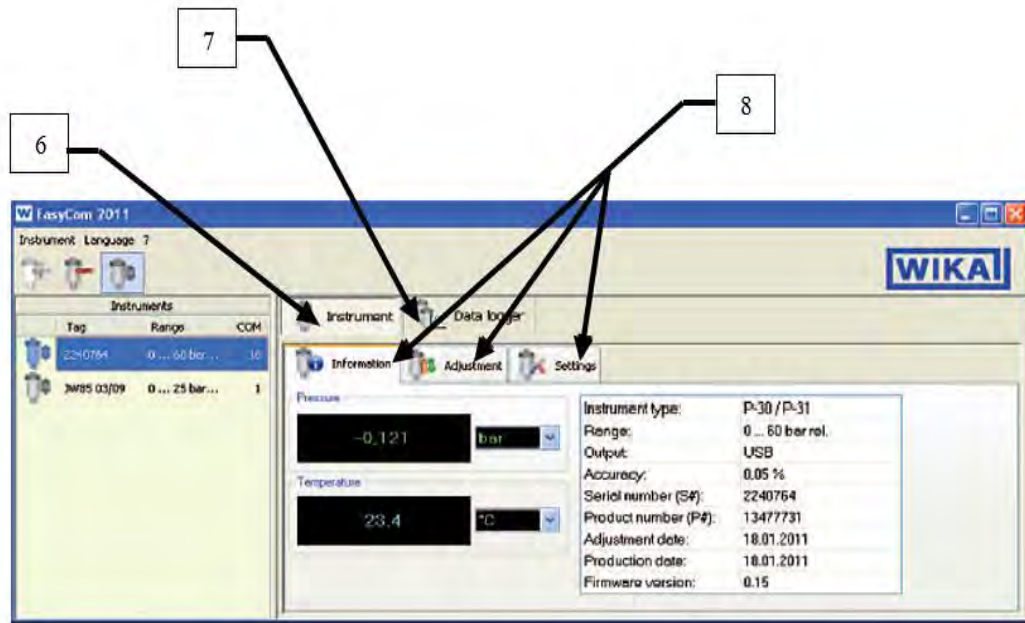


Figure C.2 Instrument menu displayed in working pane once the instrument has been connected

6 – Instrument menu; **7** – Data logger menu; **8** – Function menu including Information, Adjustment and Settings

The data logger menu contained two functions: Table view (9) and Graphical view (10). This represented the interface where the experimental results were displayed. In addition, a Settings panel was present to allow for control of the WIKA model P30 pressure transmitter. The Settings panel allowed for input of the Start condition (11) and Stop condition (12). The start of data logging could be specified as either Immediately (a) (Data logging began as soon as the Start button (15) was pressed) or Date/time (b) (Data logging began at the set day and time). The end of data logging could be specified as Date/time (c) (Data logging ended at the selected date and time), Duration (d) (Data logging ended when the set time span had expired) or Count values (e) (Data logging will end once the specified number of measured values had been reached). The Settings panel further allowed for the specification of the units for pressure and temperature (13) as well as the Measuring rate (14) which was determined from the chosen sampling frequency. Figure C.3 shows an image of the data logger interface.

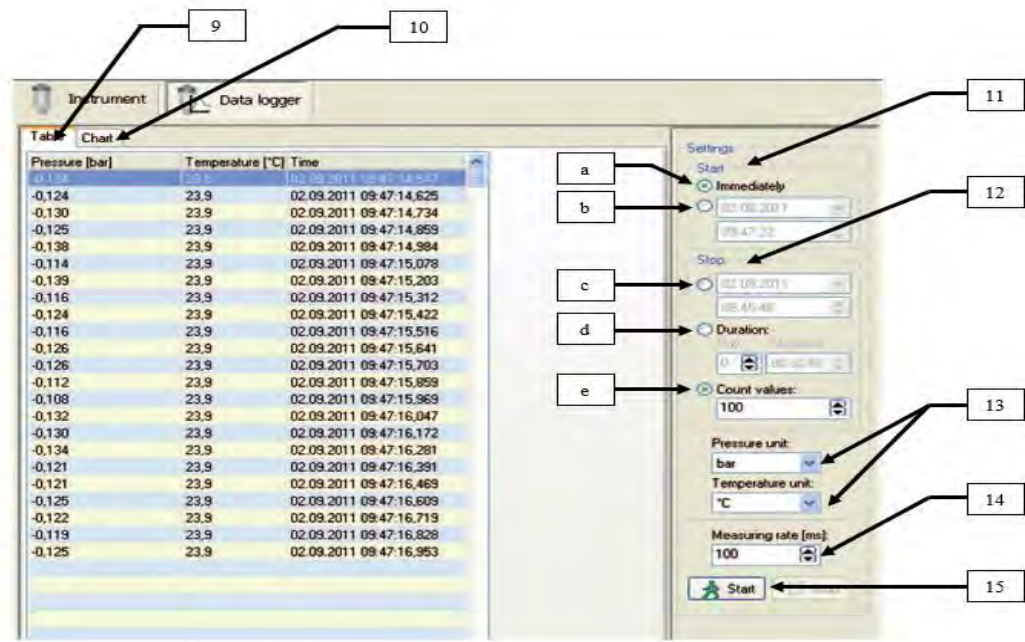


Figure C.3 Data logger menu displayed in working pane once the instrument had been connected

9 – Table view; 10 – Chart view; 11 – Start condition (a – Immediately; b – Date/time); 12 – Stop condition (c – Date/time; d – Duration; e – Count values); 13 – Unit Selection; 14 – Measuring rate; 15 – Start button